2014-10-01

Co-Firing Biomass with Biogas in Cookstoves with a Fan

Manil Poudyal
Brigham Young University - Provo

Co-Firing Biomass with Biogas in Cookstoves with a Fan

Manil Poudyal

A thesis submitted to the faculty of
Brigham Young University
in partial fulfillment of the requirements for the degree of

Master of Science

Matthew R. Jones, Chair
Randy S. Lewis
Dale R. Tree

Department of Mechanical Engineering

Brigham Young University

November 2014

ABSTRACT

Co-firing Biomass and Biogas in Cookstoves with Fan

Manil Poudyal
Department of Mechanical Engineering, BYU
Master of Science

Co-firing is a combustion process in which more than one type of fuel is used. In many cases, co-firing reduces fuel costs and/or reduces the environmental impact. The objective of this research was to test the hypothesis that adding biogas to be co-fired with biomass in a traditional cookstove reduces indoor air pollution and increases the combustion efficiency. The impact of co-firing on indoor air pollution is assessed by comparing the concentrations of carbon monoxide and particulate matter in the exhaust stream of a co-fired cookstove to a cookstove fueled with biomass alone. The concentrations of each of these pollutants were measured using a portable emissions monitoring system. Combustion efficiency is defined as the ratio of energy released by combustion to energy in the fuel. Instead of combustion efficiency, the impact of co-firing was assessed on the modified combustion efficiency, which is defined as $CO_2/(CO_2+CO)$ on a molar basis. This is because CO and CO_2 concentrations can be measured. In addition, the impact of cofiring on other parameters such as thermal efficiency, specific fuel consumption rate, and specific emission of CO, CO_2, and PM were assessed. Previous investigation of biomass combustion in traditional cookstoves indicates that power harvested using a thermoelectric generator can be used to drive a fan and increase the amount of air flowing into the combustion zone. The impact of using a fan on indoor air pollution and combustion efficiency was also assessed. It was found that co-firing biomass with optimum amount of biogas reduced the emission of CO by 32 % and PM by 33 % and increased the modified combustion efficiency by 1.3 %. It was found that using a fan reduced the emission of CO by 35 % and PM by 39 % and increased the modified combustion efficiency by 1.1 %. Finally, the combination of co-firing and use of a fan reduced the emission of CO by 58 % and PM by 71 % and increased the modified combustion efficiency by 2.8 %.

Keywords: co-firing, biogas, biomass, indoor air pollution, combustion efficiency

ACKNOWLEDGEMENTS

I am very grateful for the support and guidance of my advisor Dr. Jones. I am thankful that he gave me the freedom to direct my research. He guided me and gave constructive criticism that helped me throughout my research. Special thanks go to Matthew Duffield and members of GEO team who helped me with the experiments and set-ups. I would like to thank Dr. Lewis for his counsel and for the opportunity to conduct my research.

I want to dedicate this thesis to my loving mother (Menaka Poudyal), and father (Madan Poudyal). I thank my sister (Manila Poudyal) for her constant love and support. I am blessed to have a wonderful family who taught me to work hard under every circumstance. Having personally spent many years in the rural communities of Nepal facing the cookstove challenges, this project was focused to mitigate those challenges.

TABLE OF CONTENTS

LIST OF TABLES ..... **vi**

LIST OF FIGURES ..... **vii**

1 Chapter 1: Introduction **1**

1.1 Background 3

1.2 Motivation and Objective 5

1.3 Literature Review 8

1.4 Hypothesis 9

2 Chapter 2: Experimental Equipment, Measurements, and Methods **11**

2.1 Experimental Equipment 11

2.1.1 Wood 11

2.1.2 Biomass Cookstove 13

2.1.3 Biogas 15

2.1.4 Fan 15

2.1.5 Windbreak 16

2.1.6 Portable Emissions Monitoring System 17

2.1.7 Water Boiling Test 18

2.2 Measurements 19

2.2.1 CO Concentration (ppm) 19

2.2.2 CO_2 Concentration (ppm) 21

2.2.3 Particulate Matter (mg/m^3) 25

2.2.4 Temperature (^oC) 28

2.2.5 Scale (g) 28

2.3 Methods 29

3 Chapter 3: Experimental Analysis and Comparisons 32

3.1 Performance Parameter 33

3.1.1 Thermal Efficiency 35

3.1.2 Specific Fuel Consumption Rate 38

3.1.3 Specific Emission of Carbon Monoxide 39

3.1.4 Specific Emission of Carbon Dioxide 39

3.1.5 Specific Emission of Particulate Matter 40

3.1.6 Modified Combustion Efficiency 40

3.2 Results 41

3.2.1 Time Resolved Measurements 41

3.2.2 Integrated Results 58

3.3 Discussion 66

3.3.1 Time Resolved Results 66

3.3.2 Integrated Results 69

4 Chapter 4: Conclusion and Recommendations 72

4.1 Conclusion 72

4.2 Recommendations 75

References 77

Appendix A: Variability and Uncertainty Analysis 80

Appendix B: Emissions and Other Measurements Database 89

Appendix C: Calculating Mass Flow (g/sec) 95

Appendix D: Raw Data to Final Result 100

Appendix E: Raw Data 107

LIST OF TABLES

Table 1-1: Acronym Table 2

Table 2-1: Dimension and Number of Pieces Used for Each Test 12

Table 2-2: Dimensions of Cookstove System 14

Table 2-3: Air Velocity from the Fan 16

Table 3-1: List of Tests Being Compared 32

Table 3-2: Nomenclature for Measurement Variables 33

Table A-1: Nomenclature for Variables Introduced in Calculations 80

LIST OF FIGURES

Figure 2-1: Identically cut wood mixed together and wood weighed before the test. 13

Figure 2-2: Mobile cookstove can be wheeled out and in. 13

Figure 2-3: Top view of Peruvian cookstove. 14

Figure 2-4: Fan to provide air. Two burners to deliver biogas and a duct to supply air. 16

Figure 2-5: Filter paper being desiccated. Filter paper being weighed on microbalance. 18

Figure 2-6: CO sensor - electrochemical cell 21

Figure-2-7: Non-dispersive infrared (NDIR) CO_2 sensor 24

Figure 2-8: PM sensor with and without smoke 27

Figure 2-9: Location of flue gas thermocouple and pot water thermocouple 28

Figure 2-10: Biogas tank with regulator and flow meter. Biogas connected to burners. 31

Figure 3-1: Water is being heated in a pot. Dashed lines represent the control volume. 35

Figure 3-2: PM versus time for biomass burned alone 42

Figure 3-3: CO versus time for biomass burned alone 43

Figure 3-4: CO_2 versus time for biomass burned alone 43

Figure 3-5: PM versus time for biomass co-fired with 10% biogas 44

Figure 3-6: CO versus time for biomass co-fired with 10% biogas 45

Figure 3-7: CO_2 versus time for biomass co-fired with 10% biogas 45

Figure 3-8: PM versus time for biomass co-fired with 25% biogas 46

Figure 3-9: CO versus time for biomass co-fired with 25% biogas 47

Figure 3-10: CO_2 versus time for biomass co-fired with 25% biogas 47

Figure 3-11: PM versus time for biomass co-fired with 50% biogas 48

Figure 3-12: CO versus time for biomass co-fired with 50% biogas 49

Figure 3-13: CO_2 versus time for biomass co-fired with 50% biogas 49

Figure 3-14: PM versus time for biomass burned with fan 50
Figure 3-15: CO versus time for biomass burned with fan.....51
Figure 3-16: CO_2 versus time for biomass burned with fan 51
Figure 3-17: PM versus time for biomass co-fired with 10% biogas in addition to fan.....52
Figure 3-18: CO versus time for biomass co-fired with 10% biogas in addition to fan 53
Figure 3-19: CO_2 versus time for biomass co-fired with 10% biogas in addition to fan.....53
Figure 3-20: PM versus time for biomass co-fired with 25% biogas in addition to fan.....54
Figure 3-21: CO versus time for biomass co-fired with 25% biogas in addition to fan 55
Figure 3-22: CO_2 versus time for biomass co-fired with 25% biogas in addition to fan.....55
Figure 3-23: PM versus time for biomass co-fired with 50% biogas in addition to fan.....56
Figure 3-24: CO versus time for biomass co-fired with 50% biogas in addition to fan 57
Figure 3-25: CO_2 versus time for biomass co-fired with 50% biogas in addition to fan.....57
Figure 3-26: CO versus biogas flow rate with and without fan (Cumulative).....59
Figure 3-27: PM versus biogas flow rate with and without fan (Cumulative) 60
Figure 3-28: Thermal efficiency versus biogas flow rate with and without fan 61
Figure 3-29: Specific fuel consumption versus biogas flow rate with and without fan 61
Figure 3-30: MCE versus biogas flow rate with and without fan.....62
Figure 3-31: CO compared to PM emissions per energy delivered to the cooking pot 63
Figure 3-32: MCE versus thermal efficiency for different fuel combinations 65
Figure 3-33: Specific fuel consumption for different fuel combinations 66
Figure 3-34: Knot randomly distributed in the test wood.....69

1 CHAPTER 1: INTRODUCTION

A review of the energy access situation in developing nations was issued by the United Nations Development Program and the World Health Organization in November 2009 (Legros, Havet, Bruce, & Bonjour, 2009). This review indicates that 2.2 billion people use inefficient 'three stone' fires or highly polluting traditional cookstoves each day. Combustion of coal and biomass in these cookstoves generally results in fuel-rich flames that spew out substantial amounts of smoke, black carbon (soot) and toxic fumes, contributing to global climate change (Legros, Havet, Bruce, & Bonjour, 2009; Ramanathan & Carmichael, 2008) and harming the health of local residents.

The detriment to health and the environment resulting from biomass fuel stoves has been well documented. Studies have shown that the incomplete combustion of solid fuels produces fumes and particulate matter that increase the risk of cancer, damage immune systems, irritates airways and reduce the oxygen supplied to unborn children (Dherani, et al., 2008; World Health Organization, 2013). Approximately two million deaths per year are associated with the use of solid fuels, and more than 99% of these deaths occur in developing nations.

While the health of all members of a household is affected by the toxic fumes and particulate matter produced by primitive cookstoves, the consequences for women, infants and children, who are exposed to the poor indoor air quality the most, are disproportionately severe (World Health Organization, 2013). Widespread use of solid fuels leads to numerous other negative outcomes that also primarily impact women and children. Examples of these other

negative consequences are more likely to be burned from open fires and poorly designed cookstoves. The necessity of collecting fuel also makes them vulnerable to violent attacks and injury, and causes them to miss opportunities to attend school or engage in other activities that would result in economic or social development (World Health Organization, 2013).

Both the scope and magnitude of these problems suggest that even modest enhancements in cookstove efficiency and emissions have the potential to substantially improve the lives of the poorest of people, provided the proposed enhancements are affordable. This research focuses on traditional cooking styles in developing countries like Nepal, where it is feasible to produce modest amounts of biogas (Ukpai & Nnabuchi, 2012).

The objective of the thesis is to test the hypothesis that co-firing biomass and biogas with or without a fan reduces emissions of pollutants and increases the combustion efficiency. It is feasible to produce biogas in developing regions (Ukpai & Nnabuchi, 2012). In the following chapter, other literature reviews and experiments are analyzed in order to provide a framework for the hypothesis.

Table 1-1: Acronym Table

Acronym	Term
COPD	Chronic Obstructive Pulmonary Disease
GHG	Greenhouse Gas
HTE	Heat Transfer Efficiency
IAP	Indoor Air Pollution
LHV	Latent Heat of Vaporization
MCE	Modified Combustion Efficiency
NDIR	Non-Dispersive Infrared

Table 1-1, continued

Acronym	Term
PIC	Product of Incomplete Combustion
PM	Particulate Matter
TEG	Thermoelectric Generators
WBT	Water Boiling Test
WHO	World Health Organization
PEMS	Portable Emissions Monitoring System

1.1 **Background**

The use of clean-burning fuels such as propane and kerosene for cooking is prohibitively expensive in developing regions. Consequently, the populace is heavily dependent on firewood or dry cow dung for fuel, making it more difficult to escape poverty. Also, as mentioned previously, burning biomass contributes substantially to health problems, GHG emissions, and deforestation.

Many health hazards are caused by IAP, which is created by the PIC of biomass. Incomplete combustion occurs when fuel and oxidizer are poorly mixed or oxygen is insufficient for complete combustion. PIC includes carbon monoxide, nitrous oxide, sulfur oxides, carcinogens, and char (solid residue rich in carbon content). Women and children spend a considerable amount of time in front of the stove, making them at risk for serious eye problems such as cataracts and even blindness. Low birth weights and high mortality rates among young children are also associated with indoor cooking using wood and cow dung. IAP can also result in cancer of trachea and lungs (Elledge, et al., 2012). According to the WHO, indoor smoke is a major cause of pneumonia, which remains the single most deadly child killer, and is responsible for 2 million deaths every year. The acrid smoke also causes COPD, which is responsible for

511,000 deaths worldwide per year (Rehfuess, 2006), as well as bronchitis, asthma, and respiratory infections. Also, over 25% of arsenic in fumes produced by dung cakes is absorbed by the respiratory system, causing lung diseases (Pyati, 2012).

IAP affects the environment as dramatically as it does humans. Most PIC gases eventually form CO_2, but the remaining PIC gases have higher environmental impact per carbon atom than CO_2, and contribute more towards global warming (Smith, Uma, Kishore, Zhang, Joshi, & Khalil, Greenhouse Implications of Household Stoves: An Analysis for India, 2000). Heavy dependence on firewood also contributes to deforestation. Due to wood burning, Pakistan lost 14.7% of its forest between 1990 and 2005 (Tahir, Rafique, & Alaamer, 2010). Deforestation allows CO_2 to remain in the atmosphere, and accounts for 25 to 30 percent (or 1.6 billion tons) of all GHGs produced per year (Matthews, 2006). Land left barren by deforestation is vulnerable to soil erosion and to landslides following monsoons, making the effects of deforestation particularly concerning for mountainous countries such as Nepal.

But the good news is that there are means available to improve upon the current situation. The combustion efficiency in traditional cookstoves is around 94% (Smith, et al., 2000). At first glance, this figure seems extraordinarily high for a primitive stove. Indeed, this shows that the potential for stove improvements to reduce fuel consumption via combustion efficiency gains is modest at best. However, it is important to keep in mind that there is still sizable potential for emissions reductions. 94% combustion efficiency indicates that a significant amount of fuel carbon is leftover as PIC. Furthermore, study show that a small variation in combustion efficiency results in a large difference in the emissions of pollutants (Jetter, et al., 2012).

Successful integration of an alternative fuel to biomass will increase economic wealth in third world countries. According to the World Bank, the average Nepalese household spends 41

hours per month collecting firewood (Loughran & Pritchett, 1997). Every day, women and children spend several hours traveling long distances through thick forests in search of firewood. They risk physical assault and face the omnipresent danger of getting killed by wild animals (Berkeley, 2012). In addition to the physical risks associated with gathering biomass fuels, both time and opportunities are lost. An alternative way of using biomass that reduces the impact on people's health and on the environment could help people improve their financial condition, open doors for children to go to school, and break the vicious cycle of poverty.

1.2 **Motivation and Objective**

Because sufficiently large-scale biogas production is not feasible in developing nations, most will continue to use biomass as the primary source of fuel. However, it is quite feasible to produce enough biogas to supplement biomass combustion. The main hypothesis of this thesis is that co-firing two different fuels—biomass and biogas—leads to more complete combustion, reducing emissions and increasing combustion efficiency, compared to burning the biomass alone. Combustion efficiency is defined as the ratio of heat produced in a combustion process to the heat that would be released in complete and ideal combustion. There is an extensive literature regarding emissions from cookstoves, but no previous studies regarding co-firing of biomass with biogas have been published.

Biogas is an economically plausible solution because of the simplicity of its production. It can be produced merely by mixing dung and water (Ukpai & Nnabuchi, 2012), two resources that are abundant in Nepal. Nepal is home to many rivers, streams and lakes, and a major part of Nepal's income is dependent on agriculture and livestock. Almost every village family has cows, buffaloes, oxen, or goats, which makes the dung readily available and can be used with water to produce biogas. Moreover, construction of a biogas plant requires only simple tools and

unskilled labor. The plant is made up of bricks, stones, sand, and cement and usually built underground for stability. Once built, it requires minimal maintenance. Cow dung is mixed with water and the slurry is let into the digester after which the valve is closed. As the bacteria produce biogas inside the digester, the gas rises to the top, the pressure increases, and the slurry is forced through an outlet. Dung which is currently unused or only used as solid fuel can be used to produce biogas, a better co-firing material than other solid fuels.

In addition to the simplicity of this method of biogas production, there are a number of fringe benefits associated with the dung decomposition production method. For example, the biogas plant's outlet slurry is very good for compost manure and can be used for agriculture. Also, uncollected dung may undergo anaerobic decomposition in agricultural areas with significant production of methane and other GHGs which will contribute to the global warming (Bhattacharya, Thomas, & Salam, 1997). Since, methane is a worse greenhouse gas than CO_2, burning the biogas will convert methane into CO_2.

In third world countries such as Nepal, technology is expensive, but manual labor is cheap. This outlet slurry is very good for compost manure and can be used for agriculture. Since it is an open system, the required maintenance is minimal. If necessary, the digester is easy to clean by making sure that no biogas is left in the system. The size of the plant depends upon the quantity of available dung rather than the size of the family. Bajgain provides a table for plant size with respect to the number of cattle and dung produced (Bajgain, 1994). For instance, a four cubic meter plant is the right size for 24 kgs of dung per day produced by 2-3 cattle. Based on the population of livestock, Nepal has the potential to install 1.9 million family sized biogas plants. As of June 2009, Nepal has installed 174,591 biogas plants (Katuwal & Bohara, 2009).

Dung can produce significant quantities of biogas. For example, the anaerobic digestion of 440 kg of cow dung in an experimental digester of 800 liters at 37 ^{o}C produces about 26.9 m^3 of biogas, an energy equivalent to 592.8 MJ (164.5 KWh) with an average composition of 61 % methane. This means that about 61 ml of biogas can be obtained per kg of cow dung (Ounnar, Benhabyles, & Igoud, 2012). The biogas needs no refinement and will not have any effect on cooking appliances (Arthur, Baidoo, & Antwi, 2011). The size of the plant depends upon the quantity of available dung rather than the size of the family. Bajgain provides a table for plant size with respect to the number of cattle and dung produced (Bajgain, 1994). For instance, a four cubic meter plant can consume 24 kgs of dung per day produced by 2-3 cattle. Based on the population of livestock, Nepal has the potential to install 1.9 million family sized biogas plants. As of June 2009, Nepal has installed 174,591 biogas plants (Katuwal & Bohara, 2009).

Biogas can be burned alone, but its production can be limited for a number of reasons. First, the production of biogas is a function of temperature and the production is limited during winter months when the temperature drops (Garba, 1996). Second, the slurry requires a dung-water mass ratio of 1:2, and although water is readily available in most parts of the country, there are areas where water is scarce. Third, because families in rural areas are typically large, it is unlikely that the average family will be able to fulfill their needs solely using dung-derived biogas. That is why this research primarily investigates using biogas as a supplementary fuel in co-firing.

All of this indicates that co-firing cookstoves with biogas is plausible. However, before advocating more widespread use of co-firing cookstoves, it is essential to determine whether or not co-firing is effective at reducing emissions and increasing efficiency. And that is the intent of this thesis.

1.3 **Literature Review**

The effects of biomass combustion on the environment have been extensively studied. Much of the literature used is from the nearby countries of India and Pakistan. Smith, et al. compare biomass fuels and biogas and assess the emissions occurring when these fuels are burned in different cookstoves. PIC is much higher for biomass than for biogas (Smith, Uma, Kishore, Zhang, Joshi, & Khalil, Greenhouse Implications of Household Stoves: An Analysis for India, 2000). PM consists of tiny solid particles ranging in size and composition. Thermal efficiency is the ratio of energy used to cook the food to the energy consumed by burning wood. The thermal efficiency of biogas is high and in comparison to the most solid biomass fuels, biogas produces lower PIC (Smith, Uma, Kishore, Zhang, Joshi, & Khalil, Greenhouse Implications of Household Stoves: An Analysis for India, 2000). It can be assumed that co-firing biogas with biomass can lower PIC, lower PM, and increase thermal efficiency.

Demirbas explains how co-firing biomass with coal increases boiler efficiency and minimizes waste. He shows a reduction in the levels of CO_2, NO_x and SO_x which reduces the total emissions per unit energy produced (Demirbas, 2003). Considering that, when burned in isolation, biogas produces lower PIC, making it a more efficient fuel than coal, the same should be true when they are burned in co-firing. . It can be suggested that there is no reason that the efficiency gains from co-firing would be any less when the supplementary fuel is biogas rather than coal.

Witt performed experiments by forcing air into the stove, which resulted in an increase in flame temperature and a reduction in emissions due to complete combustion. The forced air reduced the PM and the time to boil (Witt, 2005). Co-firing biomass and biogas with air will presumably lead to even better results.

Jetter, et al. tried to standardize the system of measurement of different cookstoves (Jetter, et al., 2012). The assessments described in this thesis follow the general procedure recommended by Jetter et al., including gravimetric measurement of PM. Jetter recommends that a cookstove and a fuel be treated as a system, and that the performance of a cookstove/fuel system be compared to the performance of another cookstove/fuel system. In this research, the same cookstove was used for all tests, and the amount of biogas was varied. The tests were repeated with and without using the fan. Jetter, et al. repeats each test at least three times. Each of the tests for this research is also performed at least 3 times. For each test, there were measurements of emissions (CO, CO_2, and PM concentrations), pot water temperature, flue gas temperature. The other measurements done were mass of accumulated particulate matter, wood, charcoal, and water. According to WBT protocol, these measurements are averaged for the repeated tests, and one standard deviation is taken as their error. For this research the same emissions will be measured, but while averaging, the instrument uncertainty and variability in the results will be included to make the comparison more meaningful.

There is extensive literature regarding emissions from cookstoves, but after multiple searches of databases available through the Harold B. Lee Library, it is concluded that no previous studies regarding co-firing of biomass with biogas have been published. The key words used during the search were: co-fire, biogas, biomass, cookstove, products of incomplete combustion, and indoor air pollution.

1.4 **Hypothesis**

The purpose of this research is to investigate the hypothesis that co-firing biomass with biogas in a traditional cookstove lowers emissions (CO and PM) and increases the combustion efficiency (Smith, Uma, Kishore, Zhang, Joshi, & Khalil, Greenhouse Implications of Household

Stoves: An Analysis for India, 2000). The impact of using a fan to increase the flow of air into the combustion zone was also assessed (Witt, 2005). It is anticipated that co-firing and using the fan will reduce IAP and lessen the adverse impacts on health and environment. Moreover, if the hypothesis is proven, then this system will offer an improved cooking process that will improve lives in rural communities.

2 CHAPTER 2: EXPERIMENTAL EQUIPMENT, MEASUREMENTS, AND METHODS

Experimental equipment required for the tests and experimental setups are discussed in this chapter. Experimental setup is fairly uniform, elements such as wood, fire, cookstove, fan, windbreak, PEMS, are all set up in the same way for all the tests. To better match the controlled laboratory test to the field tests, experience with a real cookstove system is important; therefore a Peruvian traditional cookstove was used for the experiment. The measurements section discusses the measured values which were used to calculate a performance parameter in the later chapter. This chapter also discusses the methodology used to perform the experiments.

2.1 Experimental Equipment

2.1.1 Wood

Since a comparison needs to be made between the results of the combustions tests, the burning methods should be similar for all tests. For consistency, the wood used in the experiments was cut into similarly sized pieces and mixed together as seen in Figure 2-1. All of the wood was bought from the same store and came from the same type of tree, southern pine. To assess the impact of co-firing, the tests were performed in controlled conditions. The amount of wood was pre-determined by using a scale as in Figure 2-1 and no additional wood was added to the fire during the test period. The fire was uninterrupted to make sure that the process was

less dependent on the operator. Practice burns were performed to ascertain the correct method to build a fire, to determine wood dimensions, and to ascertain the proper wood mass. The log was saw-cut to the desired size. The practice tests were conducted to figure out the right dimensions and amount of wood with respect to the stove size and the hood. When 1500 grams of wood was burned there was too much fire that shut off the sensors. With 1000 grams the wood burned quickly resulting in lower burn time. Also, the smaller dimensions of wood burned quickly with fire getting lot larger. Therefore, 1200-1300 grams of wood with larger dimensions were appropriate. To start the fire there were kindling and also smaller dimensions of wood. The wood burned for about 20 minutes, leaving hardly any unburned wood left at the end of the test. The wood was cut uniformly into three types as listed in Table 2-1. To start the fire, the tinder was made from one of the small-sized, pre-weighed wood. A fixed length of paper towels was used to start the fire for each test. Also, the firewood was built similarly for each experiments being compared.

Table 2-1: Dimension and Number of Pieces Used for Each Test

*Dimensions (cm*cm*cm)*	*Number of Pieces*
3.8 * 3.8 * 35.6	3
2.5 * 2.5 * 35.6	3
2.5 * 2.5 * 20.3	2

Figure 2-1: Identically cut wood mixed together and wood weighed before the test.

2.1.2 Biomass Cookstove

Figure 2-2 shows a replica of a traditional Peruvian cookstove that was placed in the middle of a cart. There were cinder blocks on three sides to mimic a hearth, similar to those often used in homes in remote Peruvian villages.

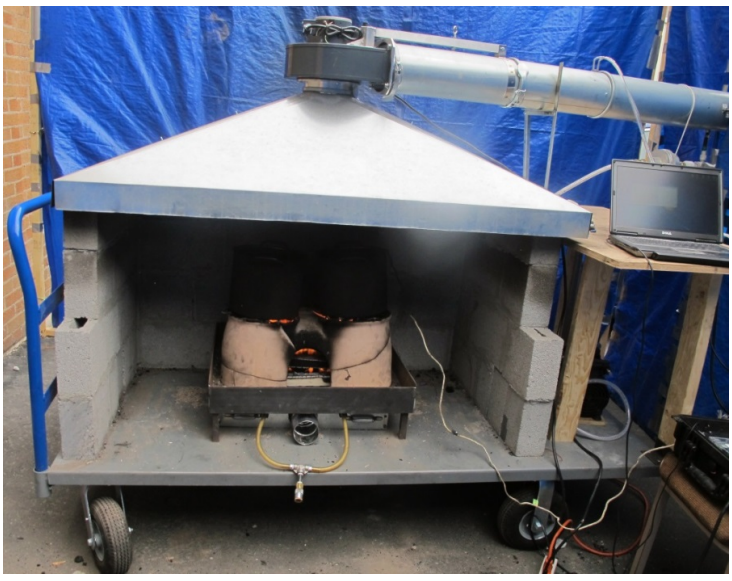

Figure 2-2: Mobile cookstove can be wheeled out and in.

Figure 2-3 shows the detailed view of the cookstove, which was made with clay. This cookstove is similar to the traditional cookstoves most widely used in Nepal. The dimensions of the cookstove are listed in Table 2-2. For the tests, the fire was at the center while wood sticks were oriented radially. The dimensions of the stoves are given in Table 2-2. The cookstove had 3 spots to place the cooking pots. The emissions test system had a hood for collecting emissions from the stoves. There was a blower attached on top of the hood. The blower drew smoke through the hood. To avoid overloading the sensor, the dilution of smoke was necessary. The increase in air to fuel ratio was done by increasing the height of the hood and cinder block wall, and increasing the overall distance from the stove to the blower.

Figure 2-3: Top view of Peruvian cookstove.

Table 2-2: Dimensions of Cookstove System

Cookstove base area	53.3 cm * 35.6cm
Cookstove height	25.4 cm
Cookstove hole 1 and 2 diameter	22.9 cm
Cookstove hole 3 diameter	14 cm

Table 2-2, continued

Windbreak base area	3.65 m * 6.1 m
Windbreak height	2.44 m
Filter paper diameter	10.2 cm
Cooking pot 1 and 2 diameter	22.8 cm
Cooking pot 1 and 2 height	20.3 cm
Cooking pot 1 and 2 thickness	0.5 mm
Cooking pot 3 diameter	15.2 cm
Cooking pot 3 height	9.1 cm
Cooking pot 3 thickness	1 mm
Cinder block wall height	78.7 cm
Hood height	35.6 cm
Cinder block wall base area (interior)	50 cm * 101 cm

2.1.3 Biogas

Biogas was simulated using a mixture of 65% methane and 35% carbon dioxide. Several literatures suggest that the composition of the biogas made from compost is 65% methane and 35% carbon dioxide (Ounnar, et al., 2012; Arthur, et al., 2011). Also this composition can be created in the field. Since biogas stores energy, it was important to make sure that when biogas was co-fired with biomass, the biogas was not the primary energy source during the process of combustion. Thus, the flow rate of biogas was vital when co-firing biogas with biomass. When biomass is burned alone for a certain period of time, the total energy with time is known. A flow rate of 10 % biogas means that biogas provides additional 10% of that total energy with time. In the tests, biogas was co-fired with biomass at flow rates of 10%, 25%, and 50% of total energy with time.

2.1.4 Fan

Figure 2-4 shows a fan from a desktop computer with a duct that was used to supply air. An anemometer was used to calculate the velocity of the air from the fan as listed in Table 2-3.

Figure 2-4 shows the duct which was located at the very center of the cookstove, the diameter of the duct is 7.6 cm.

Figure 2-4: Fan to provide air. Two burners to deliver biogas and a duct to supply air.

Table 2-3: Air Velocity from the Fan

Voltage (V)	*Velocity (m/s)*	*Volumetric Flow Rate (m^3/s)*
4.8	4.2	0.019

2.1.5 Windbreak

For safety reasons, the test had to be performed outside. To minimize the effect of wind, an outside factor that would affect the outcome of the experiment, a windbreak was used to shield the flame from gusts of air. It was made up of plastic tarps. The dimensions of the windbreak are given in Table 2-2. The windbreak was three-sided and the fourth side was the building which shielded the air during the experiment.

2.1.6 Portable Emissions Monitoring System

The PEMS consists of a flow measurement system, sampling system for emissions, and a data acquisition system. The PEMS measured flue gas temperature and emissions of CO_2, CO, and PM. This measurement was used to quantify the reduction in harmful emissions from cooking stoves and to calculate various metrics. The emissions from the stove were collected into a steel hood. There was a blower attached to the top of the hood which blew out the fuel gas to the sampling duct. The sampling duct consisted of tubes which were used to measure the flow rate and emissions. A thermocouple measured the exhaust temperature. The emissions sample reached the analyzer through a sample line with the help of a suction pump. A pitot tube array was used to measure the flue gas velocity in the sampling duct, and by measuring velocity, temperature, and pressure, flue gas mass flow was determined. A separate thermocouple was used to measure the water temperature inside the pot.

To obtain an accurate PM measurement, particulate were collected on a filter and weighed gravimetrically. The gravimetric system consists of a particle separator, which is a cyclone that allows only particles equal or smaller to 2.5 micron meters in diameter to pass. The PM was collected in a filter paper. In this research the larger particles (greater than 2.5 microns) were not collected. Before the experiment, the filter paper was dried in a vacuum chamber for 12 hours using desiccant and then it was weighed using a microbalance as shown in Figure 2-5. After the experiment, the filter paper was wet because of evaporated water from the pot and combustion water vapor. It was again dried and weighed. The difference between the final and initial filter paper mass was the PM collected.

Figure 2-5: Filter paper being desiccated. Filter paper being weighed on microbalance.

2.1.7 Water Boiling Test

To measure the energy generated by the cookstove, a subset of the tests that comprise the WBT protocol was performed. The WBT measures repeatability of the test by measuring how much energy is transferred to boil the water. The WBT consists of three phases. The first phase is the cold-start, high-power test where the stove is at room temperature. A certain amount of pre-weighed wood was used to boil a pre-measured quantity of water. The second phase called the hot-start, high-power test starts immediately after the first phase. The second phase is similar to the first phase; the only difference is that the stove temperature is initially hot instead of at room temperature. And in the third phase, the water is simmering. In the third phase the experiment is started immediately after the second phase. Here, the water is simmered at just below boiling. For the third phase, the tester determines the right amount of wood to simmer the measured amount of water. This is to simulate the cooking of beans and legumes. During the

test, the cooking pot was uncovered as specified by the WBT protocol (Bailis, Ogle, MacCarty, & Still, 2006).

The WBT is usually used to compare different stoves but for this research, we were investigating the impact of fuel. Only the high-power, cold-start test was performed as emissions tend to be high during this phase, especially for large thermal mass stoves, and also thermal energy delivered to the cooking pot was not completely measured in the lower-power phase of the WBT (Jetter, et al., 2012).

2.2 **Measurements**

To calculate the performance parameters in the next chapter CO, CO_2, PM, temperature of flue gas and water, mass of wood, charcoal, water, and filter paper were being measured. The following paragraphs explain the measured values.

2.2.1 CO Concentration (ppm)

Carbon monoxide is a colorless, odorless, and tasteless toxic gas which is measured by a CO sensor. The PEMS included a CO sensor which is an electrochemical cell that produces a current proportional to the concentration of carbon monoxide. As shown in Figure 2-6, the electrochemical cell consists of a container, inside of which there is a working electrode, a counter electrode, and an electrolyte for ion conduction in between them. As seen in the Equation (2-1), when carbon monoxide comes in contact with working electrode, oxidation of CO gas will occur. On the working electrode, a chemical reaction occurs between CO gas and water molecules in the air to form CO_2, $2H^+$ and $2e^-$.

Working Reaction,

$$CO + H_2O \rightarrow CO_2 + 2H^+ + 2e^- \quad \textbf{(2-1)}$$

The generated electrons flow through the circuit to the counter electrode while the generated H+ ions flow through the ion conductor to the counter electrode. As shown in Equation (2-2), a reaction between H^+ ions and oxygen in the air will occur on the counter electrode to form H_2O.

Counter Reaction,

$$2H^+ + \frac{1}{2}O_2 + 2e^- \rightarrow H_2O \quad \textbf{(2-2)}$$

Without any of the cells components being consumed, the magnitude of the current flowing through the circuit is directly proportional to the concentration of CO. Therefore, the measurement of current flowing through the circuit is a basic gas sensor (CO sensor, 2013).

Net Reaction,

$$CO + \frac{1}{2}O_2 \rightarrow CO_2 \quad \textbf{(2-3)}$$

The electrochemical cell has a linear output to CO concentration, requires less power and has a longer lifetime than other technologies available on the market (CO detector, 2013). The sensor is calibrated with 100 ppm calibration gas and this calibration can be used to measure up to 1000 ppm of CO (Aprovecho, 2012). The stored measurement of the concentration of CO (ppm) was an instantaneous measurement that is written to a file every two seconds. The manufacturer has provided repeatability and resolution of the instrument, which is used to estimate the uncertainty. For more details regarding the uncertainty analysis, refer to Appendix A.

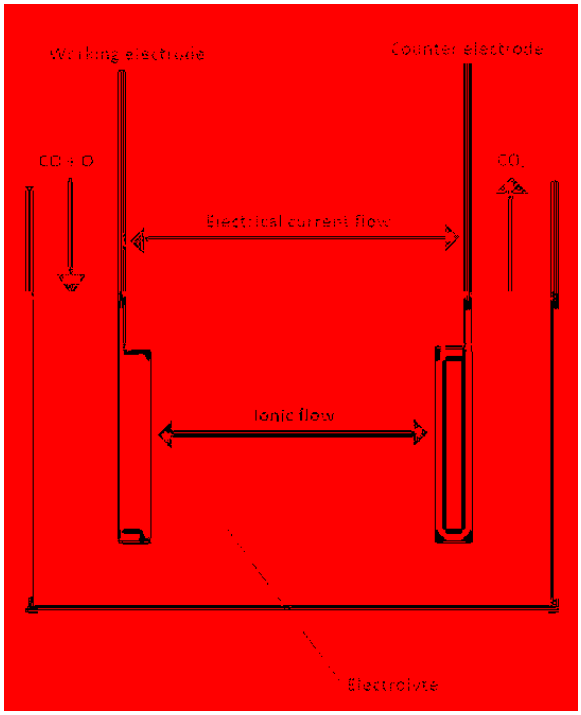

Figure 2-6: CO sensor - electrochemical cell

2.2.2 CO_2 Concentration (ppm)

The PEMS also includes a CO_2 sensor to measure the concentration of CO_2 in ppm in the exhaust stream. The actual measurement is the voltage output by the detector when the chamber in Figure 2-7 contains CO_2 and when it does not contain CO_2. The CO_2 concentration measurement is based on the absorption of infrared radiation passing through the NDIR cell shown in Figure 2-7. The sensor consists of an infrared source, a light tube, an optical filter, and an infrared detector. Exhaust gases flow steadily through the cell, and attenuation of the radiation emitted by the source due to absorption by CO_2 molecules is related to the concentration of CO_2 based on the following analysis.

Assuming the exhaust stream may be modeled as a cold (non-emitting), non-scattering medium at the wavelengths of interest, the spectral intensity incident on the detector is obtained by solving the simplified radiative transfer equation (Howell, et al., 2010).

$$\frac{dI_\lambda}{ds} = \kappa_\lambda I_\lambda \tag{2-4}$$

subject to the condition

$$I_\lambda(0) = I_{\lambda,o} \tag{2-5}$$

where $I_{\lambda,o}$ is the spectral intensity emitted by a light emitting diode (LED).

Proper selection of the LED insures it emits radiation in a narrow spectral band in which CO_2 is strongly absorbing and which does not over overlap the spectra of other radiatively participating species such as CO and H_2O.

Assuming CO_2 is the only radiatively participating species, the spectral absorption coefficient is equal to the product of the specific spectral absorption cross section of CO_2 and the volumetric concentration of CO_2 (Howell, et al., 2010).

$$\kappa_\lambda = \beta_\lambda C_{CO_2} \tag{2-6}$$

where β_λ (m^2/kmol) is the specific spectral absorption cross section of CO_2 on a molar basis.

Assuming the concentration of CO_2 is uniform along the path between the LED and the detector is uniform, solving Equation (2-4) subject to Equations (2-5) and (2-6) gives an expression for the concentration of CO_2.

$$C_{CO_2} = \frac{\ln\left(\frac{I_{\lambda,0}}{I_{\lambda,L}}\right)}{\beta_\lambda L} \tag{2-7}$$

where L is the distance between the LED and the sensor.

If the detector responds linearly to the incident intensity, the voltage reading obtained when the NDIR cell does not contain any CO_2 is given by

$$V_o = \frac{I_{\lambda,o}}{S_\lambda} \tag{2-8}$$

where S_λ is the spectral sensitivity of the detector. Similarly, the voltage reading obtained when the NDIR cell contains an unknown amount of CO_2 is given by

$$V = \frac{I_\lambda}{S_\lambda} \tag{2-9}$$

Substitution of Equations (2-8) and (2-9) into Equation (2-7) gives

$$C_{CO_2} = \frac{\ln\left(\frac{V_0}{V}\right)}{\beta_\lambda L} \tag{2-10}$$

The final step required is to determine the spectral absorption volume of the NDIR cell, which is the product of β_λ and the average path length between the source and the detector in the NDIR cell, L. The product of $\beta_\lambda L$ may be obtained using a calibration gas with a known concentration of CO_2. Defining V_{cal} as the voltage reading obtained when the NDIR cell contains a gas with a known concentration of CO_2, which is equal to C_{cal} and rearranging Equation (2-10) gives

$$\beta_\lambda L = \frac{\ln\left(\frac{V_o}{V_{cal}}\right)}{C_{cal}} \tag{2-11}$$

Substituting Equation (2-11) into Equation (2-10) gives the final relationship between the concentration of CO_2 in the NDIR and measured voltages.

$$C_{CO_2} = C_{cal} \frac{\ln\left(\frac{V}{V_o}\right)}{\ln\left(\frac{V_{cal}}{V_o}\right)} \quad \textbf{(2-12)}$$

In summary, V_o is the voltage measured when the chamber is filled with gas containing no CO_2, which is referred to as the zero gas and V is the voltage measured when the chamber is filled with the target gas. Nitrogen is usually used as the zero gas since nitrogen has no IR absorption. The second calibration, known as span calibration, is needed to solve the second unknown parameter, $\beta_\lambda L$. In the span calibration, the optical path L is exposed to a gas mixture with a known concentration.

For the span calibration, the CO_2 sensor is calibrated using 3000 ppm span gas (Aprovecho, 2012). The sensor outputs a reading every 2 seconds. All the CO_2 graphs are available in Appendix B. The manufacturer has provided accuracy and resolution of the instrument that is used to estimate the uncertainty. For more details regarding the uncertainty analysis, refer to Appendix A.

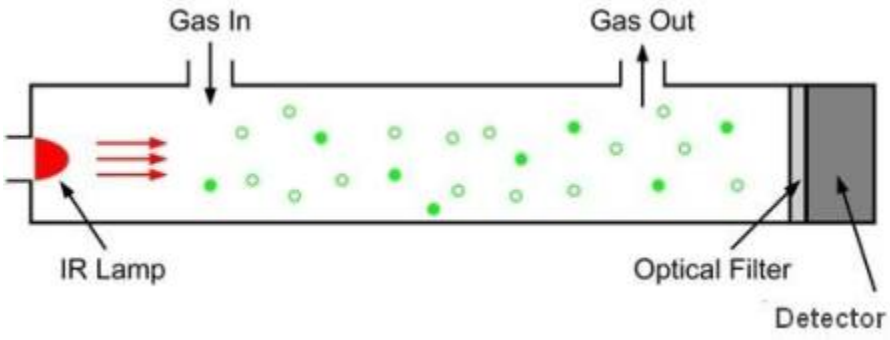

Figure-2-7: Non-dispersive infrared (NDIR) CO_2 sensor

2.2.3 Particulate Matter (mg/m^3)

Particulate matter (PM) consists of tiny solid air pollutants ranging in size and composition. The PM measured in the tests, PM 2.5, has diameters than 2.5 μm. PM 2.5 is harmful as it is inhaled easily into the lungs. In addition to sensors that detect the concentrations of CO and CO_2, the PEMS includes a system to measure the concentration of PM. The PM concentration measurement system is comprised of two components - a gravimetric system and a scattering photometer.

The gravimetric system uses a cyclone separator to channel the PM 2.5 through as system that collects the particle in filter paper. Measurement of the weight of the filter paper before and after the tests provides an estimate of the total mass of PM emitted during the test.

The scattering photometer is illustrated in Figure 2-8. Radiation scattered from the red laser beam is detected by the photometer as shown in Figure 2-8. The laser shines at a wavelength of 635 nm (Aprovecho, 2012) and a photo sensor diode acts as a receiver. When the chamber is clear the laser shines through and returns very little signal to the receiver. However, when smoke is in the sensing chamber, radiation is scattered by particles suspended in the smoke in the direction of the receiver. The scattered radiation that is incident on the detector causes the detector to produce a voltage that is proportional to the irradiation incident on the detector. Therefore, measurement of the signal from the detector can be used to infer the irradiation incident on the detector. This mechanism is based upon the 'static light scattering', a technique that measures the average molecular weight of the particle. Scattering data is usually represented by excess Rayleigh ratio, Equation (2-16) (Zimm, 1948). In Figure 2-8, I_θ is the scattered light intensity of the incident radiation, measured by the detector at angle θ.

$$I(\theta) = \frac{I_O N \Delta V}{(kr)^2} i(\theta) \quad \textbf{(2-13)}$$

where I_o is the incident intensity from the laser beam, N number of identical particles/molecules per ml illuminated by the laser beam, ΔV is the illuminated scattering volume from which scattered light reaches the detector, r is the distance from the point of scattering, and $i(\theta)$ is the scattering function of a single particle.

$$k = \frac{2\pi n_O}{\lambda_O} \quad \textbf{(2-14)}$$

where n_o is the refractive index of the suspending fluid and λ_o is the vacuum wavelength of the incident light, 635 nm (Aprovecho, 2012). The excess Rayleigh ratio, $R(\theta)$ is given by

$$R(\theta) = \frac{I(\theta) r^2}{I_O \Delta V} \quad \textbf{(2-15)}$$

Substituting Equation (2-13) in Equation (2-15) to get Equation (2-16)

$$R(\theta) = \frac{N i(\theta)}{k^2} \quad \textbf{(2-16)}$$

When the intensity $I(\theta)$ is received at the detector, the photo detecting circuit uses a photo detecting device to produce a voltage. The detector includes a timing generator for generating a timing signal in every 2 seconds. In the data analysis process, estimate of the total mass of the PM obtained from the gravimetric system is needed to interpret the measurements from the scattering PM sensor. Please refer to Appendix D for detailed description.

Although these types of particle counters are beneficial in providing real-time information they have some limitations. For example, some particles are more reflective than others. Also, the suspended particles are non-spherical, so their orientation will determine the

amount of light being scattered (Particle Measuring Systems, 2011). The particle size and composition are used to calculate mass, creating larger uncertainty.

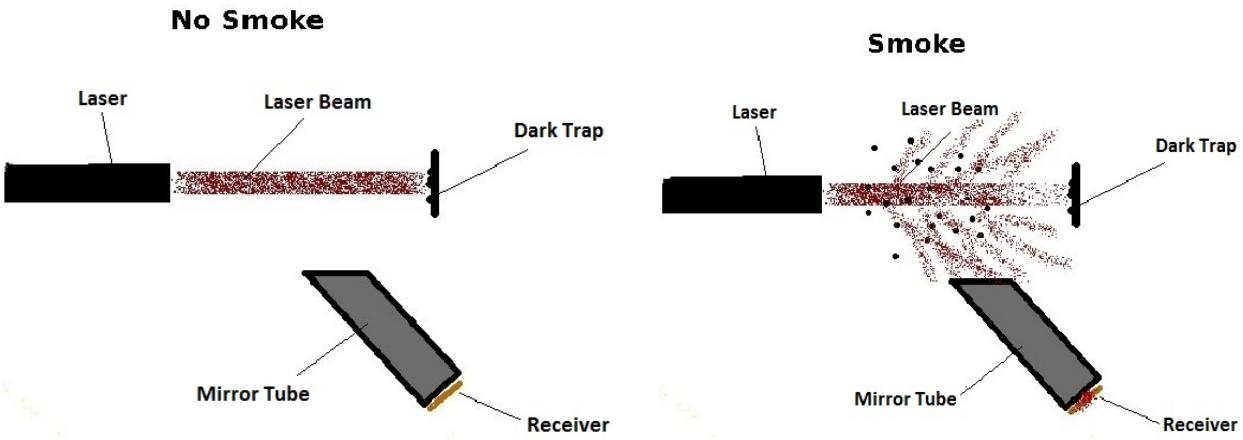

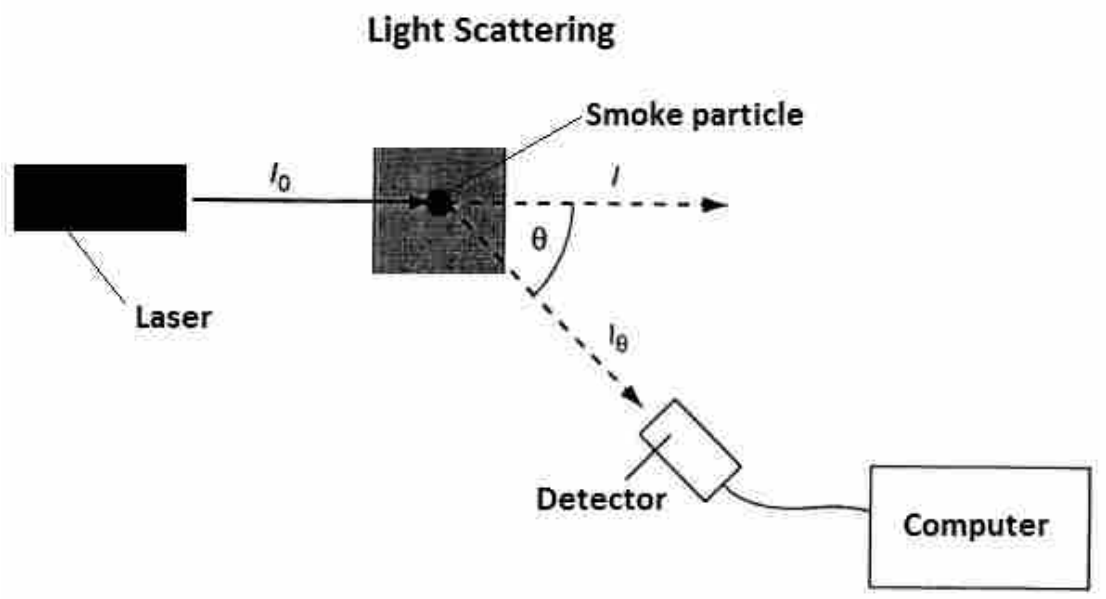

Figure 2-8: PM sensor with and without smoke

2.2.4 Temperature (^{o}C)

The sampling duct consists of a thermocouple to measure the exhaust temperature which is later used to calculate flue gas mass flow. A separate thermocouple was used to measure the temperature of the water inside the pot. These thermocouples measure the temperatures continuously. The locations of these thermocouples are shown in Figure 2-9.

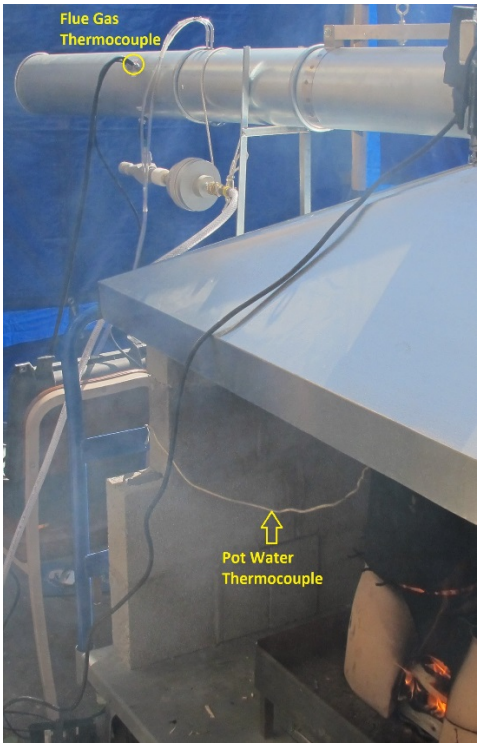

Figure 2-9: Location of flue gas thermocouple and pot water thermocouple

2.2.5 Scale (g)

A digital scale was used to weigh the mass of wood, charcoal, and water while a micro scale was used to weigh the mass of filter paper. The instrument specification was used from the

manufacturer to estimate the uncertainty. For more details regarding the uncertainty analysis, refer to Appendix A.

2.3 **Methods**

The filter paper was placed in a desiccant jar overnight by placing it with some desiccant inside of a sealed container. The mass of the filter paper is measured on a microbalance. Put the filter paper on the filter paper chamber, rough end facing towards the flow. The stove is rolled out of the building for safety purposes and surrounded by the windbreak. The magnehelic sensor should be adjusted so that it points at zero. Now the PEMS is turned on and between one to four minutes the blower is turned on. The blower speed can be changed to make the magnehelic sensor around 0.4. On the test data sheet, record the full flow calibration reading of the magnehelic pressure gauge. The background period starts after 4 minutes of the PEMS on. The background period should be at least ten minutes. During the background period the pre-weighed wood (around 1200 grams) is built in the stove. About a foot long paper towel is used as a fire-starting material for each test. For all the tests three pots were used. When the practice tests were conducted with one or two pots, the fire would shoot up through open hole. The three pots with pre-weighed water are placed on the stove. The flat base stainless steel cooking pots were used for the experiment. The dimensions of the pots are listed in Table 2-2. Also pots 1, 2, and 3 contained around 1400, 1400, and 400 milliliters of water. The initial temperature of water from each pot was recorded. After ignition the door is not opened until the end of the test. At the time of ignition, the gravimetric pump was turned on which began collection on the filter paper. The test runs for about 20 minutes. The 1200 grams of wood almost burns completely around the end of 20 minutes. At the end of the test the PEMS, gravimetric pump, and blower is turned off. Also the water temperature from each pot is recorded again. The charcoal is collected in the charcoal

container. Sheet metal is used to cover the charcoal, cutting the oxygen supply to discontinue the process of combustion. After the test the PEMS is run by itself with clean air for about 10 minutes to clear the gases out of the sensor boxes.

For biomass with a fan test, the fan is turned on at the ignition. For biomass co-fired with biogas test, the biogas is supplied at the time of ignition. There are two burners located underneath the fire to provide the biogas at different flow rates. Figure 2-10 shows the regulator and the flow meter – (Matheson 605), to control the flow of simulated biogas. Figure 2-10 (right) shows the gas pipe being connected to the two burners for co-firing. After the WBT, the charcoal is weighed. The ashes are meticulously collected in a charcoal container using a brush to be as accurate as possible. The water in the pots is again weighed to know how much water has vaporized. The filter paper is again desiccated overnight and weighed in microbalance the next day.

For three repeated tests, the fire was videotaped and a stopwatch was started at the time it was ignited. In order to timestamp the video, the stopwatch was in front of the video camera at regular intervals. This was done in order to document the variability in emissions for repeated tests.

Figure 2-10: Biogas tank with regulator and flow meter. Biogas connected to burners.

3 CHAPTER 3: EXPERIMENTAL ANALYSIS AND COMPARISONS

Chapter 2 gives an overview of the experiment setup and the test outputs. Also, Chapter 2 explains the measured values used to calculate performance parameter in this chapter. The objective of this chapter is to investigate results to determine the impact of co-firing biogas and using air as an oxidizer during the process of combustion of biomass. This requires a comparison of the results between the tests listed in Table 3-1. The results are also explained in detail. Measurement of simple biomass combustion is used as the base-case for comparison in this study. The comparisons are done by using the measurements obtained by the processes explained in the previous chapter. Chapter 3 also talks about variability in emissions over time. The amount of emissions are recorded and graphed for comparisons. Tests are performed in triplicate and results were reported as averages with errors involving uncertainty analysis and variability (Appendix A).

Table 3-1: List of Tests Being Compared

Test Number	*Type*
1	Biomass alone
2	Biomass co-fired with Biogas 10 %
3	Biomass co-fired with Biogas 25 %
4	Biomass co-fired with Biogas 50 %

Table 3-1, continued

Test Number	*Type*
5	Biomass with Fan
6	Biomass co-fired with Biogas 10 % and Fan
7	Biomass co-fired with Biogas 25 % and Fan
8	Biomass co-fired with Biogas 50 % and Fan

3.1 **Performance Parameter**

The literature review and objective sections of Chapter 1 describe the impact of co-firing on combustion efficiency, as well as its impact on various emission components, such as PIC and PM. In this chapter, combustion efficiency and emission components generated from the test are defined and discussed as performance parameter.

Combustion efficiency, thermal efficiency, and fuel consumption rate were calculated using a part of the WBT protocol. For each WBT test, the emissions (CO, CO2, and PM) were simultaneously calculated using the PEMS. Emissions were calculated on the basis of fuel wood consumed and cooking energy delivered. Jetter, et al., 2012, recommend calculating on the basis of cooking energy delivered. According to the WBT specification, the lower heating value of fuel was used (Bailis, Ogle, MacCarty, & Still, 2006).

Table 3-2: Nomenclature for Measurement Variables

Variable	*Defined As*	*Units*
U	Internal Energy	J
T	Time	S
$\dot{Q}_P$	Rate of heat utilized to heat the water	W
h_e	Enthalpy exiting the control system	J/kg

Table 3-2, continued

Variable	*Defined As*	*Units*
h_{fg}	Enthalpy of vaporization	J/kg
η_{th}	Thermal efficiency	
C	Specific heat capacity of water	*kJ/kg.K*
m_i	Mass of liquid water before test	*G*
m_f	Mass of liquid water after test	*G*
T_f	Final water temperature of each pot	^oC
T_i	Initial water temperature of each pot	^oC
ΔT	T_f - T_i	^oC
h_{fg}	Enthalpy of vaporization	*J/g*
m_v	Mass of vaporized water	*G*
m_w	Mass of dry wood consumed	*G*
LHV	Lower heating value of fuel	*kJ/kg.K*
SC	Specific fuel consumption rate	
m_P	Mass of empty pot	*G*
m_{Pf}	Mass of pot with water after test	*G*
SEM_{CO}	Specific CO emissions per energy	*g/MJ*
SEM_{CO2}	Specific CO_2 emissions per energy	*g/MJ*
SEM_{PM}	Specific PM emissions per energy	*mg/MJ*
η_C	Combustion efficiency	
m_{CO}	Total mass of CO emissions	*G*
m_{CO2}	Total mass of CO_2 emissions	*G*
m_{PM}	Total mass of PM emissions	*G*
P	Atmospheric pressure	Pa
V	Volume of the water in the pot	m^3
$\dot{m}_e$	Mass flow rate exiting the control system	kg/s

3.1.1 Thermal Efficiency

The thermal efficiency is defined as the ratio of heat utilized while heating the water to the total heat produced from the fuel during combustion (Ahuja, Joshi, Smith, & Venkataraman, 1987). The heat utilized is the sum of the change in the internal energy of the water in the pot and the enthalpy of vaporization of evaporated water. A higher thermal efficiency means that a larger fraction of fuel energy is transferred to heat the cooking pot and thus less wood is consumed. Thermocouples were used to measure changes in water temperature and a scale was used to measure the mass of wood and water. The equation to measure the thermal efficiency is derived by taking the water in the pot as the control volume. In Figure 3-1 dashed lines represent the control volume which is the water inside the pot. Equation (3-1) comes from the energy balance of the control volume. The changes in kinetic and potential energies are neglected.

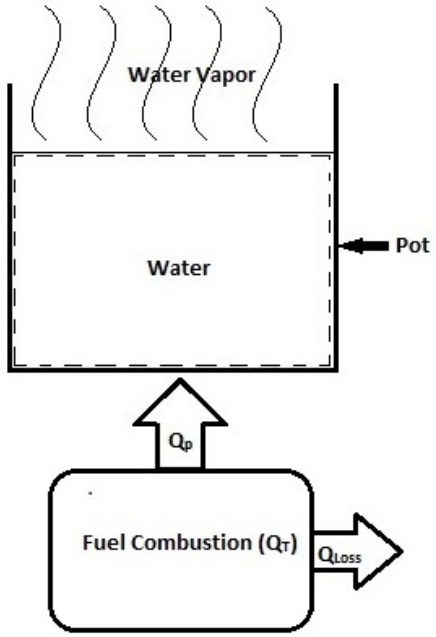

Figure 3-1: Water is being heated in a pot. Dashed lines represent the control volume.

$$\frac{dU}{dt} = \dot{Q}_p - P\frac{dV}{dt} - \dot{m}_e h_e \quad \textbf{(3-1)}$$

$$\dot{Q}_p = \frac{dU}{dt} + P\frac{dV}{dt} + \dot{m}_e h_e \quad \textbf{(3-2)}$$

Enthalpy is the sum of internal energy and product of volume and pressure applied to the volume. Also the change in pressure is zero.

$$\frac{dH}{dt} = \frac{d(U+PV)}{dt} = \frac{dU}{dt} + P\frac{dV}{dt} \quad \textbf{(3-3)}$$

Equation (3-3) is substituted in Equation (3-2) to get Equation (3-4). Equation (3-4) is also integrated from initial time to final time. t_{sat} is the time at which the liquid is heated to a saturated liquid.

$$\int_0^{t_f} \dot{Q}_p dt = \int_0^{t_{sat}} \frac{dH}{dt} dt + \int_{t_{sat}}^{t_f} \frac{dH}{dt} dt + \int_0^{t_f} \dot{m}_e h_e \quad \textbf{(3-4)}$$

The first right hand side expression of Equation (3-4) is expanded. From the initial time to t_{sat} the initial mass of the water does not change. Hence it is taken out of the integral in Equation (3-5) as a constant.

$$\int_0^{t_{sat}} \frac{dH}{dt} dt = \int_0^{t_{sat}} \frac{d(m_i c_p T)}{dt} dt = m_i c_p \Delta T \quad \textbf{(3-5)}$$

$$\Delta T = T_{sat} - T_i \quad \textbf{(3-6)}$$

The second right hand side expression of Equation (3-4) is expanded. Since the pressure is constant:

$$h = h_f = \text{constant} \quad \textbf{(3-7)}$$

$$\int_{t_{sat}}^{t_f} \frac{dH}{dt} dt = \int_{t_{sat}}^{t_f} \frac{d(mh)}{dt} dt = h_f \int_{t_{sat}}^{t_f} \frac{dm}{dt} dt = h_f \Delta m \quad \textbf{(3-8)}$$

It is approximated that evaporation of water is negligible until the water is heated to the saturation temperature. Therefore, the initial mass of the water does not change from the initial time to t_{sat}. Thus,

$$\Delta m = m_f - m_i \quad \textbf{(3-9)}$$

Now, applying conservation of mass to the control volume

$$\frac{dm}{dt} = -\dot{m}_e \quad \textbf{(3-10)}$$

Substituting Equation (3-10) to the last term of Equation (3-4)

$$h_e = h_g = \text{constant} \quad \textbf{(3-11)}$$

$$\int_0^{t_f} \dot{m}_e h_e dt = \int_0^{t_f} -\frac{dm}{dt} h_g dt = -h_g \int_0^{t_f} \frac{dm}{dt} dt = -h_g \Delta m \quad \textbf{(3-12)}$$

Since,

$$\Delta m = m_f - m_i \quad \textbf{(3-13)}$$

m_v = mass of water vaporized

$$m_v = m_i - m_f = -\Delta m \quad \textbf{(3-14)}$$

Substituting Equation (3-12) to (3-4)

$$Q_p = m_i c \Delta T + h_f \Delta m - h_g \Delta m \quad \textbf{(3-15)}$$

$$Q_p = m_i c \Delta T - \Delta m (h_g - h_f) \quad \textbf{(3-16)}$$

$$Q_p = m_i c \Delta T + m_v h_{fg} \quad \textbf{(3-17)}$$

Therefore heat utilized to heat the water is the sum of sensible heat and latent heat. The woods used were southern pine with LHV of 18,600 KJ/kg.

$$\eta_{th} = \frac{\text{heat utilized to heat the water } (Q_p)}{\text{total heat produced from the fuel during combustion } (Q_T)} \quad \textbf{(3-18)}$$

$$Q_T = m_w \cdot LHV \quad \textbf{(3-19)}$$

$$\eta_{th} = \frac{m_i \cdot c \cdot \Delta T + h_{fg} \cdot m_v}{m_w \cdot LHV} \quad \textbf{(3-20)}$$

3.1.2 Specific Fuel Consumption Rate

The specific fuel consumption rate is defined as the mass of fuel consumed per liter of water remaining in the pot at the completion of the test (Jetter, et al., 2012). Specific fuel consumption is used to calculate the fuel used to perform a task and the time required to do so. Lower specific fuel consumption means that the water boils quickly which saves time to perform a cooking task. When the water boils quickly, there is less time for water to evaporate and the amount of remaining water will be greater which lowers the specific fuel consumption. The temperature corrected terms help to compare tests that start with different initial temperatures of water. Bailis, Ogle, MacCarty, & Still, 2006, define specific fuel consumption rater as “the fuelwood required to produce a unit output”. But the fuel wood required can be calculated by weighing the mass of wood burned. A different name such as “Fuel used and time required performing a task” is recommended. Also the thermal efficiency is not related to specific fuel consumption. For lower specific fuel consumption where water boils quickly the thermal efficiency can be higher. But for higher specific fuel consumption where water boils slowly the

thermal efficiency can still be higher because the heat was used to evaporate the water, making the amount of water left in the pot smaller when the water reached the boiling point.

$$SC = \frac{m_w}{m_{Pf} - m_P} \times \frac{T_{Sat} - T_i}{T_f - T_i} \quad \textbf{(3-21)}$$

$\frac{T_{Sat} - T_i}{T_f - T_i}$ = temperature corrected terms

3.1.3 Specific Emission of Carbon Monoxide

Specific CO emission is the emission of CO (g) per energy delivered to the pot (J) (Bailis, Ogle, MacCarty, & Still, 2006). All the specific emission performance metrics are calculated as emissions per energy delivered to the cooking pot instead of emissions per energy released from the fuel burned. This is because biomass cookstoves have lower thermal efficiency than liquid or gas cookstoves. Thus the emission of PIC will be higher if it is calculated per energy delivered to the cooking pot (Smith, et al., 2000).

$$SEM_{CO} = \frac{CO\,emissions(g)}{Energy\,delivered\,to\,pot(J)} = \frac{m_{CO}}{\eta_{th} \cdot m_w \cdot LHV} \quad \textbf{(3-22)}$$

3.1.4 Specific Emission of Carbon Dioxide

Specific CO_2 emission is the emission of CO_2 (g) per energy delivered to the pot (J) (Bailis, Ogle, MacCarty, & Still, 2006). It is recommended that pollutant emissions should be measured per cooking energy delivered to allow valid comparisons between the fuels, thus creating the fundamental desired output of cooking energy (Jetter, et al., 2012). For the tests performed there will be a direct comparison between the fuels, such as biomass burned alone and biomass co-fired with different amounts of biogas.

$$SEM_{CO_2} = \frac{CO_2\ emissions(g)}{Energy\ delivered\ to\ pot(J)} = \frac{m_{CO_2}}{\eta_{th} \cdot m_w \cdot LHV} \quad \textbf{(3-23)}$$

3.1.5 Specific Emission of Particulate Matter

Specific PM emission is the emission of CO_2 (g) per energy delivered to the pot (J) (Bailis, Ogle, MacCarty, & Still, 2006).

$$SEM_{PM} = \frac{PM\ emissions(g)}{Energy\ delivered\ to\ pot(J)} = \frac{m_{PM}}{\eta_{th} \cdot m_w \cdot LHV} \quad \textbf{(3-24)}$$

3.1.6 Modified Combustion Efficiency

The combustion efficiency is the ratio of heat produced in a combustion process to the heat that would be released in complete combustion, or the amount of chemical energy in fuel converted to heat (Jetter, et al., 2012). Heat produced in a combustion process is required to compute the combustion efficiency. Device like bomb calorimeter is used to measure the heat of combustion which makes the calculation of combustion efficiency harder. But the measured CO and CO_2 can be used to calculate the MCE. Linear regression of combustion efficiency showed excellent agreement with MCE as CO and CO_2 accounted for almost all emitted carbon species by mass. MCE is a reasonable substitute for true combustion efficiency (Johnson, Edwards, Berrueta, & Masera, 2010). MCE is defined as

$$\eta_C = \left(\frac{CO_2}{CO_2 + CO} \right) \times 100\% \quad \textbf{(3-25)}$$

MCE is also related to thermal efficiency. Thermal efficiency is the product of HTE and MCE. HTE is equal to the amount of heat released during combustion that is actually transferred to perform the cooking task. The harmful effects on health due to emissions of pollutants are a strong function of MCE (Jetter, et al., 2012).

3.2 **Results**

The results from the experiment are discussed into two categories; time resolved results and integrated results. Time resolved results show the behavior of emission in the process of combustion by giving real time information of CO and PM emissions for all the repeated tests. It is also useful to integrate the time resolved results to obtain measurement of the total emissions to know cumulative emission during a cooking task, which are presented as integrated results. The graphs in this section show variations for different tests and give the overview of the output of the experiments.

3.2.1 Time Resolved Measurements

All the different tests listed in Table 3-1 were repeated three times. Figures 3-2 to 3-25 are the plots of emissions (PM, CO and CO_2) with respect to the burn time for all the tests. Each plot has three graphs for the repeated tests. The CO versus time plot the bands represent the uncertainty in the measurements based on manufacture specifications. For PM versus time the uncertainty estimate based on the information available from the instrument manufacturer is negligible (Resolution: 15 ug/m3), and these are not shown in the plot. The time resolved measurement of PM emission is recorded through a scattering photometer sensor. The sensor uses the concentration provided by manufacturer which is obtained from a specific test and stove (Aprovecho, 2012). The given concentration can be used to calculate the total PM but if the stove or fuel is different from the ones used by manufacturer then the PM calculation is not accurate (Jetter, et al., 2012). To mitigate this inaccuracy it is necessary to calibrate and the calibration is done by scaling the gravimetric concentration which is specific for a test. Appendix D shows the detailed calculation of calibration.

When biomass was burned alone, the time resolved measurements show that concentrations of PM and CO rise steadily from the time of ignition to 200 seconds. Both PM and CO concentrations are relatively flat between 200 and 600 seconds and drop off after 600 seconds. PM concentration decreases as fire burns out, but CO concentration increases. As shown in Figure 3-2, during Test 1, the PM concentration spikes between approximately 490 – 510 seconds.

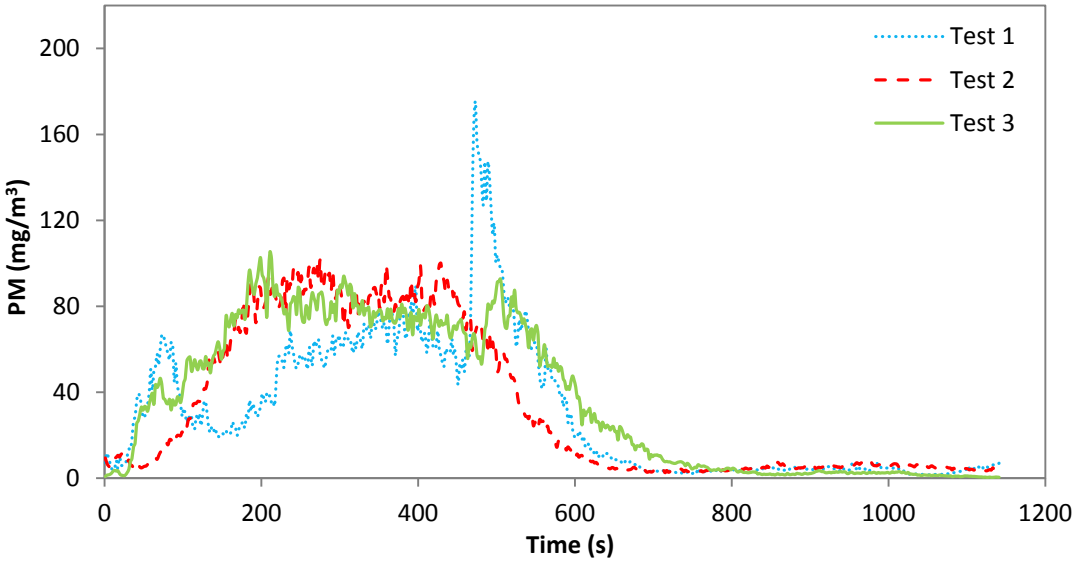

Figure 3-2: PM versus time for biomass burned alone

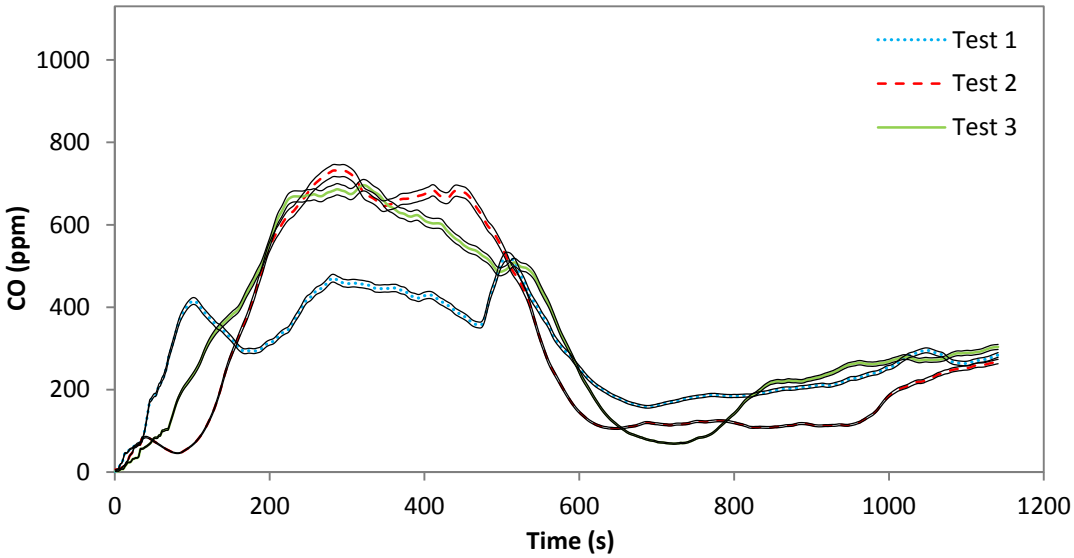

Figure 3-3: CO versus time for biomass burned alone

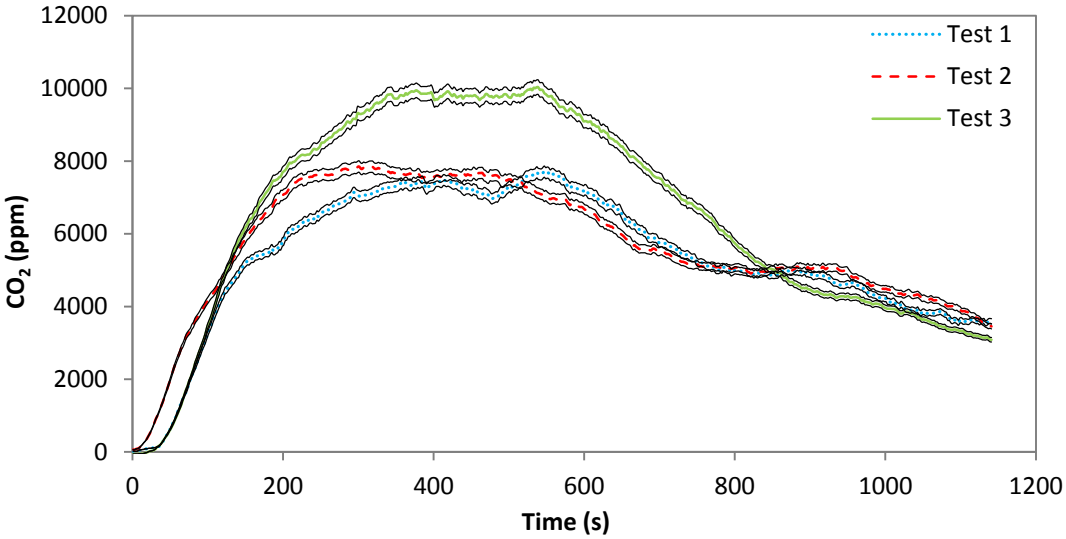

Figure 3-4: CO_2 versus time for biomass burned alone

For biomass co-fired with 10% biogas, the time resolved measurements show that both PM and CO spike after the ignition and fluctuate during the test. When the flame is nearing the end, the CO concentration starts to rise but PM concentration continues to lessen. In Figure 3-5,

the PM concentration for the repeated tests does not show uniform trend. It can be observed that the Test 1 is very different from the Tests 2 and 3. After around 600 seconds, the concentration of PM for all the tests continues to diminish. For the Test 3, the PM concentration increases to around 1050 seconds and decreases again. In Figure 3-6, CO concentration rises steadily from the time of ignition to 200 seconds. The CO concentration remains relatively flat between 200 and 550 seconds and drops off after 550 seconds. Between the 200 and 550 seconds, the level of CO is different for all the repeated tests. After 1000 seconds, the CO can be observed to rise again to about 200 ppm.

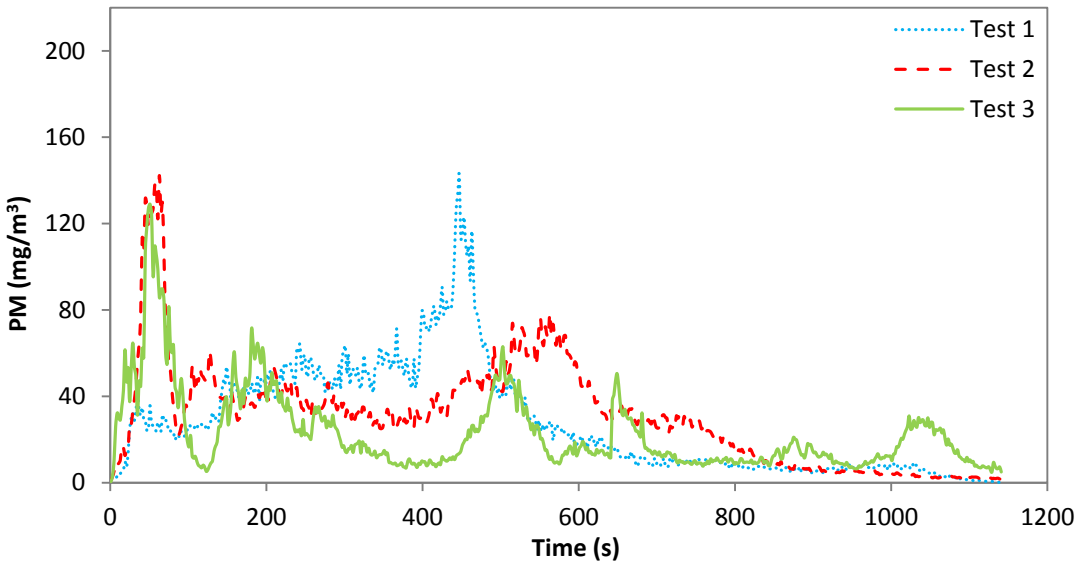

Figure 3-5: PM versus time for biomass co-fired with 10% biogas

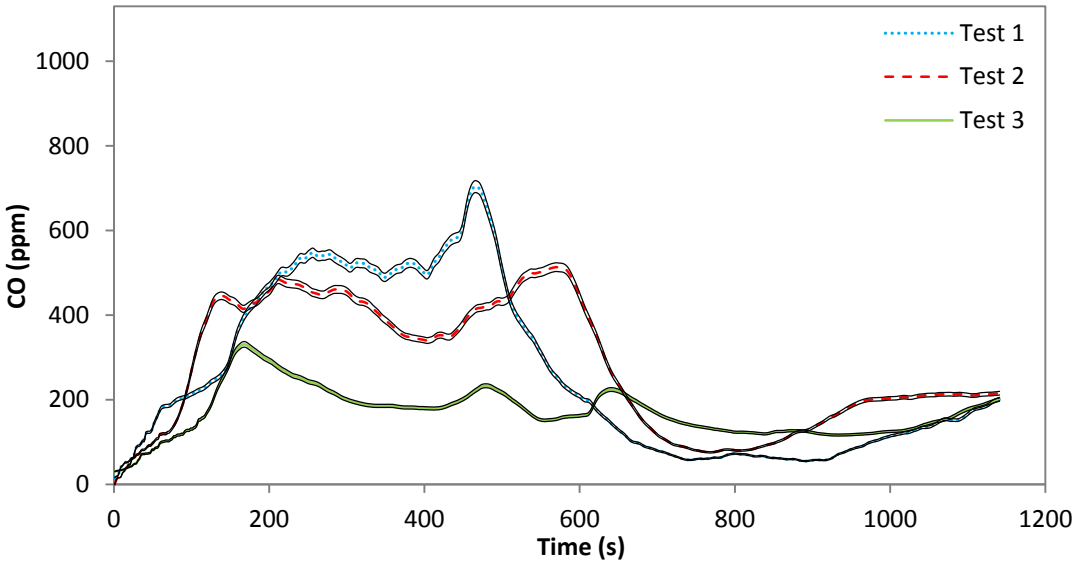

Figure 3-6: CO versus time for biomass co-fired with 10% biogas

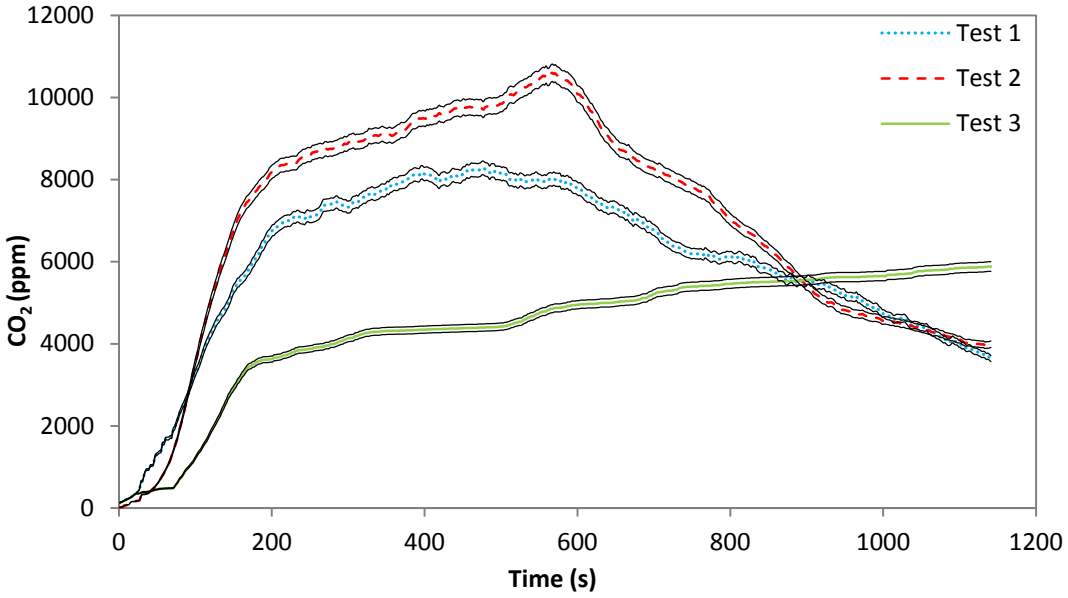

Figure 3-7: CO_2 versus time for biomass co-fired with 10% biogas

For biomass co-fired with 25% biogas, there is a lot of variability in PM for the entire repeated tests as seen in Figure 3-8. The PM concentration continues to diminish after around 600 seconds. At around 750 seconds, PM concentration for the Test 3 follows a different trend

from the remaining two tests. It slightly rises and drops off again. In Figure 3-9, CO concentration rises rapidly from the time of ignition. The repeated tests are different from each other. When combustion nears the end, CO concentration for Tests 1 and 3 rises but CO concentration for Test 2 does not.

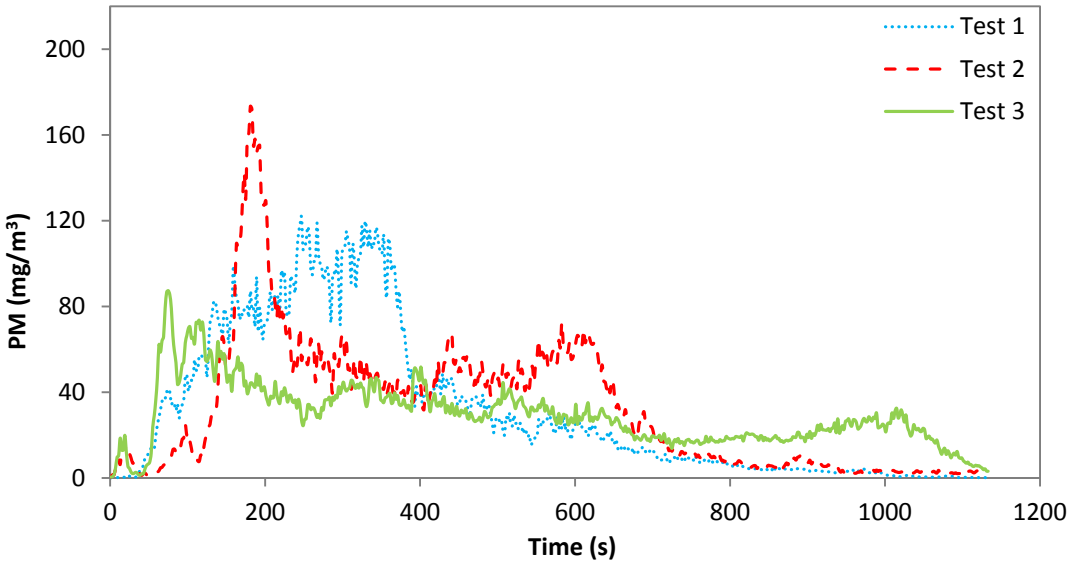

Figure 3-8: PM versus time for biomass co-fired with 25% biogas

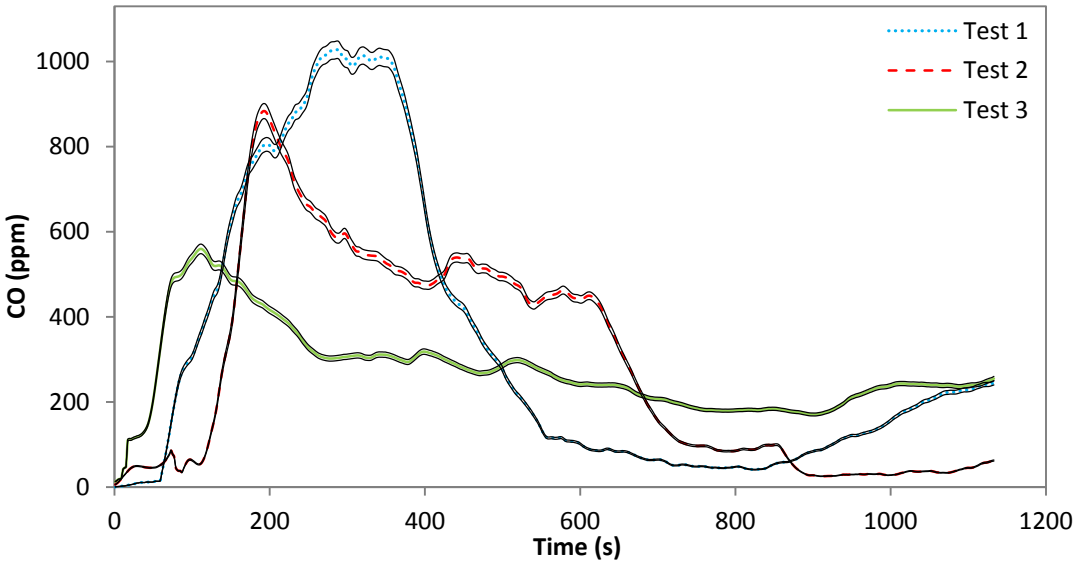

Figure 3-9: CO versus time for biomass co-fired with 25% biogas

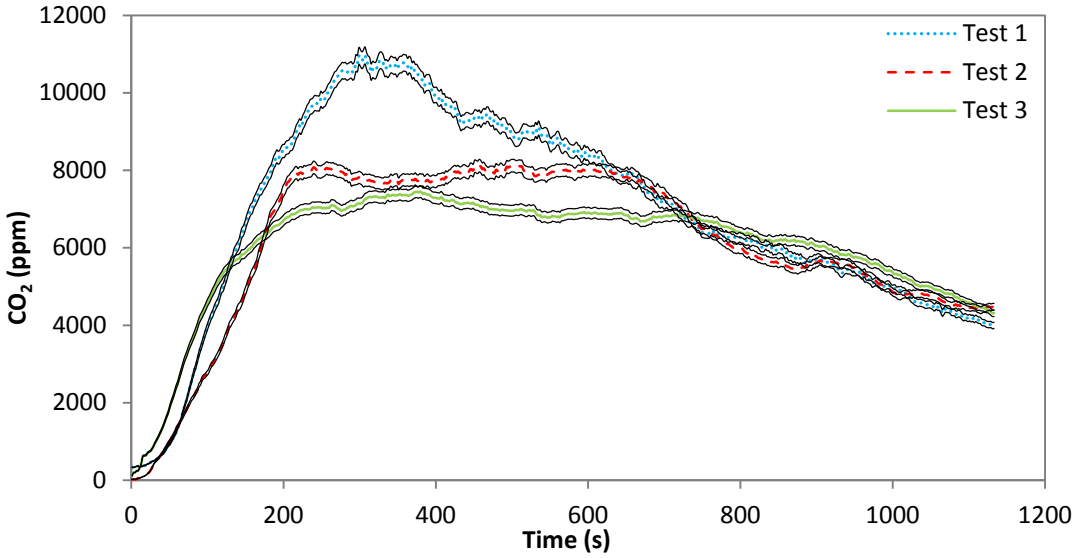

Figure 3-10: CO_2 versus time for biomass co-fired with 25% biogas

For biogas co-fired with 50% biogas, PM concentration rises rapidly from the time of ignition for Tests 2 and 3, as seen in Figure 3-11. For Test 1, PM concentration rises rapidly, but only after 100 seconds from the ignition. The PM concentration for Test 1 is also the highest

around 200 mg/m^3 in comparison to other two repeated tests. It is at its peak at around 250 seconds and drops rapidly from 250 seconds to 400 seconds. Then it again rises till 600 seconds and diminishes. The PM concentration for Tests 2 and 3 continue to diminish after 500 seconds. In Figure 3-12, CO concentrations for repeated tests are highly variable. However, interestingly, Test 1 has a similar trend for both CO and PM concentrations. Both PM and CO take about 100 seconds to rise after the ignition and both rise rapidly till 250 seconds. As observed in other tests, CO concentration starts to rise but PM concentrations continue to diminish as combustion nears completion. PM and CO concentrations for Test 2 also complement each other.

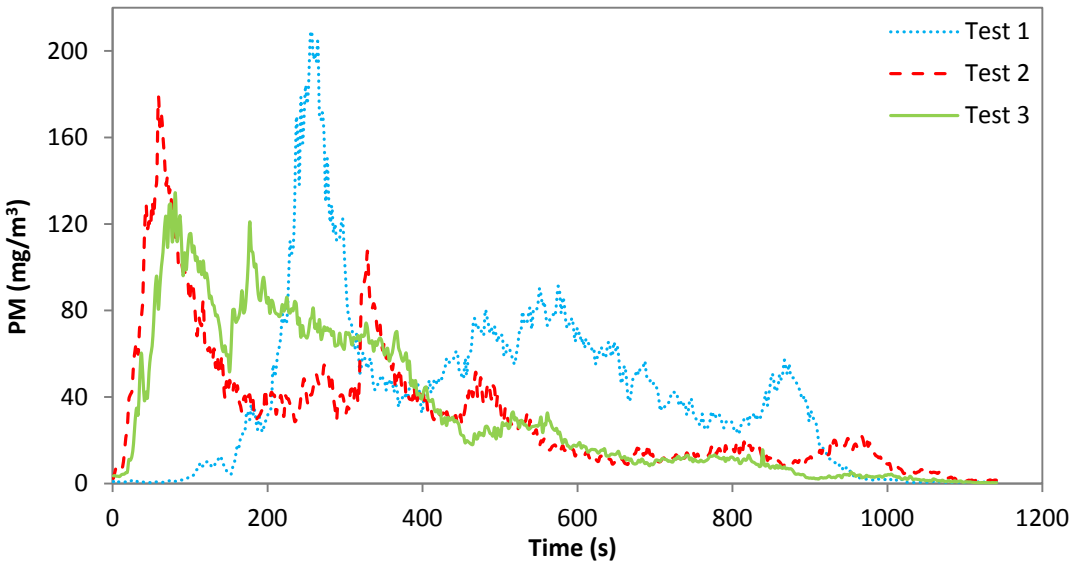

Figure 3-11: PM versus time for biomass co-fired with 50% biogas

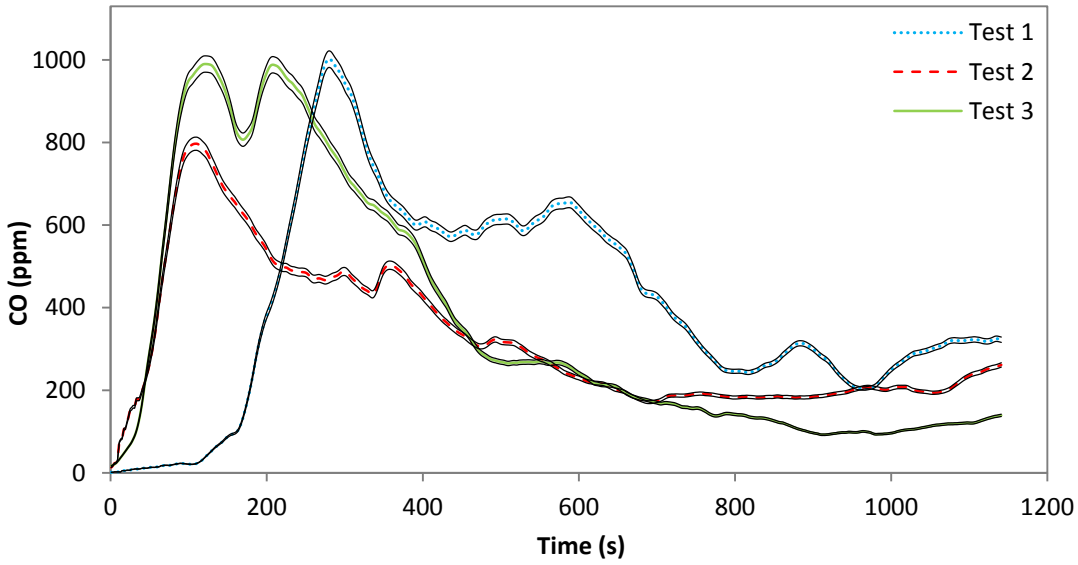

Figure 3-12: CO versus time for biomass co-fired with 50% biogas

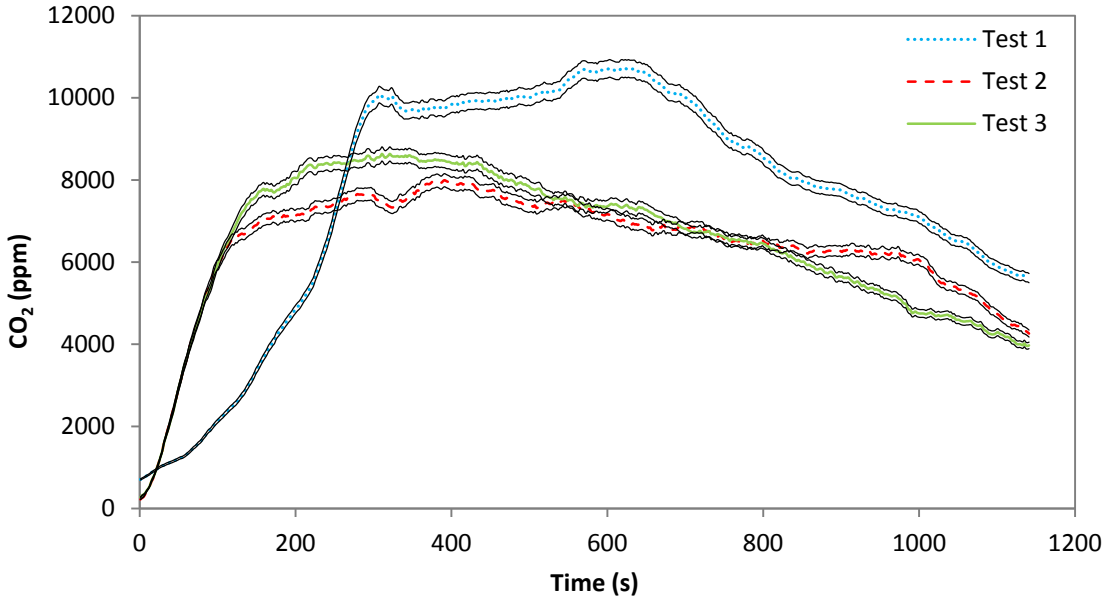

Figure 3-13: CO_2 versus time for biomass co-fired with 50% biogas

For biomass burned with fan, the three repeated tests for both PM and CO are different from ignition to around 500 seconds. PM concentration in Test 1 rises up to 190 mg/m^3 at around

75 seconds whereas in Test 2 it spikes to about 200 mg/m^3 at around 390 seconds. After 500 seconds, the repeated tests for both PM and CO concentrations follow similar pattern. In Figure 3-14, PM concentration starts to diminish at around 400 seconds and in Figure 3-15, CO concentration gradually rises up at around 600 seconds. At around 600 seconds, the flames start to diminish too. In Figure 3-15, the CO concentration for Test 1 raises high for the second time at around 390 seconds.

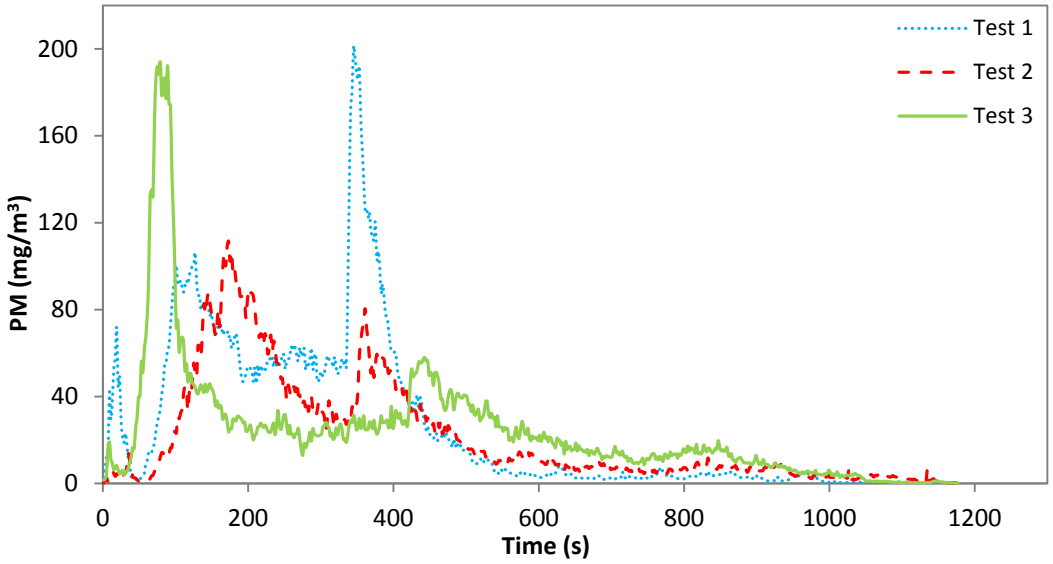

Figure 3-14: PM versus time for biomass burned with fan

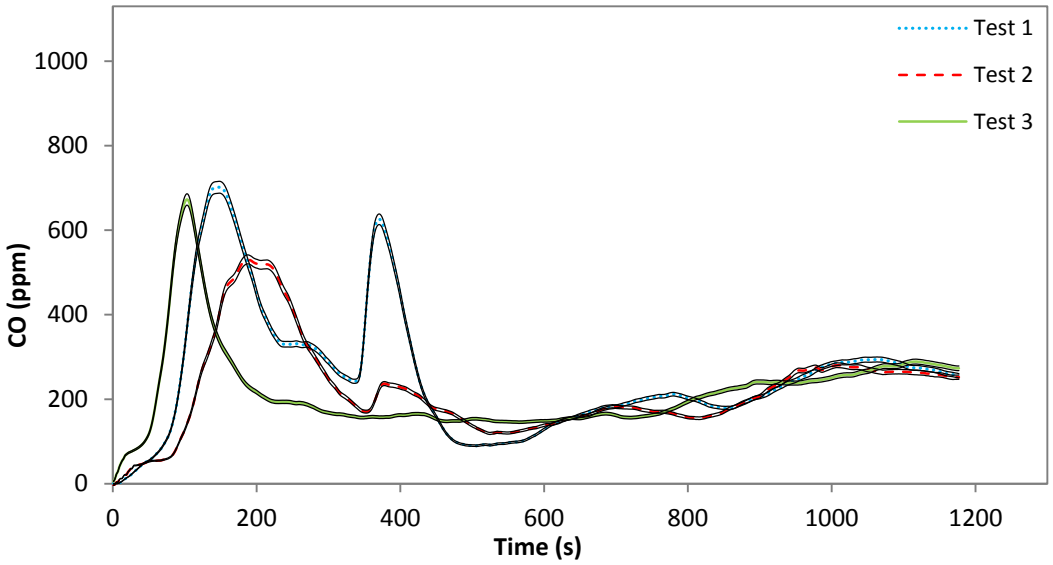

Figure 3-15: CO versus time for biomass burned with fan

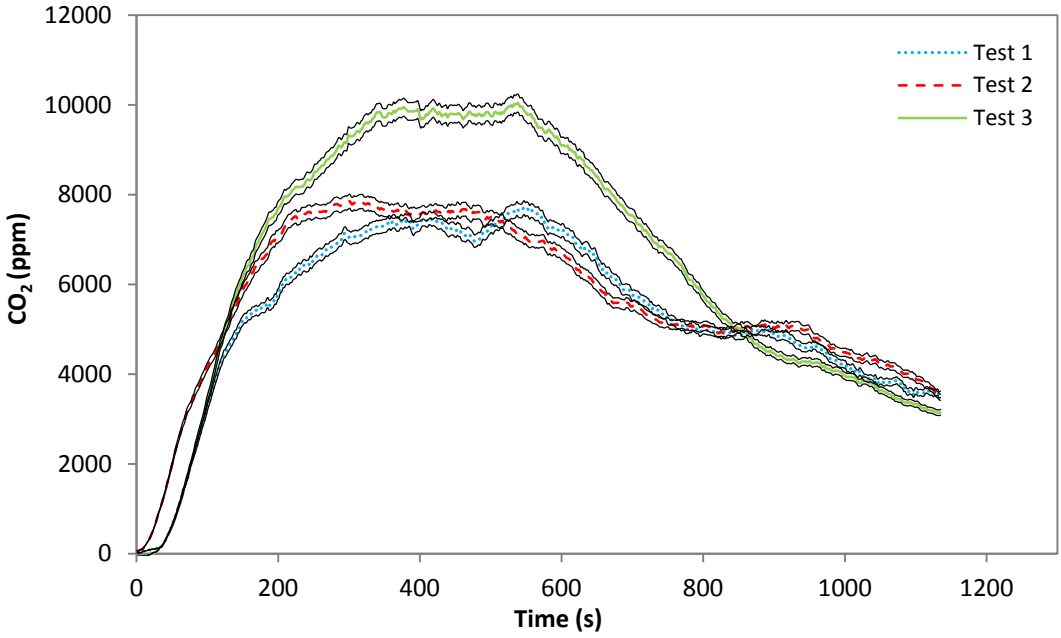

Figure 3-16: CO_2 versus time for biomass burned with fan

For biomass co-fired with biogas 10% and a fan, the repeated tests for PM and CO concentrations vary a lot. In Figure 3-17, Test 2 PM rises rapidly after the ignition and goes up to

195 mg/m^3, whereas Test 1 takes around 100 seconds from the ignition to rise. After 180 seconds the PM concentrations for all the repeated tests do not rise above 40 mg/m^3. Similarly in Figure 3-18, for all the repeated tests, the CO concentration remains below 200 ppm after around 200 seconds. For Tests 1 and 3, there is occasional rise in PM concentration around 650 seconds and 400 seconds respectively. In Figure 3-18, the CO concentration for all the repeated tests rises and drops from ignition to around 250 seconds. From 250 seconds to about 750 seconds, the CO concentration for all the tests is relatively flat. After around 800 seconds, the CO concentration gradually increases, whereas the PM continues to diminish.

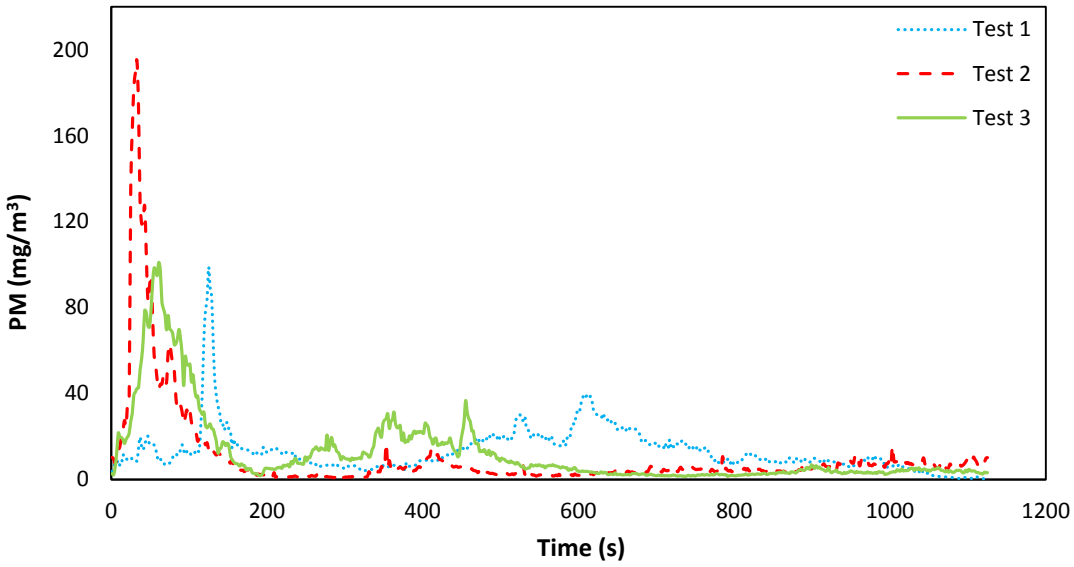

Figure 3-17: PM versus time for biomass co-fired with 10% biogas in addition to fan

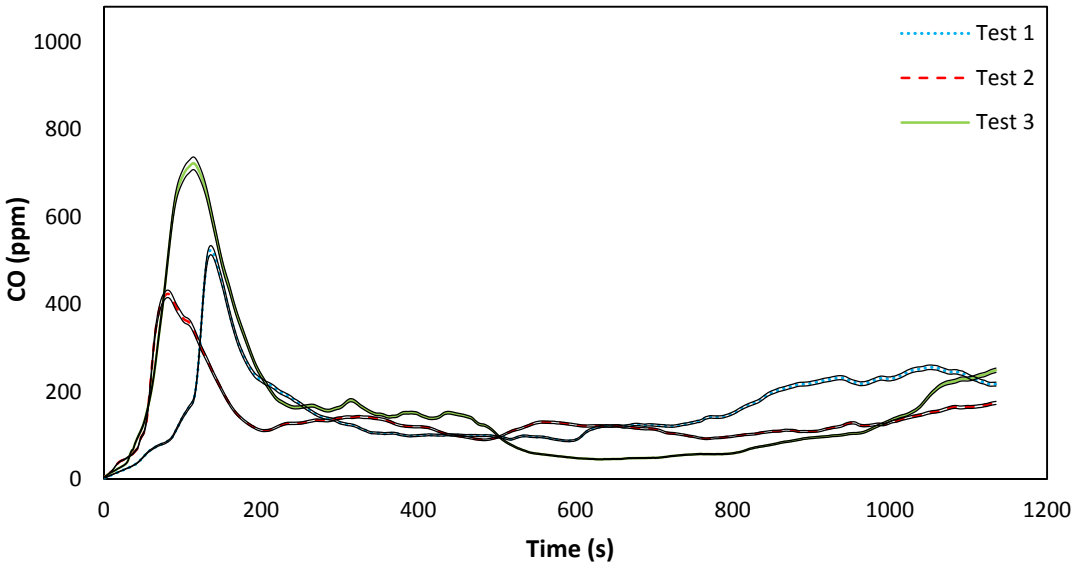

Figure 3-18: CO versus time for biomass co-fired with 10% biogas in addition to fan

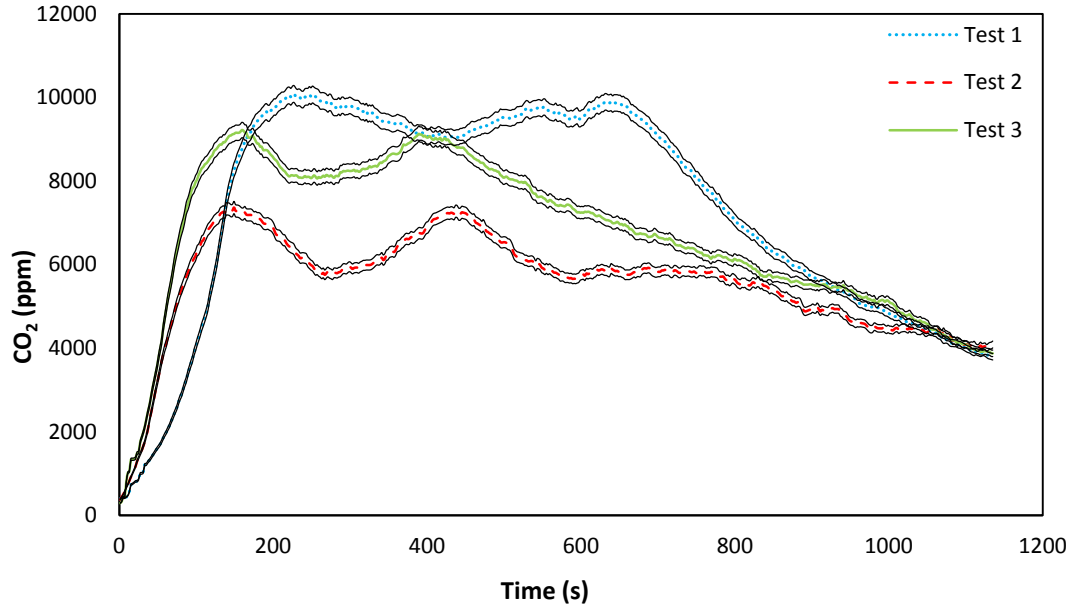

Figure 3-19: CO_2 versus time for biomass co-fired with 10% biogas in addition to fan

For biomass co-fired with biogas 25% in addition to fan, the repeated tests for PM and CO concentrations vary a lot. In tests 2 and 3, PM rises after the ignition and goes up to 80

mg/m^3 whereas Test 1 takes around 50 seconds from the ignition to rise as seen in Figure 3-20. There is a sudden rise in PM concentration for Test 3 around 300 seconds and the PM concentration reaches around 190 mg/m^3. There is also a sudden rise in PM concentration for Test 1 around 420 seconds where it rises up to 120 mg/m^3. After 500 seconds, the PM concentrations for all the repeated tests continue to diminish. Similarly as seen in Figure 3-21, for all the repeated tests, the CO concentration continues to drop around 500 seconds, but starts to rise up around 850 seconds.

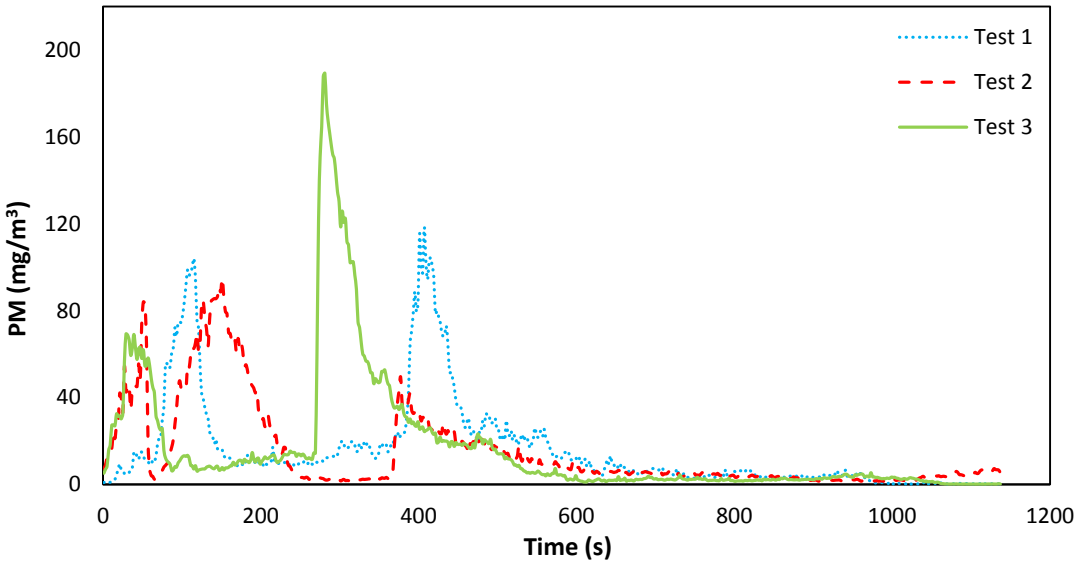

Figure 3-20: PM versus time for biomass co-fired with 25% biogas in addition to fan

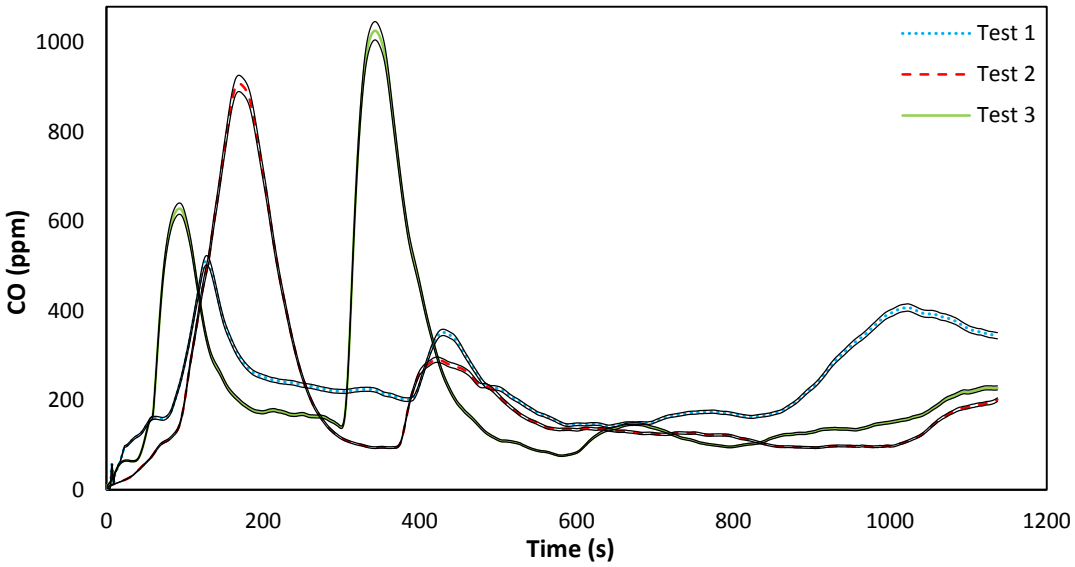

Figure 3-21: CO versus time for biomass co-fired with 25% biogas in addition to fan

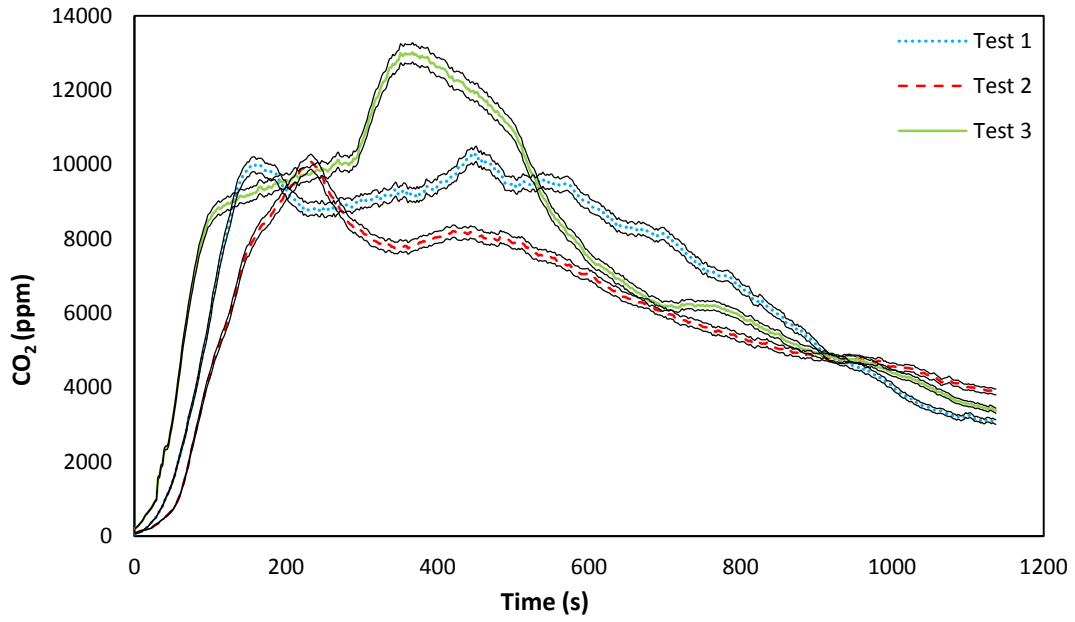

Figure 3-22: CO_2 versus time for biomass co-fired with 25% biogas in addition to fan

For biomass co-fired with biogas 50% in addition to fan, the three repeated tests for both PM and CO concentrations are different. In Figure 3-23, around 50 seconds, the PM

concentration is relatively higher for all the three tests. And from 100 to 600 seconds, the PM concentration for all the tests are relatively flat at around 40 mg/m^3 and after about 600 seconds, the PM concentration starts to drop down. In Figure 3-24, the CO concentration for all the repeated tests rises rapidly after ignition. CO concentrations for the Test 2 continue to increse until 1100 ppm and quickly drops down to 400 ppm within the interval of about 100 seconds. Also, CO concentration for Test 2 increases rapidly to about 600 ppm when the flame nears its end.

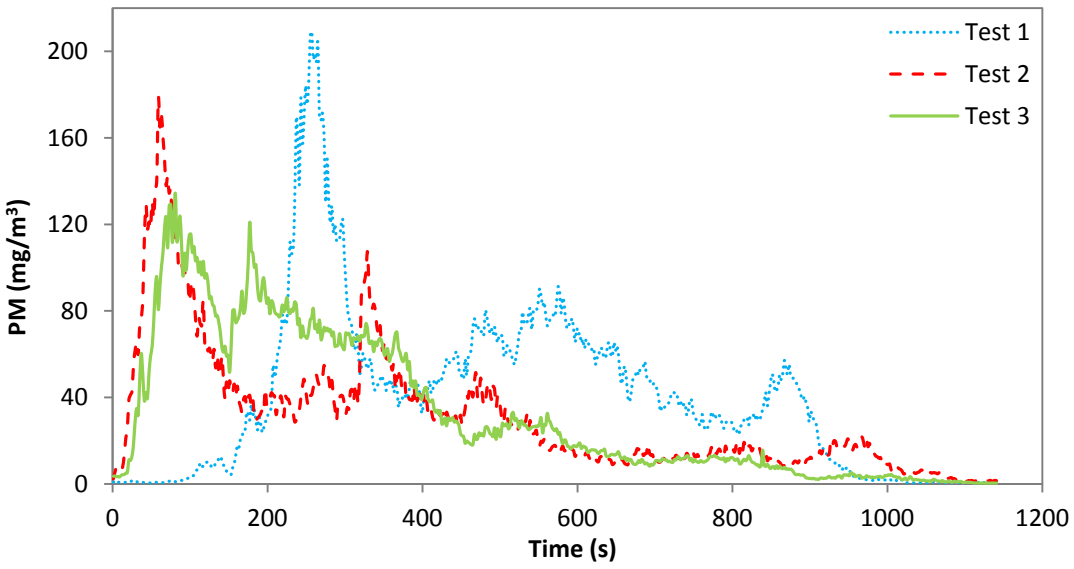

Figure 3-23: PM versus time for biomass co-fired with 50% biogas in addition to fan

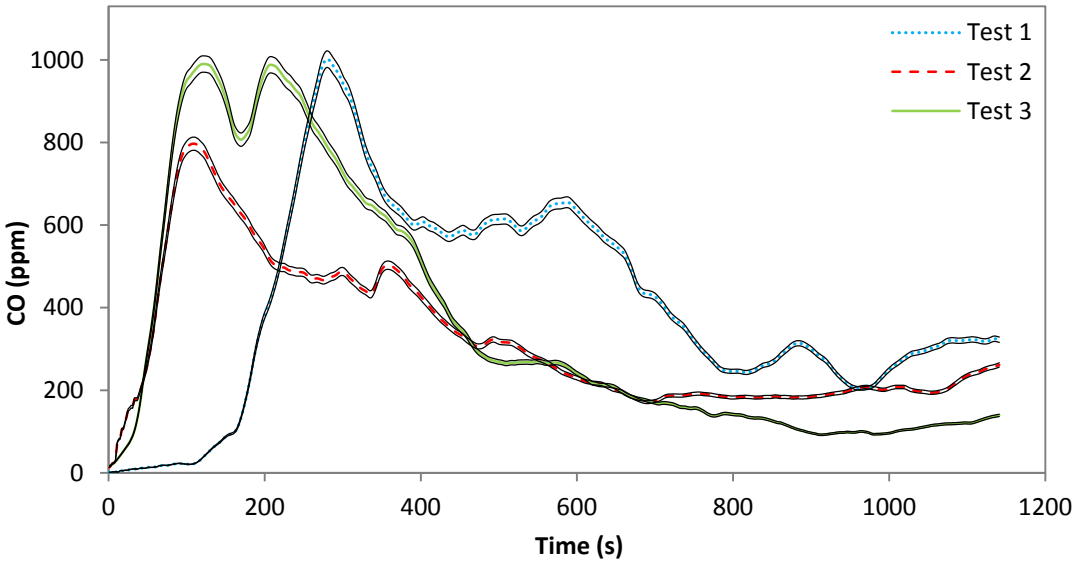

Figure 3-24: CO versus time for biomass co-fired with 50% biogas in addition to fan

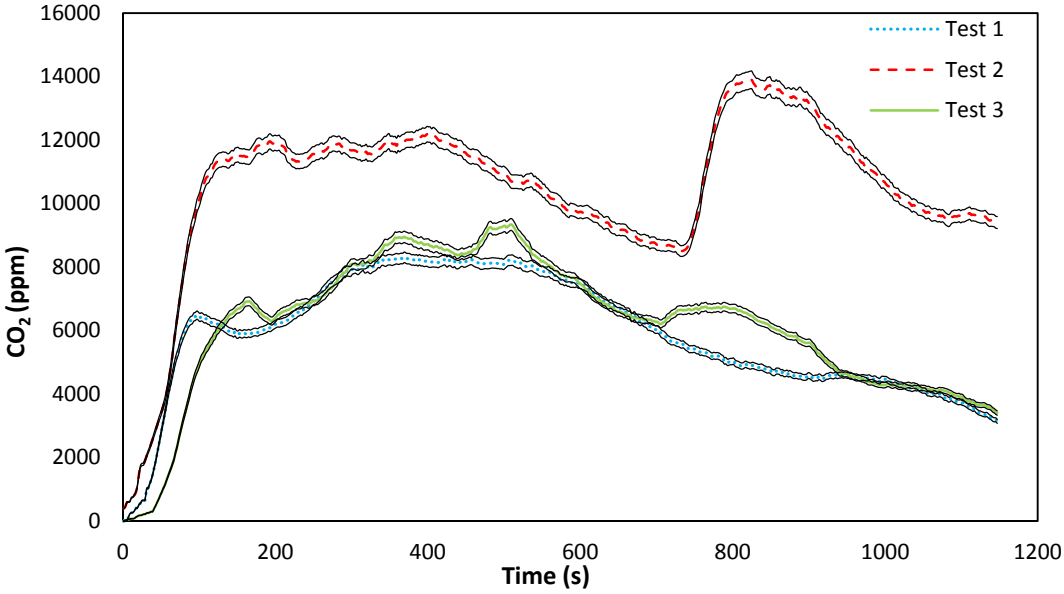

Figure 3-25: CO_2 versus time for biomass co-fired with 50% biogas in addition to fan

The time resolved measurement explains the behavior of emission during the entire process of combustion. It is also useful to integrate the time resolved measurements to obtain measurement of the total emissions to know cumulative emission during a cooking task. The

total emissions produced during the burn can be compared to assess the impact of co-firing (Jetter, et al., 2012). It is explained in the discussion that the total PM is used to measure the average PM concentration and this value would be used to calibrate the real time concentration measured by the PM laser.

3.2.2 Integrated Results

The time resolved results are integrated to calculate the total emissions. Out of all the different tests listed in Table 3-1, the emissions of CO, CO_2, and PM per wood being burned from the repeated tests were similar. Also the other measurements discussed in Chapter 2 were similar too. The total emissions produced during the burn can be compared to assess the impact of co-firing (Jetter, et al., 2012). As per WBT protocol specifications, the results are reported as an average values among the repeated tests (Bailis, Ogle, MacCarty, & Still, 2006). A detailed discussion of the uncertainty estimates is given in Appendix A. The results shown in this section are pollutant emissions per energy delivered to the cooking pot instead of emissions per energy released from the fuel burned. This is because biomass cookstoves have lower thermal efficiency than liquid or gas cookstoves. Thus the emission of PIC will be higher if it is calculated per energy delivered to the cooking pot (Smith, et al., 2000). It is also recommended that pollutant emissions should be measured per cooking energy delivered to allow valid comparisons between the fuels, thus creating the fundamental desired output of cooking energy (Jetter, et al., 2012). For the tests performed there will be a direct comparison between the fuels, such as biomass burned alone and biomass co-fired with different amounts of biogas. Both the results of emissions per energy delivered to the cooking pot and emissions per fuel energy can be found in Appendix B. These two results lead to the same conclusions regarding the performance of a stove.

In Figure 3-26, biomass burned alone produced the highest mass of CO (g) per energy delivered to the cooking pot (MJ). When the biomass is co-fired with 10% biogas the CO reduces but with addition of more biogas the CO gradually increases. In comparison to biomass co-fired with 10% biogas, the level of CO is lower when biomass is burned with fan. Biomass co-fired with 10% biogas in addition to the fan significantly lowers the CO. The same trend of increase in CO with the increase in biogas flow rate is seen with and without the fan.

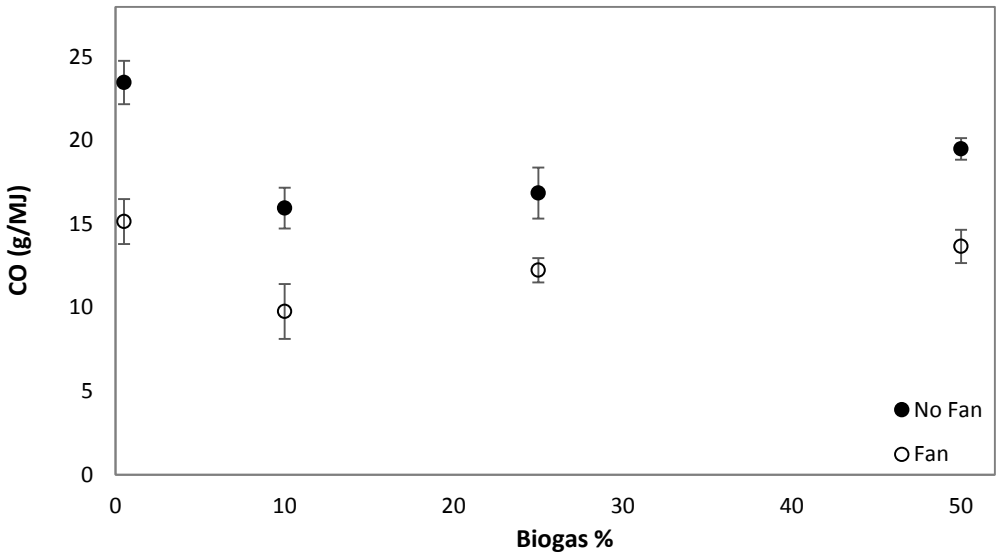

Figure 3-26: CO versus biogas flow rate with and without fan (Cumulative)

In Figure 3-27, biomass burned alone produces the highest PM. PM versus biogas flow rate and CO versus biogas flow rate shows the same trend.

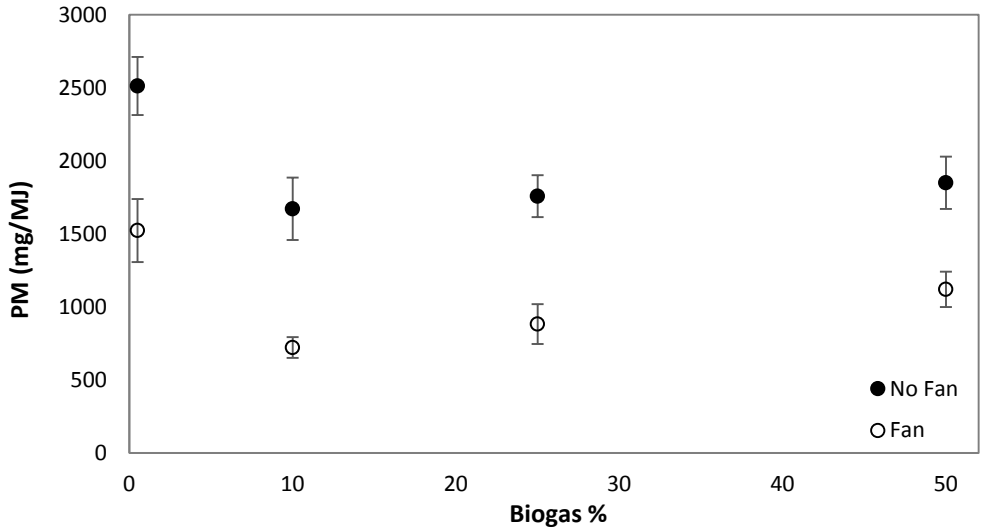

Figure 3-27: PM versus biogas flow rate with and without fan (Cumulative)

As seen in the Figure 3-28, thermal efficiency is lowest for the biomass alone. The efficiency gradually rises with the increase in the flow rate of biogas. In comparison to biomass co-fired with biogas without the fan the increment in thermal efficiency is minor for biomass co-fired with biogas in addition to the fan. However the error bars are large enough to show there is likely no difference.

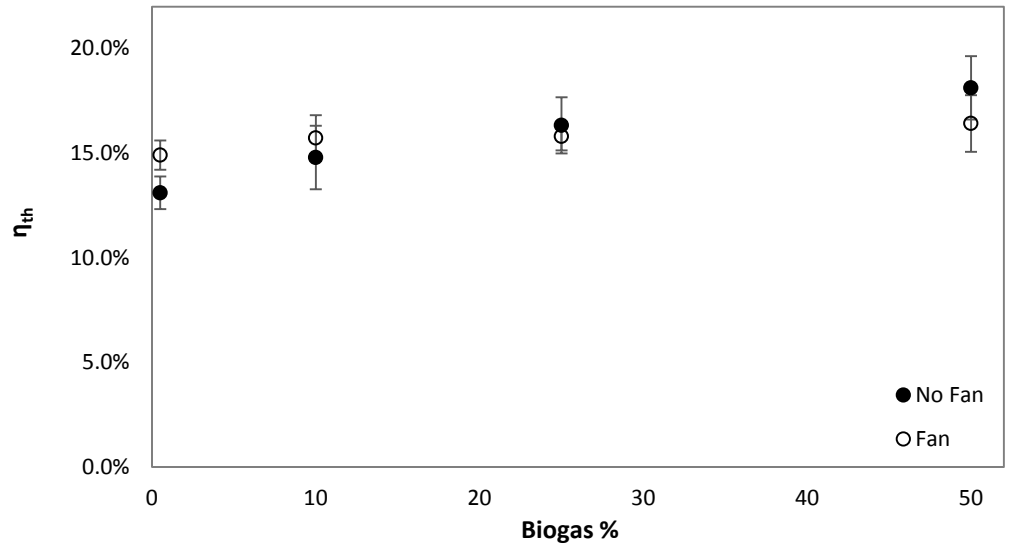

Figure 3-28: Thermal efficiency versus biogas flow rate with and without fan

Figure 3-29 shows the comparison of specific fuel consumption with and without the fan. Specific fuel consumption hardly increases without the fan. But it gradually increases with the increase in biogas flow rate for fan on. 10% biogas with the addition of fan has the lowest specific fuel consumption.

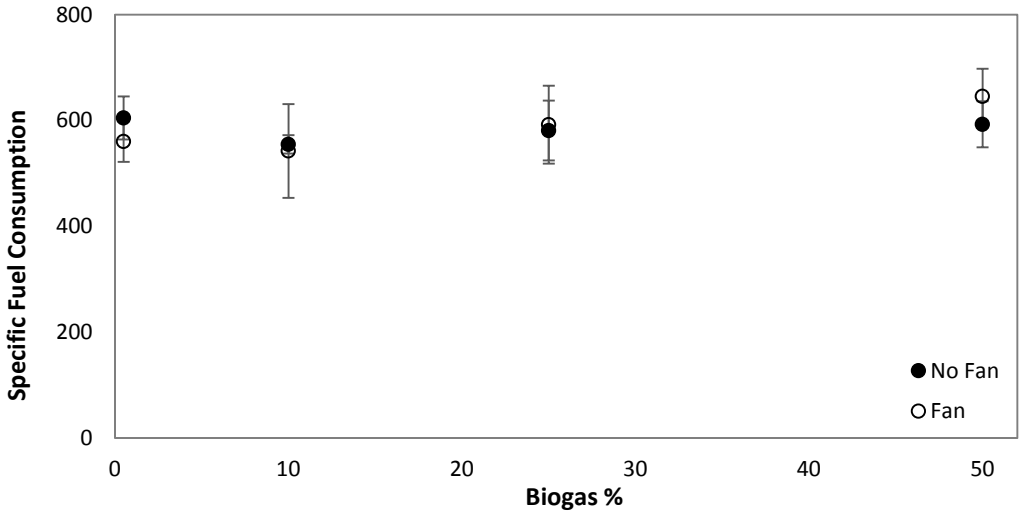

Figure 3-29: Specific fuel consumption versus biogas flow rate with and without fan

In Figure 3-30, MCE is high but many studies done in the past show that a small variation in MCE results in a large difference in the emissions of pollutants (Jetter, et al., 2012). Thus the plot of MCE versus flow rate is the reverse of PM and CO versus flow rate. When biomass is burned alone it produces the lowest MCE. When the biomass is co-fired with 10% biogas the MCE increases but with addition of more biogas the MCE gradually decreases. MCE is similar in biomass co-fired with 10% biogas and biomass burned with fan. Biomass co-fired with 10% biogas in addition to the fan significantly increases MCE. The same trend of decrease in MCE with the increase in biogas flow rate is seen with the addition of fan too.

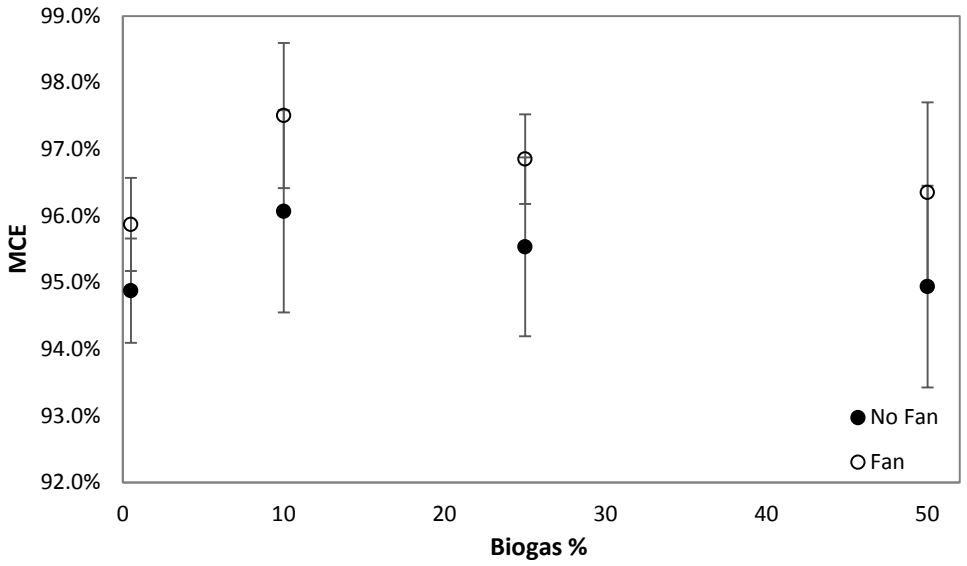

Figure 3-30: MCE versus biogas flow rate with and without fan

Figure 3-31 compares cumulative CO and PM emissions per energy delivered to the cooking pot; the tests with the largest emissions are in the upper right corner. When the biomass was burned alone, the CO emission (around 23 g/MJ), and PM emission (around 2500 mg/MJ) were the highest. When the biomass was burned with the fan, the CO emission was reduced to 15

g/MJ and the PM emission was reduced to around 1500 mg/MJ. When the biomass was co-fired with 10% biogas, the CO emission was around 16 g/MJ and the PM emission was around 1700 mg/MJ which is much lower than the emissions from the biomass alone. There were significantly fewer emissions observed when the biomass was co-fired with 10% biogas, 25% biogas, and 50% biogas with addition of the fan. The least amount of emissions (CO around 10 g/MJ and PM around 700 mg/MJ) was created when biomass was co-fired with 10% biogas in addition with the fan. CO and PM emissions for the biomass with fan and the biomass co-fired with 10% biogas were similar. For both cases, with or without the fan, the emissions gradually increased with the increase of biogas flow rate.

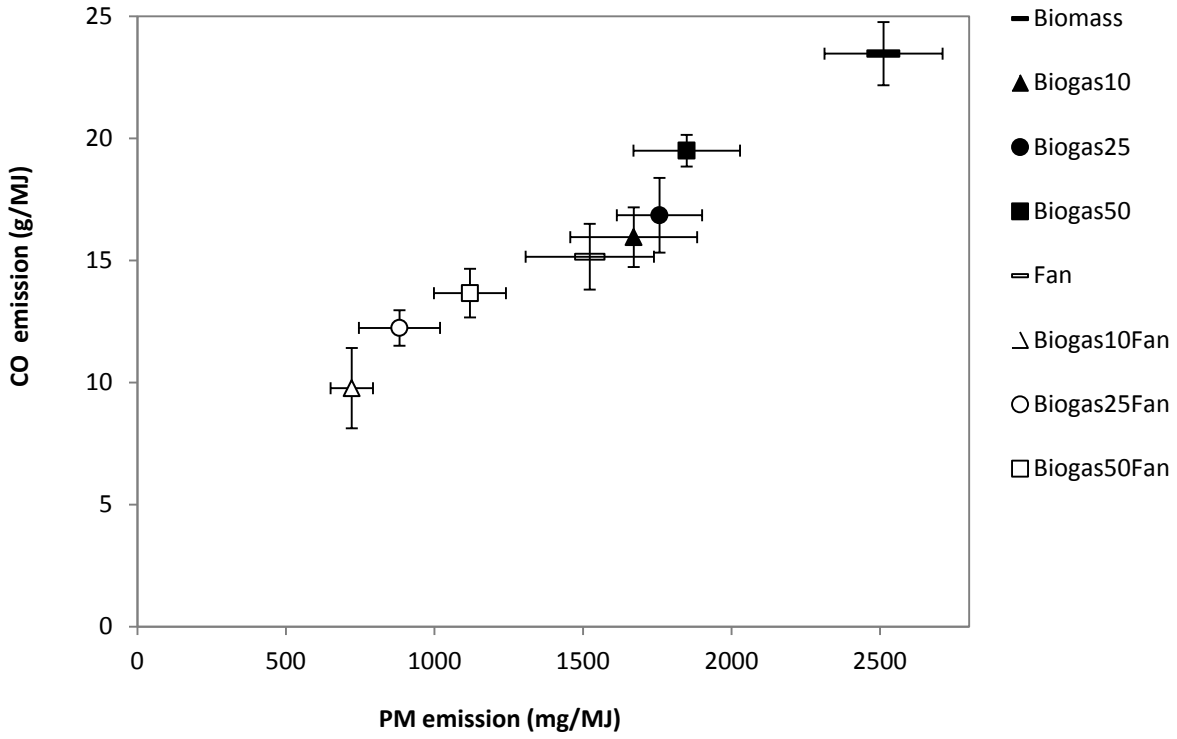

Figure 3-31: CO compared to PM emissions per energy delivered to the cooking pot

Figure 3-32 shows the MCE and the thermal efficiency for all the tests while performing a subset of the tests that comprise the WBT protocol. The more efficient fuel combinations resided in the top right corner of the figure. The highest MCE was observed when biomass co-fired with 10% biogas burned with the fan. The least MCE was measured when biomass was burned alone and when biomass was co-fired with 50% biogas. For biomass co-fired with biogas, MCE gradually decreased with the increase in biogas flow rate. Similarly, biomass co-fired with 10% biogas with fan had a better MCE than biomass co-fired with 25% biogas and 50% biogas with fan. The highest thermal efficiency was observed when 50% biogas was co-fired with biomass and the least thermal efficiency was measured when biomass was burned alone. The thermal efficiency gradually increased with the increase in the flow rate of biogas. But when burned with fan, the thermal efficiency hardly increased with the increase in flow rate of biogas (Appendix B). The thermal efficiencies for biomass co-fired with biogas, with or without the fan, were higher in comparison to biomass burned alone.

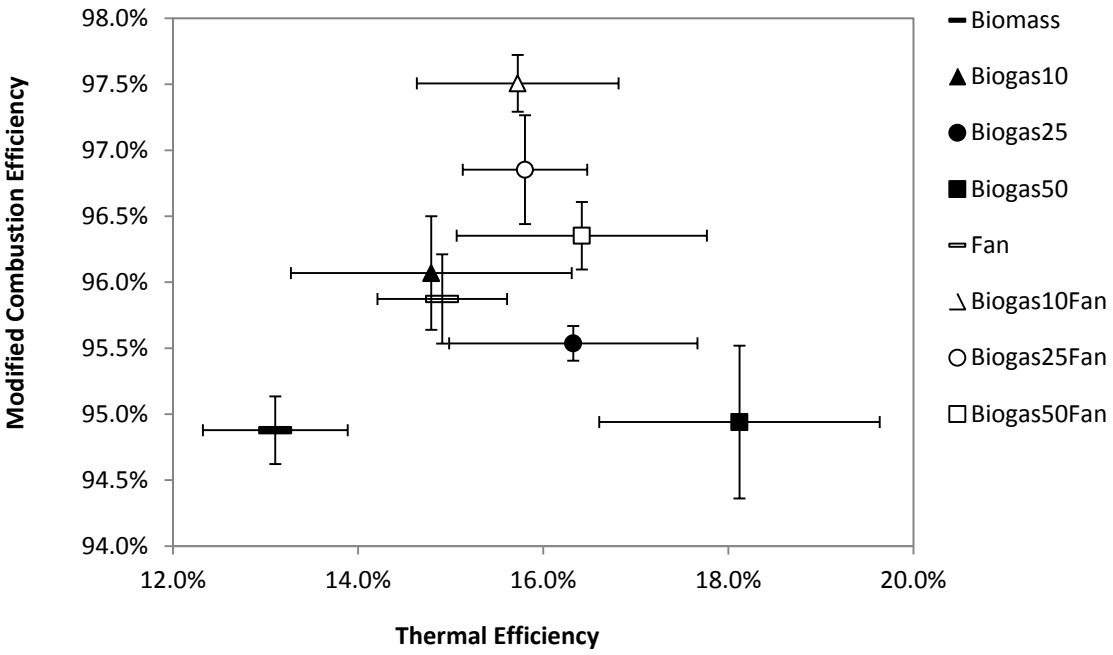

Figure 3-32: MCE versus thermal efficiency for different fuel combinations

Figure 3-33 shows the specific fuel consumption rate. It can be observed that the rate was highest when biomass was co-fired with 50% biogas with fan, and lowest when biomass was co-fired with 10% biogas with the fan. Biomass burned with the fan and biomass co-fired with 10% biogas had almost the same fuel consumption rate. For both cases, biomass co-fired with biogas and biomass co-fired with biogas in addition to fan, the fuel consumption rate continued to increase gradually with the increase in biogas flow rate. The fuel consumption rate had larger spread for the biomass co-fired with biogas (10%, 25%, and 50%) with the fan, compared to biomass co-fired with biogas without the fan. Biomass co-fired with biogas (10%, 25%, and 50%) was lower than the biomass burned alone. With the addition of the fan, 10% biogas was lower, 25% biogas was similar, and 50% biogas was higher than the biomass burned alone. Statistically the specific fuel consumption for the tests is likely the same due to the error bars.

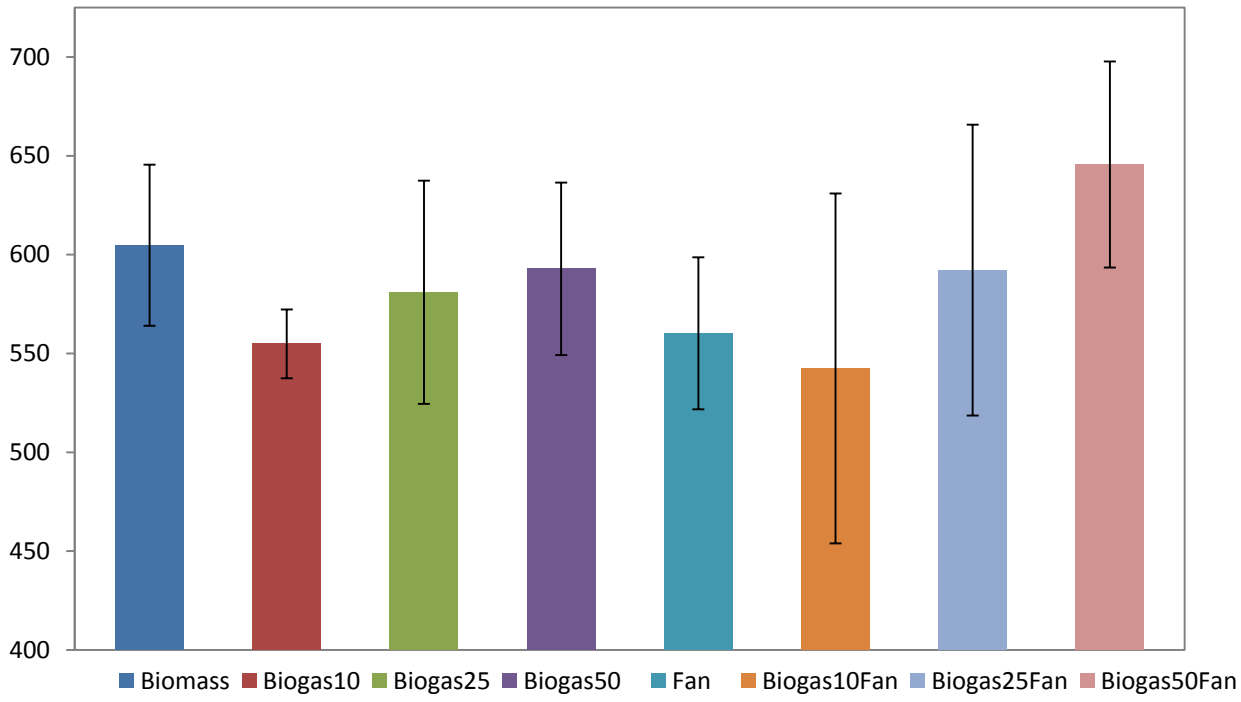

Figure 3-33: Specific fuel consumption for different fuel combinations

3.3 Discussion

3.3.1 Time Resolved Results

The PM sensor is a red laser scattering photometer with a laser and a light receiver inside a sensing chamber. The concentration measured by laser in real time is provided by manufacturer which is obtained from a specific test and stove (Aprovecho, 2012). The given concentration can be used to calculate the total PM but it should be calibrated for every test (Jetter, et al., 2012). When the PM concentration given by the manufacturer was used without calibration for the tests done for this thesis, it was found that the integrated PM from the sensor was about 50-75% lower than the gravimetric measurements. The reason behind this disparity is that the concentration

measured by laser in real time which is given by the manufacturer was obtained from a different kind of stove or test. The stove, burning style, fuel being used in the tests for this thesis are different from the test the manufacturer used to obtain the real time laser concentration value. To mitigate this inaccuracy, it is necessary to calibrate and the calibration is done by scaling the gravimetric concentration which is specific for a test. The scattering photometer measurements alone are unreliable, but they are valuable because they can collect real time information. If the real time concentration from the laser is not calibrated by the user then there should be a higher instrument uncertainty but the uncertainty calculated from the information provided by the manufacturer was very small. Upon further investigation, the manufacturer confirmed that the PM sensor is still a work in progress and did not meet the uncertainty reported for all particulate (Aprovecho, 2012).

PM and CO are often what are usually measured as emissions from cookstoves. As seen in the Figures 3-2 to 3-25, when the flame was nearing the end, the CO started to rise, but PM continued to diminish. When the visible flame was dying, the wood was mostly converted to charcoal and when the flame started to extinguish, the PIC increased which resulted in the rise of CO. Around the same time that the fire was dying, the fluidization velocity of the flames reached its minimum. Fluidization velocity is an upward drag force caused by the moving fluid (flue gas) and it was not sufficient to overcome the weight of the solid particles. This resulted in the PM settling at the bottom or around the stove, thus lowering the PM.

It can be seen that there is a lot of variability in the graphs. This holds true for all the repeated tests executed for this thesis. A significant amount of time was spent understanding and interpreting the data, and analyzing the graphs at instantaneous time. The video of the fire was watched carefully to account for occurrences of spikes and to document the variability. PM

spiked up whenever there was a rise in flame or a spark around the fire. Similarly, the CO spiked up whenever there was more smoke than usual. But it was difficult to see the behavior of fire inside the stove.

All the repeated experiments were performed meticulously. The fire was built in similar fashion and the wood dimensions were the same. Still there was a lot of variability seen in the instantaneous graphs among almost all the repeated experiments. It was impossible to control the fire spreading within the wood which is one of the main reasons of variability. Even though the same dimensions of small and large wood were used each time, after ignition, the fire would spread within the wood in different ways. For some tests, large logs would catch the fire first and for others, smaller ones would catch the fire first. This created variability in graphs of PM, CO, and CO_2 for each repeated test.

Another cause for the variation was wood knots that were distributed randomly in the wood as seen in Figure 3-34. Also, at the end of the repeated tests the remainder of unburned wood was inconsistent. The fire was not identical, even though it was built similarly. The kindling's thickness to start the fire in each repeated tests were not identical either. The dimensions were similar, but there were small differences.

Figure 3-34: Knot randomly distributed in the test wood

Another strong factor that brought the variability in the procedure was wind. Even though there was a windbreak, it was not perfect and small gusts of wind were entering and exiting through the corners. Also there was no roof on the windbreak.

3.3.2 Integrated Results

The total amounts of emissions per energy delivered to the cooking pot, emissions per energy released from the fuel burned, thermal efficiency, and combustion efficiency were almost the same for each of the repeated experiments. As seen in Figure 3-31, when biomass was burned alone, there was an incomplete combustion. With addition of biogas, the combustion was more complete with less PIC. Biomass co-fired with 10% biogas with the fan had the lowest emission. It can also be observed that when the percentage of biogas co-fired was increased, the amount of emissions increased too. One can attribute the increased emissions to the limited amount of air (oxidizer) available locally inside the fire. Also to mimic the traditional cookstove, the bottom of the fire was sealed with mud. Thus, inside the fire there was limited air. Biogas, being in its gaseous state, burned rapidly and consumed most of the oxygen molecules. Therefore, less

oxygen for biomass was available to burn. The result was a gradual increase in emission with an additional increase in biogas.

One could postulate that the additional air to biomass co-fired with biogas would lower the emissions. Biomass co-fired with 10% biogas in addition to the fan, significantly lowered the CO emission by 58% and reduced the PM by 71% from biomass burned alone. These percentages were calculated from the cumulative emissions of PM and CO. The extra air from the fan gave enough oxygen molecules for biogas and wood to burn, lowering the emission significantly. Likewise, there was a gradual increase in emission with increase in the flow rate of biogas during the experiment with the fan. At higher biogas flow rates, the air from the fan was not enough due to the design of the duct. As in Figure 2-4, the air duct sat at the very center of the fire. The area of the duct from where air was coming out was around 46 square centimeters while the base area of the fire was around 1900 square cm. Though the air was supplied, about 97% of the area on the base of the stove did not receive the extra air. Although the volume flow rate of air from the fan might have been adequate, the fan's location and the way the air was directed was not enough to distribute the air locally. In Figure 2-4., there is a gas burner with a much larger surface area and the biogas is distributed more evenly. Thus, the air coming out of the duct might have been enough for fire burning at the center, but the air did not reach towards the wall of the stove. The amount of air was still limited near the wall with the addition of the fan. When the biogas flow rate was increased, it used up most of the oxygen molecules and there was less oxygen for biomass to burn.

As seen in Figure 3-32, a lesser amount of thermal efficiency was seen with 25% biogas, and 10% biogas, but the thermal efficiency was still higher than biomass burned alone. All other tests had higher thermal efficiency and much lower pollutant emissions than biomass alone. For

10% biogas with the fan, MCE was the highest, thermal efficiency was average, and emissions of all pollutants were the lowest. In comparison to the tests without the fan, the MCE increased with the addition of fan because of a more complete combustion due to air. Thermal efficiency is the product of HTE and MCE. Thermal efficiency is the ratio of useful energy delivered while cooking to potential energy in the fuel. HTE is how much of the heat released during combustion that is actually transferred to perform the cooking task. High thermal efficiency means the consumption of wood is less to perform a cooking task. In Figure 3-32, when the biomass was co-fired with 50% biogas, the thermal efficiency was the highest, and the modified combustion efficiency was the lowest. Since MCE is a strong function of emissions of pollutants, 50% biogas has the second largest emissions of CO and PM as seen in Figure 3-31, biomass being the first. 50% Biogas had MCE similar to the biomass burned alone, but showed the highest thermal efficiency. Biomass, co-fired with 50% biogas has higher HTE and performs more cooking tasks while consuming a similar amount of fuel because the large quantity of biogas acts as an extra fuel source, but generally produces higher emissions per wood consumed. For all the tests, MCE is high, but many studies done in the past show that a small variation in MCE results in a large difference in the emissions of pollutants (Jetter, et al., 2012). This relation of MCE and emissions of pollutants was observed in the tests.

4 CHAPTER 4: CONCLUSION AND RECOMMENDATIONS

This section gives an overview and summarizes the results and discussion from Chapter 3. It also examines the results obtained through the tests to see whether they are similar to the hypothesis. This chapter also suggests improved methodology and things to avoid in future tests. It also explains how the experimental setup affects the results of the test.

4.1 Conclusion

The objective of the research documented in this thesis was to investigate the extent to which co-firing biomass with biogas reduces indoor air pollution and increases combustion efficiency. It can be concluded that all the cases studied has lower emissions, and higher thermal efficiency in comparison to biomass burned alone. With or without the use of the fan, biogas addition performed better than biomass burned alone. As expected from the literature review, biomass co-fired with biogas in addition to the fan significantly lowered the emission. The CO emission was reduced by 58% and the PM emission was reduced the by 71% from biomass burned alone. As the biogas flow rate gradually increased, the amount of emissions increased too and this was true for both, with or without the fan. The increase in emissions would be due to the limited amount of air (oxidizer) inside the fire. Biogas, being in its gaseous state, burned rapidly and consumed most of the oxygen molecules found locally. Therefore, less oxygen for biomass was available to burn.

From the results and discussion above, one can conclude that biogas with low flow rate generated the best results for this set-up. The test results show that the 10% biogas to be the most effective at reducing emissions when compared to the 25% and 50% of biogas. 10% biogas is also a more practical and cost-effective option because the production of biogas is limited. Compared with the biomass fired alone, reduction in PM was more than half, fuel consumption and CO emissions were much lower when co-fired with 10% biogas. This shows that if the fan is not an option, then 10% biogas is better than burning biomass alone.

The tests conducted showed that there is a high level of variability in the results, despite meticulous efforts to repeat the experiments exactly. Although the fire was built in similar style, there was a lot of variability with instantaneous graphs among almost all the repeated experiments. The PM sensor which consists of a red laser scattering photometer was used to generate the instantaneous graph. The concentration for the laser in real time is provided by the manufacturer which was obtained from a different kind of stove or test (Aprovecho, 2012). If the given concentration is used for a different type of stove or test then the PM calculation is not accurate. PM coefficient can be used to calculate the total PM but it is considered less accurate (Jetter, et al., 2012). When the PM concentration given by the manufacturer was used for the tests done for this thesis, it was found that the total PM from the sensor was about 50-75% lower than the gravimetric measurement. To mitigate this inaccuracy the integrated continuous measurement was scaling the gravimetric concentration. Gravimetric concentration was derived from the total PM obtained from gravimetric system (filter paper). The scattering photometer measurements are unreliable but if calibrated, they are valuable and can collect real time information.

The conclusion from integrated results is that co-firing with right amount of biogas reduces PM and CO emissions, and gives better performance. Also, addition of the fan to the co-firing of biogas would be even more efficient and can contribute to significant reduction in emissions.

The main purpose of this thesis was to investigate the impact of biomass co-fired with biogas with and without fan. Compared to biomass burned alone, the biogas co-firing technique with and without fan, improves indoor air quality and combustion efficiency. The results show that small amounts of biogas can lower the emissions.

The production of adequate biogas from a digester requires enough dung, water and larger digester. In the rural communities of Nepal, water might be scarce due to topographical features, dung might be limited, and building a larger digester costs more money. Also the production of biogas is lower during winter because of the drop in temperature (Garba, 1996). Due to the limited production of biogas people do not build biogas digesters and continue to burn biomass. It is anticipated that if the benefits of co-firing biomass with a small amount of biogas is made known to the people in rural communities then many will reconsider the idea of small biogas digesters which are financially possible. Since the amount of biogas required during co-firing is small, a couple of families can collaborate and invest in one biogas plant. There are cultural impediments while deploying any technology. It is also believed that the co-firing technology will have less cultural impediments because people will still be using biomass. If implemented this technique would improve health conditions and lower the environmental degradation.

4.2 **Recommendations**

There were certain constraints in the design due to some limitations. For instance, the speed of the fan could not be increased as it resulted in higher temperature and stopped the blower. There is an automatic safety shut off which shuts the blower in higher temperature to protect the blower's motor. It is recommended that more tests with higher fan speed are required to really know the impact of the fan.

As seen in discussion, the air duct covered about 3% of the base area of the stove and it was located at the very center. Though there was extra air, it was not well distributed locally. More of a burner design that would spread at the base of the stove is recommended to supply the air. Compared to air, the biogas was well oriented with two small burners, but it might be even better if the burners were bigger and covered more base area of the stove.

As seen in the result, the lowest biogas 10% with or without the fan gave better result in comparison to higher biogas. But Figure 3-26 and Figure 3-27, suggest that biogas less than 10% would even be better for producing the lowest emission. So, the optimum amount of biogas percentage is still unknown. A rotameter (Matheson 605) was available and the lowest flow rate it could give was 10% biogas. In the future, a rotameter or any gas flow controller with lower flow rate capacity is suggested in order to measure lower flow rates of biogas. Also, more tests of different biogas flow rates are recommended to know the behavior of amount of biogas in the process of co-firing.

The windbreak used during the experiment was not able to completely stop the wind. The wind was still entering and exiting through the corners and the open top. The test would be better controlled if performed in a room where there was no wind.

Some of the tests done for this thesis required fan and a power generator was used to power the fan. In the field, TEG or other source would be needed. Experiments showed that it takes a long time for the TEG to start powering the fan. A battery or other means to store energy is needed.

REFERENCES

Ahuja, D. R., Joshi, V., Smith, K. R., & Venkataraman, C. (1987). Thermal performance and emission characteristics of unvented biomass-burning cookstoves: A proposed standard method for evaluation. *Biomass*, 247-270.

Aprovecho, R. (2012, August 21). *Instructions for Use of the Portable Emissions Monitoring System (PEMS)*. Cottage Grove.

Arthur, R., Baidoo, M. F., & Antwi, E. (2011). Biogas as a potential renewable energy source: A Ghanaian case study. *Renewable Energy*, 1510-1516.

Ashekuzzaman, S., & Poulsen, T. G. (2011). Optimizing feed composition for improved methane yield during anaerobic digestion of cow manure based waste mixtures. *Bioresource Technology*, 2213-2218.

Bailis, R., Ogle, D., MacCarty, N., & Still, D. (2006). *The Water Boiling Test (WBT)*. London: Shell Foundation.

Bajgain, S. (1994, September). *Nepal Biogas Plant - Construction Manual*. Retrieved from journeytoforever: http://journeytoforever.org/biofuel_library/methane_nepal.html

Berkeley, L. N. (2012, 4 26). *BERKELEY LAB*. Retrieved from Cookstove Project: Darfur: http://cookstoves.lbl.gov/darfur.php

Bhattacharya, S., Thomas, J. M., & Salam, A. P. (1997). Greenhouse gas emissions and the mitigation potential of using animal wastes in Asia. *Energy*, 1079–1085.

CO detector. (2013, March 14). Retrieved July 2, 2013, from wikipedia.org: http://en.wikipedia.org/wiki/Carbon_monoxide_detector#Electrochemical

CO_2 sensor. (2012, May 1). Retrieved July 3, 2013, from CO_2Meter.com: http://www.co2meter.com/blogs/news/6010192-how-does-an-ndir-co2-sensor-work

Demirbas, A. (2003). Sustainable Co-firing of Biomass with Coal. *Energy Conversion and Management*, 1465-1479.

Dherani, M., Pope, D., Mascarenhas, M., Smith, K. R., Weber, M., & Bruce, N. (2008). Indoor air pollution from unprocessed solid fuel use and pneumonia risk in children aged under five years: a systematic review and meta-analysis. *Bull World Health Organ*, 390–398.

Elledge, M. F., Phillips, M. J., Thornburg, V. E., Everett, K. H., & Nandasena, S. (2012). A Profile of Biomass Stove Use in Sri Lanka. *International Journal of*, 1097-1110.

Figliola, R. S., & Beasley, D. E. (2011). *Theory and Design for Mechanical Measurements.* Clemson: John Wiley & Sons, Inc.

Garba, B. (1996). Effect of Temperature and Retention Period on Biogas Production from Lignocellulosic Material. *Renewable Energy* , 938-41.

Jetter, J., Zhao, Y., Smith, K. R., Khan, B., Yelverton, T., DeCarlo, P., & Hays, M. D. (2012). Pollutant Emissions and Energy Efficiency under Controlled Conditions for Household Biomass Cookstoves and Implications for Metrics Useful in Setting International Test Standards. *Environ. Sci. Technol.* , 10827−10834.

Johnson, M., Edwards, R., Berrueta, V., & Masera, O. (2010). New Approaches to Performance Testing of Improved Cookstoves. *Environ. Sci. Technol.*, 368-374.

Katuwal, H., & Bohara, A. K. (2009). Biogas: A promising renewable technology and its impact on rural households in Nepal. *Renewable and Sustainable Energy Reviews*, 2668–2674.

Legros, G., Havet, I., Bruce, N., & Bonjour, S. (2009, November). *WHO, UNDP.* Retrieved from The energy access situation in developing countries: http://content.undp.org/go/cms-service/stream/asset/?asset_id=2205620

Loughran, D., & Pritchett, L. (1997). *Environmental Scarcity, Resource Collection, and the Demand for Children in Nepal.* World Bank.

Malm, W. C., Sisler, J. F., Huffman, D., Eldred, R. A., & Cahill, T. A. (1994). Spatial and seasonal trends in particle concentration. *JOURNAL OF GEOPHYSICAL RESEARCH,*, 1347-1370.

Matthews, C. (2006, September 4). *Food and Agriculture Organization of the United Nations*. Retrieved from FAONewsroom: http://www.fao.org/newsroom/en/news/2006/1000385/index.html

McIlveen-Wright, D., Huang, Y., Rezvani, S., Mondol, J., Redpath, D., Anderson, M., . . . Williams, B. (2011). A Techno-economic assessment of the reduction of carbon dioxide emissions through the use of biomass co-combustion . *Fuel*, 11-18.

Ounnar, A., Benhabyles, L., & Igoud, S. (2012). Energetic Valorization of Biomethane Produced from Cow-Dung. *Procedia Engineering*, 330-334.

Particle Measuring Systems. (2011). Retrieved from A Simple Guide to How Aerosol Particle Counters Work.

Pyati, A. T. (2012, March 6). *Those dung cakes could be harmful: Study*. Retrieved from Deccan Herald: http://www.deccanherald.com/content/232244/those-dung-cakes-could-harmful.html

Ramanathan, V., & Carmichael, G. (2008). Global and regional climate changes due to black carbon. *Nature Geoscience*, 221–227.

Rehfuess, E. (2006). *Fuel for life : household energy and health.* Geneva: WHO Press.

Roden, C. A., Bond, T. C., Conway, S., & Pinel, A. B. (2006). Emission Factors and Real-Time Optical Properties of Particles Emitted from Traditional Wood Burning Cookstoves. *Environ. Sci. Technol.*, 6750-6757.

Smith, K. R., Uma, R., Kishore, V., Zhang, J., Joshi, V., & Khalil, M. (2000). Greenhouse Implications of Household Stoves: An Analysis for India. *Annu. Rev. Energy Environ.*, 741–63.

Tahir, S., Rafique, M., & Alaamer, A. (2010). Biomass fuel burning and its implications: Deforestation and greenhouse gases emissions in Pakistan. *Environmental Pollution*, 2490–2495.

Tikuisis, P., Kane, D., McLellan, T., Buick, F., & Fairburn, S. (1992). Rate of formation of carboxyhemoglobin in exercising humans exposed to carbon monoxide. *Applied Physiology*, 1311–9.

Ukpai, P., & Nnabuchi, M. (2012). Comparative study of biogas production from cow dung, cow pea and cassava peeling using 45 litres biogas digester. *Advances in Applied Science Research*, 1864-1869.

Witt, B. M. (2005). *An Improved Wood Cookstove: Harnessing Fan Driven Forced Draft for Cleaner Combustion.* Hartford: Aprovecho Research Center.

World Health Organization. (2013, February 14). Retrieved from Indoor Air Pollution and Health: http://www.who.int/mediacentre/factsheets/fs292/en/

APPENDIX A: VARIABILITY AND UNCERTAINTY ANALYSIS

In any assessment process, it is very important to include variability and uncertainty. These errors are inherent to any measurement. The available data from PEMS maybe of unknown quality, thus including uncertainty and variability will make the analysis or assessment much more meaningful. This Appendix explains the calculations to find variability and uncertainty.

Table A-1: Nomenclature for Variables Introduced in Calculations

Variable	*Defined As*	*Units*
u_v	Variable uncertainty	
$t_{v,p}$	Student's t distribution	
$s_{\bar{x}}$	Random uncertainty	
s_x	Standard deviation	
N	Number of samples	
u_R	Repeatable uncertainty	
u_c	Error propagation	
u_i	Instrument uncertainty	
u_A	Accuracy uncertainty	
θ_i	Partial derivative with respect to the measured variable	
Π_{th}	Thermal efficiency	
C	Specific heat capacity of water	*kJ/kg.K*

Table A-1, continued

Variable	*Defined As*	*Units*
T_f	Final water temperature of each pot	^oC
T_i	Initial water temperature of each pot	^oC
ΔT	T_f - T_i	^oC
h_{fg}	Enthalpy of vaporization	*J/g*
m_v	Mass of vaporized water	*g*
m_w	Mass of dry wood consumed	*g*
LHV	Lower heating value of fuel	*kJ/kg*
SC	Specific fuel consumption rate	
m_P	Mass of empty pot	*g*
m_{Pf}	Mass of pot with water after test	*g*
SEM_{CO}	Specific CO emissions per energy	*g/MJ*
SEM_{CO2}	Specific CO_2 emissions per energy	*g/MJ*
SEM_{PM}	Specific PM emissions per energy	*mg/MJ*
Π_C	Combustion efficiency	
Π_{th}	Thermal efficiency	
m_{CO}	Total mass of CO emissions	*g*
m_{CO2}	Total mass of CO_2 emissions	*g*
m_{PM}	Total mass of PM emissions	*g*
m_l	Mass of liquid water	*g*

Variable uncertainty considers the variability of all measured variables and the controllability of the test operating conditions. It also includes the effects of resolution. Random uncertainty ($s_{\bar{x}}$) estimates the probable range of random error. Student t distribution is the probability distribution of the random variable. It is used when the sample size is small and

population standard deviation is unknown. The t distribution also considers the confidence intervals for the difference between the population means. To calculate the variable uncertainty, 95% confidence level is used. The equations used in this appendix are used from the book (Figliola & Beasley, 2011).

$$u_v = t_{v,P} \cdot s_{\bar{x}} \quad \textbf{(A-1)}$$

$$s_{\bar{x}} = \frac{s_x}{\sqrt{N}} \quad \textbf{(A-2)}$$

The tests were repeated three times making the sample size, $N = 3$. The t distribution for $N = 3$ at 95% confidence level is $t_{95} = 4.303$ (Figliola & Beasley, 2011). Also, there are sensors and scales that have their own instrument uncertainties. The final error combines the instrument uncertainty with variability. The total uncertainty estimates is calculated for each measurements.

Carbon Monoxide

The following information was gathered from PEMS specifications sheet:

CO sensor:

Range: 0 – 1000 ppm

Repeatability: 2%

Resolution: 1ppm

$$SEM_{CO} = \frac{\text{CO emissions}\left(\text{g}\right)}{\text{Energy delivered to pot}\left(\text{J}\right)} = \frac{m_{CO}}{\eta_{th} \cdot m_w \cdot LHV} \quad \textbf{(A-3)}$$

Calculating Instrument uncertainty: The instruments being used to calculate SEM_{CO} are the CO sensor and the scale (to measure the mass of the wood). The only known information

about the scale is the resolution of ± 1 gram. There are two instrument uncertainties for CO sensor: repeatability and resolution. Variable uncertainty which will be calculated already accounts for the error from resolution (Figliola & Beasley, 2011). The full scale operating range which will account for maximum possible error is calculated as:

$$r_o = \text{Max Range - Min Range} \quad \textbf{(A-4)}$$

The uncertainty from repeatability is calculated as:

$$u_{R,CO} = u_{R\%,CO} \cdot r_{o,CO} \quad \textbf{(A-5)}$$

$$u_{R,CO} = 2\ \%(1000 - 0)\ ppm \quad \textbf{(A-6)}$$

$$u_{R,CO} = 20\ \text{ppm}\ \times\ 28\left(\frac{g}{mole}\right) \quad \textbf{(A-7)}$$

where, $28\left(\frac{g}{mole}\right)$ is the molecular weight of CO

Equation (A-6) gives the instrument uncertainty of the CO sensor. In Equation (A-3), SEM_{CO} is the dependent variable and m_{CO} is a measured variable. The instrument uncertainty is in the term m_{CO}. To calculate the uncertainty for SEM_{CO} a partial derivative of Equation (A-3) is taken to measure the sensitivity that arises from the changes in m_{CO}. This is also known as the propagation of error which is calculated as:

$$u_c = \left[\sum_{i=1}^{L}\left(\theta_i \cdot u_i\right)^2\right]^{\frac{1}{2}} \quad \textbf{(A-8)}$$

where L is the number of independent variables

$$u_{c,CO} = \left[\left(\theta_{R,CO} \cdot u_{R,CO}\right)^2\right]^{\frac{1}{2}} \quad \textbf{(A-9)}$$

$$\theta_{R,CO} = \frac{\partial SEM_{CO}}{\partial m_{CO}} \quad \textbf{(A-10)}$$

$$\theta_{R,CO} = \frac{1000000}{\eta_{th} \cdot m_w \cdot LHV}\left(MJ^{-1}\right) \quad \textbf{(A-11)}$$

$$u_{c,CO} = \frac{1000000}{\eta_{th} \cdot m_w \cdot LHV}\left(MJ^{-1}\right) \times \frac{20 \times 28}{1000000}\left(g\right) \quad \textbf{(A-12)}$$

$$u_{c,CO} = \frac{560}{\eta_{th} \cdot m_w \cdot LHV}\left(\frac{g}{MJ}\right) \quad \textbf{(A-13)}$$

Calculating variability: The uncertainty from variability of three repeated tests is calculated as

$$u_{v,CO} = t_{v,P} \cdot s_{\bar{x}\ CO}\left(95\%\right) \quad \textbf{(A-14)}$$

Therefore, the overall error for SEM_{CO}:

$$u_{CO} = \left[{u_{c,CO}}^2 + {u_{v,CO}}^2\right]^{\frac{1}{2}} \quad \textbf{(A-15)}$$

Carbon Dioxide

CO_2 sensor:

Range: 0 – 10,000 ppm

Accuracy: 10 %

Resolution: 2 ppm

$$SEM_{CO_2} = \frac{\mathrm{CO_2\ emissions\left(g\right)}}{\text{Energy delivered to pot}\left(\mathrm{J}\right)} = \frac{m_{CO_2}}{\eta_{th} \cdot m_w \cdot LHV} \quad \textbf{(A-16)}$$

Calculating Instrument uncertainty: The instruments being used to calculate SEM_{CO2} are the CO_2 sensor and the scale. The resolution of the scale is ± 1 gram. There are two instrument uncertainties for CO_2 sensor: accuracy and resolution. Variable uncertainty which will be calculated already accounts for the error from resolution (Figliola & Beasley, 2011). The full scale operating range which will account for maximum possible error is calculated as:

$$r_o = \text{Max Range - Min Range} \quad \textbf{(A-17)}$$

The uncertainty from accuracy is calculated as:

$$u_{A,CO_2} = u_{A\%,CO_2} \cdot r_{o,CO_2} \quad \textbf{(A-18)}$$

$$u_{A,CO_2} = 10\ \%(10000 - 0)\ ppm \quad \textbf{(A-19)}$$

$$u_{A,CO_2} = 1000\ \text{ppm} \times 44\left(\frac{\text{g}}{\text{mole}}\right) \quad \textbf{(A-20)}$$

where, 44 $\left(\frac{g}{mole}\right)$ is the molecular weight of CO_2

Equation (A-20), $u_{A,CO_2} = 1000\ \text{ppm} \times 44\left(\frac{\text{g}}{\text{mole}}\right)$

(A-20 gives the instrument uncertainty of the CO_2 sensor. In order to calculate uncertainty with SEM_{CO2} measurement, a partial derivative of Equation (A-16) is taken which will include the sensitivity that arises from the changes in m_{CO2}. This is also known as the propagation of error which is calculated as:

$$u_{c,CO_2} = \left[\left(\theta_{A,CO_2} \cdot u_{A,CO_2}\right)^2\right]^{\frac{1}{2}} \quad \textbf{(A-21)}$$

$$\theta_{A,CO_2} = \frac{\partial SEM_{CO_2}}{\partial m_{CO_2}} = \frac{1000000}{\eta_{th} \cdot m_w \cdot LHV}\left(MJ^{-1}\right) \quad \textbf{(A-22)}$$

$$u_{c,CO_2} = \frac{1000000}{\eta_{th} \cdot m_w \cdot LHV}\left(MJ^{-1}\right) \times \frac{1000 \times 44}{1000000}(g) \quad \textbf{(A-23)}$$

$$u_{c,CO_2} = \frac{44000}{\eta_{th} \cdot m_w \cdot LHV}\left(\frac{g}{MJ}\right) \quad \textbf{(A-24)}$$

Calculating variability: The uncertainty from variability of three repeated tests is calculated as

$$u_{v,CO_2} = t_{v,P} \cdot s_{\bar{x}\ CO_2}\ (95\%) \quad \textbf{(A-25)}$$

Therefore, the overall error for SEM_{CO2}:

$$u_{CO_2} = \left[u_{c,CO_2}{}^2 + u_{v,CO_2}{}^2 \right]^{\frac{1}{2}} \quad \textbf{(A-26)}$$

Particulate Matter

The following information was gathered from PEMS specifications sheet:

PM sensor:

Range: 0 – 60,000 ppm

Resolution: 15 ug/m^3

$$SEM_{PM} = \frac{\text{PM emissions}\left(\text{g}\right)}{\text{Energy delivered to pot}\left(\text{J}\right)} = \frac{m_{PM}}{\eta_{th} \cdot m_w \cdot LHV} \quad \textbf{(A-27)}$$

Since variability includes the effects of resolution (Figliola & Beasley, 2011). The overall error for SEM_{PM} would be the uncertainty from variability of repeated tests.

$$u_{PM} = u_{v,PM} \quad \textbf{(A-28)}$$

$$u_{v,PM} = t_{v,P} \cdot s_{\bar{x}\ PM}\left(95\%\right) \quad \textbf{(A-29)}$$

Specific fuel consumption rate

$$SC = \frac{m_w}{m_{Pf} - m_P} \times \frac{T_{Sat} - T_i}{T_f - T_i} \quad \textbf{(A-30)}$$

W_w, P_{wf}, and ΔT are calculated using a scale and thermometer. The scale has a resolution of ± 1 gram and the thermometer has a resolution of ± 0.1^0C which would be their instrument uncertainties. But the variable uncertainty which will be calculated accounts for the error from resolution (Figliola & Beasley, 2011).

The uncertainty from variability is calculated as:

$$u_{v,SC} = t_{v,P} \cdot s_{\bar{x}\ SC}(95\%) \quad \textbf{(A-31)}$$

The number of tests is about three. That means the student's t distribution is higher and the uncertainty from variability is much higher than other instrument uncertainties if they were available.

Thermal Efficiency

$$\eta_{th} = \frac{\mathrm{m_l} \cdot c \cdot \Delta \mathrm{T} + \mathrm{h_{fg}} \cdot \mathrm{m_v}}{m_w \cdot LHV} \quad \textbf{(A-32)}$$

To calculate the thermal efficiency, the instruments involved would be scale and thermometer. The only information available about the instruments are their resolutions. The error from resolution is already accounted in variability. As in specific fuel consumption, the overall uncertainty would be from variability.

$$u_{v,\eta_{th}} = t_{v,P} \cdot s_{\bar{x}\ \eta_{th}}(95\%) \quad \textbf{(A-33)}$$

Combustion Efficiency

$$\eta_C = \left(\frac{CO_2}{CO_2 + CO} \right) \times 100\% \quad \textbf{(A-34)}$$

Combustion efficiency is a function of CO_2 and CO. To estimate uncertainty for η_C, the uncertainty of CO_2 and CO should be considered. To calculate the propagation of error partial derivative of Equation (A-34) is taken with respect to CO_2 and CO.

Error propagation

$$u_c = \left[\sum_{i=1}^{L} (\theta_i \cdot u_i)^2 \right]^{\frac{1}{2}} \quad \textbf{(A-35)}$$

where, L is the number of independent variables

$$u_{c,\eta_C} = \left[\left(\theta_{R,CO} \cdot u_{R,CO} \right)^2 + \left(\theta_{A,CO_2} \cdot u_{A,CO_2} \right)^2 \right]^{\frac{1}{2}} \quad \textbf{(A-36)}$$

$$\theta_{R,CO} = \frac{\partial \eta_C}{\partial CO} = \frac{-CO_2}{\left(CO_2 + CO \right)^2} \quad \textbf{(A-37)}$$

In Equation (A-34), CO and CO_2 are in molar basis.

$$u_{R,CO} = 20\, ppm\left(mole \right) \quad \textbf{(A-38)}$$

$$\theta_{A,CO_2} = \frac{\partial \eta_C}{\partial CO_2} = \frac{CO}{\left(CO_2 + CO \right)^2} \quad \textbf{(A-39)}$$

$$u_{A,CO_2} = 1000\, ppm\left(mole \right) \quad \textbf{(A-40)}$$

The uncertainty from variability of three repeated tests is calculated as

$$u_{v,\eta_C} = t_{v,P} \cdot s_{\bar{x}\,\eta_C} \left(95\% \right) \quad \textbf{(A-41)}$$

Therefore, the overall error for η_C:

$$u_{\eta_C} = \left[{u_{c,\eta_C}}^2 + {u_{v,\eta_C}}^2 \right]^{\frac{1}{2}} \quad \textbf{(A-42)}$$

APPENDIX B: EMISSIONS AND OTHER MEASUREMENTS DATABASE

As seen in the Figure B1, thermal efficiency is lowest when biomass is burned alone. The efficiency gradually rises with the increase in the flow rate of biogas. Biomass co-fired with 10% biogas has similar thermal efficiency to the biomass burned with the fan. In comparison to biomass co-fired with biogas without the fan, the increment in thermal efficiency is slow for biomass co-fired with biogas with the fan. Thermal efficiency is the ratio of energy used to heat the water to total heat units in the fuel consumed by burning wood. A higher thermal efficiency means that a larger fraction of fuel energy is transferred to heat the cooking pot and thus less wood is consumed. The error bar in the figure is calculated in Appendix A.

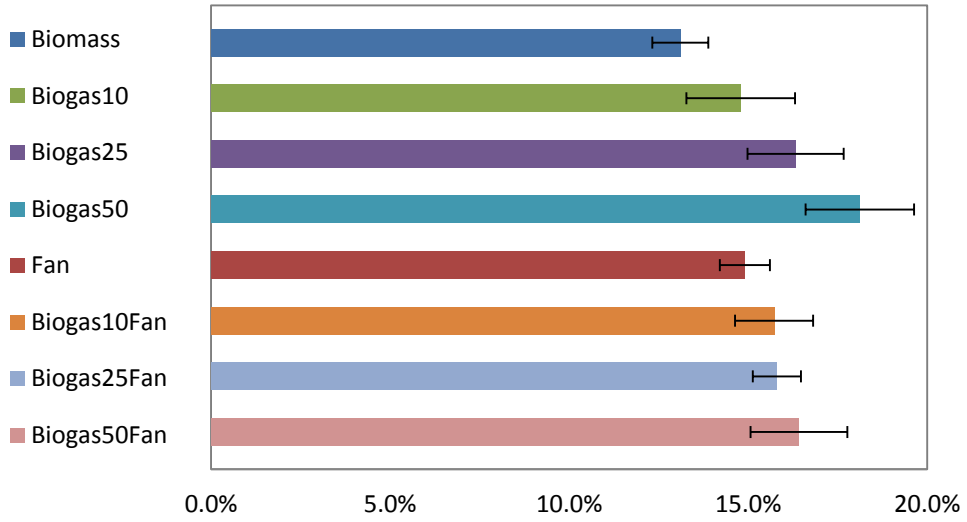

Figure B 1: Comparison of Thermal Efficiency among all the different Tests

Figure B2 shows the comparison of specific fuel consumption among all the different /tests. Specific fuel consumption is the mass of fuel consumed per liter of water remaining in the pot at the completion of the test (Jetter, et al., 2012). Lower specific fuel consumption means that the water boils quickly and saves time to perform a cooking task. When the water boils quickly, there is less time for water to evaporate and the amount of remaining water will be greater. This lowers the specific fuel consumption. Biomass burned alone is the base case for comparison here. It has average specific fuel consumption in comparison to other tests. The fuel consumption gradually increases with the increase in biogas flow rate for both cases, with fan or without fan off. For the test with 10% biogas with fan, the water will boil the fastest as it has the lowest specific fuel consumption.

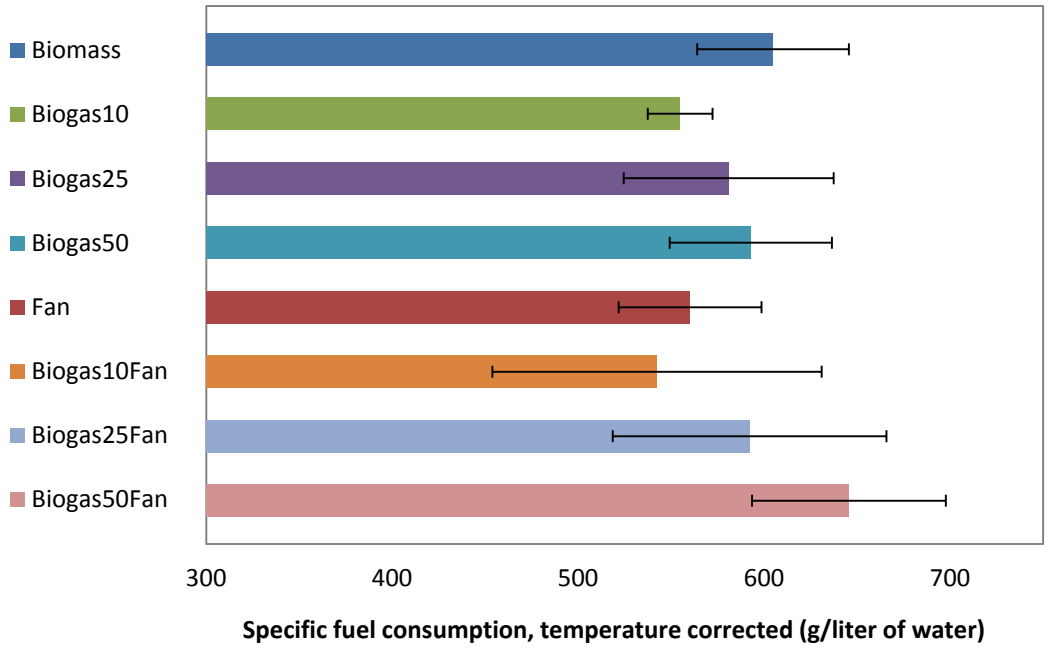

Figure B 2: Comparison of Specific Fuel Consumption among all the different Tests

The result shown in Figure B3 is CO emission per energy delivered to the cooking pot whereas; Figure B4 shows CO emission per energy released from the fuel burned. It is recommended that pollutant emissions should be measured per cooking energy delivered (Jetter, et al., 2012). In Figure B3, the CO emission is highest for biomass burned alone and is lowest for biomass co-fired with 10% biogas in addition to the fan. The CO emission gradually increases with increases of biogas flow rate with or without fan. The only difference in Figure B3 in comparison to Figure B4 is that biomass burned with 50% biogas has the highest CO emission.

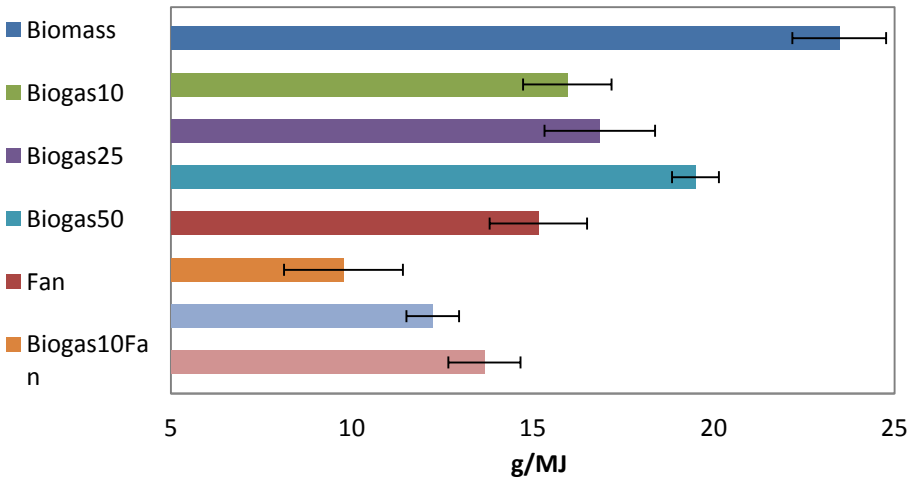

Figure B 3: Comparison of CO Emission per Energy Delivered to Cooking Pot among all the Tests

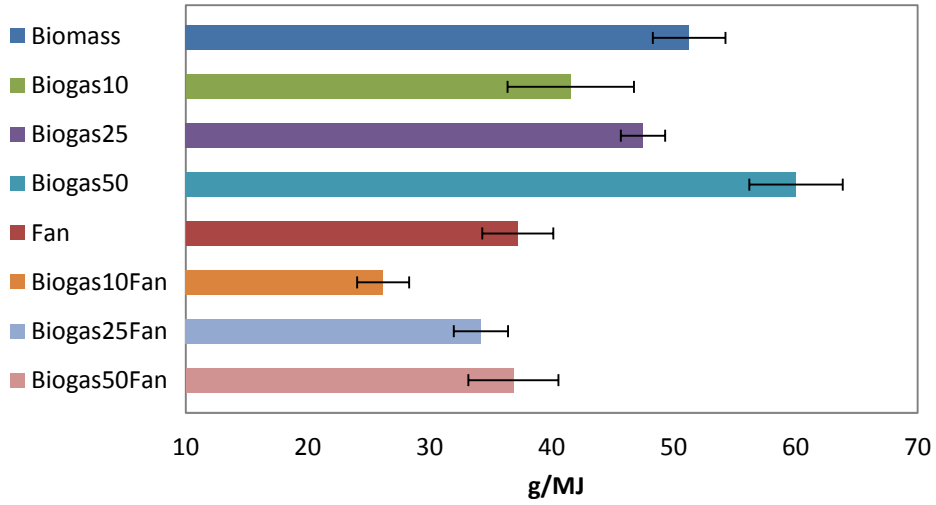

Figure B 4: Comparison of CO Emission per Fuel Energy among all the Tests

Figure B5 shows CO_2 emission per energy delivered to the cooking pot, whereas Figure B6 shows CO_2 emission per energy released from the fuel burned. In both cases the error is large for the CO_2 data. In Figure B5, the CO_2 is highest for biomass burned alone and lowest for biomass burned with fan. In Figure B6, biomass co-fired with 50% biogas produces the largest CO_2, whereas biomass burned with fan produces the lowest CO_2.

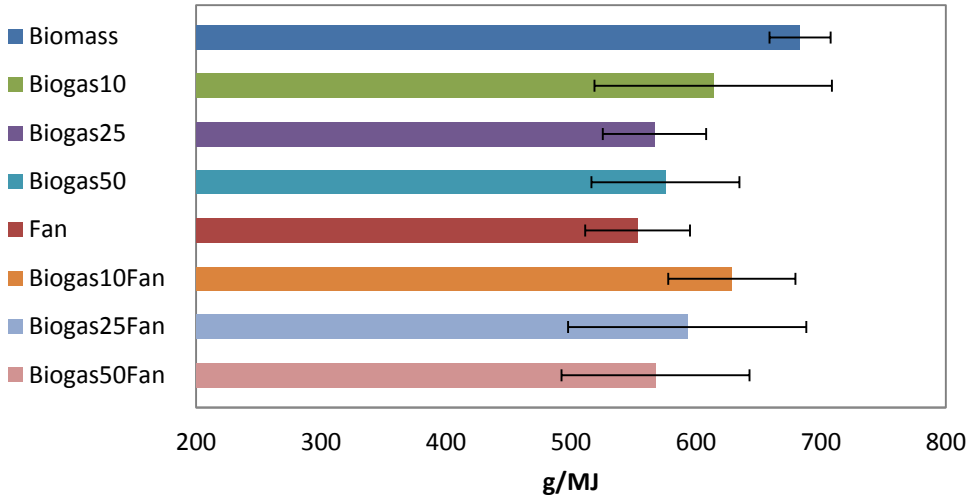

Figure B 5: Comparison of CO_2 Emission per Energy Delivered to Cooking Pot among all the Tests

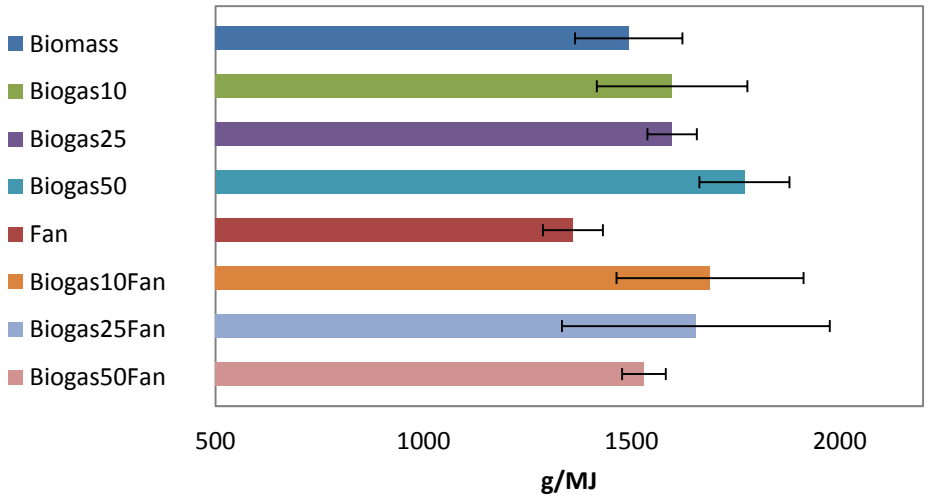

Figure B 6: Comparison of CO_2 Emission per Fuel Energy among all the Tests

Figure B7 shows PM emission per energy delivered to the cooking pot as it allows valid comparisons between the fuels, creating the fundamental desired output of cooking energy. In Figure B7, biomass burned alone produces the highest PM, whereas biomass co-fired with 10% biogas produces lowest PM. In Figure B8, biomass burned alone and biomass co-fired with 50% biogas produce same amount of PM. The lowest PM is still produced when biomass is co-fired with 10 % biogas with the addition of fan.

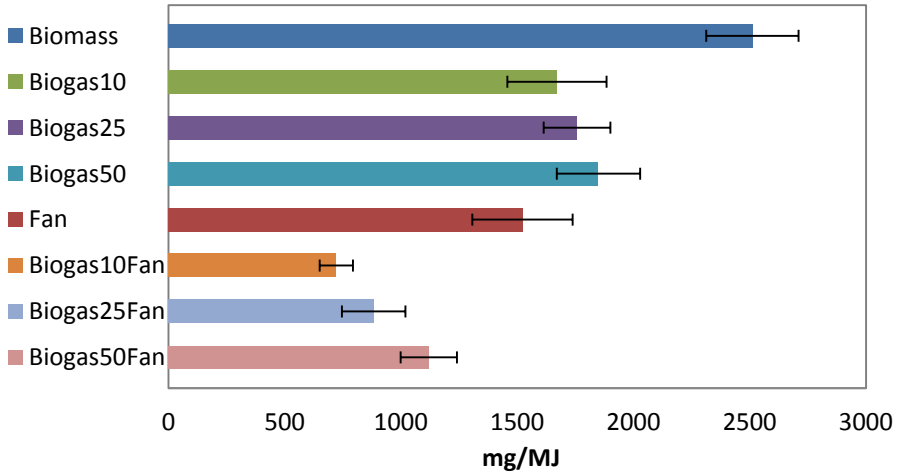

Figure B 7: Comparison of PM Emission per Energy Delivered to Cooking Pot among all the Tests

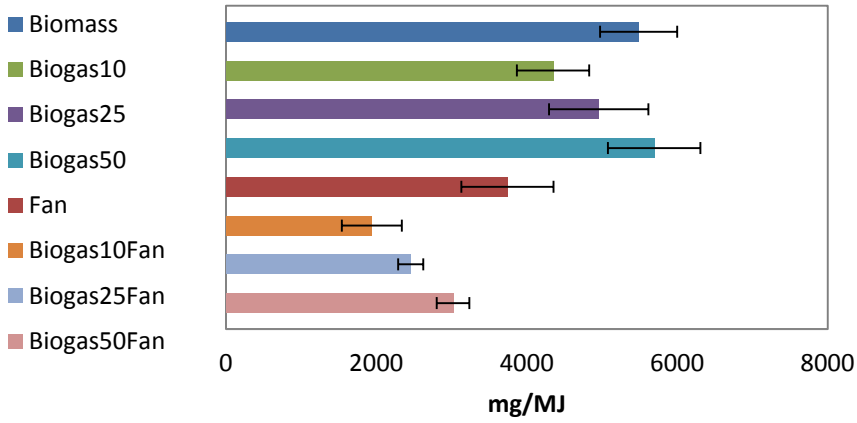

Figure B 8: Comparison of PM Emission per Fuel Energy among all the Tests

Figure B9 compares the MCE among all the tests. Each test is repeated three times. True combustion efficiency is the ratio of heat produced in a combustion process to the heat that would be released in complete or ideal combustion. MCE is a reasonable substitute for true combustion efficiency (Johnson, Edwards, Berrueta, & Masera, 2010). For all the tests, MCE is high, but many studies done in the past show that a small variation in MCE results in a large difference in the emissions of pollutants (Jetter, et al., 2012). MCE is lowest for biomass burned alone. There is a rise in MCE when biomass is co-fired with 10% biogas. But, with the increase in flow rate of biogas, MCE decreases. This trend is true with the addition of fan too. Biomass co-fired with 10% biogas in addition with the fan produces the highest MCE.

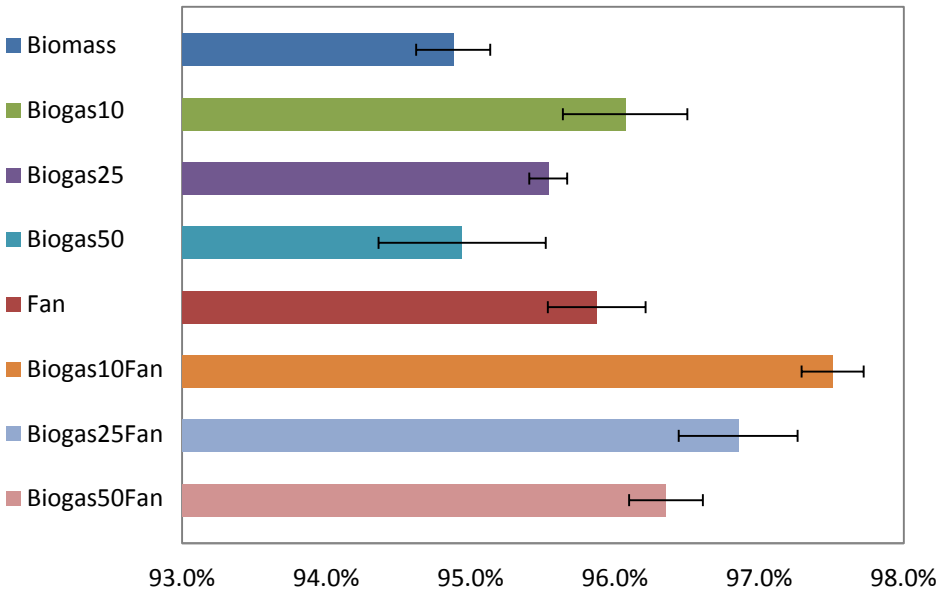

Figure B 9: Comparison of MCE among all the different Tests

APPENDIX C: CALCULATING MASS FLOW (G/SEC)[1]

This appendix explains how the flue gas mass flow rate within the duct is calculated. For pitot tube, Bernoulli's equation states that stagnation pressure (P_t) is the sum of static pressure (P_s) and dynamic pressure ($\rho v^2/2$). This equation includes density as a variable which estimates a more accurate flow. The theoretical velocity of a pitot tube is

$$v = \sqrt{\frac{2\Delta P}{\rho}} \qquad \textbf{(C-1)}$$

$$v = velocity\left(\frac{m}{s}\right)$$

$$\Delta P = stagnant\ and\ static\ pressure\ differential\left(Pa\right)$$

$$\rho = density\left(\frac{kg}{m^3}\right)$$

The pressure differential is measured and recorded using the magnesense pressure transducer which is a part of PEMS. The pressure differential from PEMS is in the units of inches of H_2O where it is converted to Pascal by the following conversion.

$$1 in H_2 0 = 249.09\, Pa \qquad \textbf{(C-2)}$$

If the pitot tube is located in the duct at the radius where $v = \bar{v}$ (average velocity) then the flow rate in the duct is represented by

[1] Adapted and Modified from Reference (Aprovecho, 2012)

$$\dot{v} = C_1\sqrt{\frac{2\Delta P}{\rho}} \qquad \textbf{(C-3)}$$

$\dot{v} = flow\,rate\left(\frac{m^3}{s}\right)$

$C_1 = cross\,sectional\,area\left(m^2\right)$

$\Delta P = pressure\,differential\,of\ flow\,grid\left(Pa\right)$

The flow grid is not a theoretical pitot tube, there is an amplification factor. The flow rate through the flow grid is represented by

$$\dot{v} = C_1 C_2\sqrt{\frac{2\Delta P}{\rho}} \qquad \textbf{(C-4)}$$

$C_1 = cross\,sectional\,area\left(m^2\right)$

$C_2 = amplification\ factor$

These constants can be combined into one: $C = C_1 C_2\sqrt{2}$, and the equation becomes

$$\dot{v} = C\sqrt{\frac{\Delta P}{\rho}} \qquad \textbf{(C-5)}$$

$\dot{v} = flow\,rate\left(\frac{m^3}{s}\right)$

$C = constant\left(\frac{\frac{m^3}{s}}{\sqrt{\frac{Pa\cdot m^3}{kg}}}\right)$

$\Delta P = pressure\,differential\left(Pa\right)$

$\rho = density\left(\frac{kg}{m^3}\right)$

The calibration constant is provided with the flow grid (Aprovecho, 2012)

$$\Rightarrow C = 0.0165\left(\frac{\frac{m^3}{s}}{\sqrt{\frac{Pa \cdot m^3}{kg}}}\right) \quad \textbf{(C-6)}$$

The volumetric flow rate is

$$\dot{v} = 0.0165\sqrt{\frac{\Delta P}{\rho}} \quad \textbf{(C-7)}$$

$$\dot{v} = volumetric\ flow\ rate\left(\frac{m^3}{s}\right)$$

$$\Delta P = pressure\ differential\ of\ \ flow\ grid\left(Pa\right)$$

$$\rho = density\left(\frac{kg}{m^3}\right)$$

Next, the mass flow rate

$$\dot{m} = \rho\dot{v} = \rho \times 0.0165\sqrt{\frac{\Delta P}{\rho}} = 0.0165\sqrt{\Delta P \rho} \quad \textbf{(C-8)}$$

$$\dot{m} = mass\ flow\left(\frac{kg}{sec}\right)$$

$$\Delta P = pressure\ differential\ of\ \ flow\ grid\left(Pa\right)$$

$$\rho = density\left(\frac{kg}{m^3}\right)$$

The density is calculated from the flue temperature. The ideal gas law is

$$\rho = \frac{P}{RT} \quad \textbf{(C-9)}$$

And the gas constant: $R_{air} = 287\left(\frac{J}{kg \cdot K}\right) or \left(\frac{Pa \cdot m^3}{kg \cdot K}\right)$

Note: The gas in the duct is treated as air, since it is over 99% air and less than 1% other gases (Aprovecho, 2012).

Substituting Equation (C-9) into (C-8) gives the mass flow

$$\dot{m} = \frac{0.0165}{\sqrt{287}}\sqrt{\frac{\Delta P \cdot P}{T}} \quad \textbf{(C-10)}$$

$\dot{m} = mass\ flow\left(\frac{kg}{sec}\right)$

$\Delta P = pressure\ differential\ of\ \ flow\ grid\left(Pa\right)$

$P = ambient\ pressure\left(Pa\right)$

$T = temperature\left(K\right)$

To convert the mass flow to (grams/sec)

$1\ kg\ \ =\ \ 1000\ g$

The pressure differential reading from the flow grid must be converted to (Pa)

$1 in H_2 0 = 249.09\ Pa$

The temperature sensor output must be converted to Kelvin

$°K = °C + 273.15$

Equation (C-10) becomes

$$\dot{m} = \frac{0.0165\sqrt{249.09}}{\sqrt{287}} \times \sqrt{\frac{\Delta P \cdot P}{T + 273.15}} \times 1000 \quad \textbf{(C-11)}$$

$$\dot{m} = 15.3\sqrt{\frac{\Delta P \cdot P}{T + 273.15}} \quad \textbf{(C-12)}$$

$\dot{m} = mass\ flow\left(\frac{g}{sec}\right)$

$\Delta P = pressure\, differential\, of\ flow\, grid\left(inH_2O\right)$

$P = ambient\ pressure\left(Pa\right)$

$T = temperature\left(^{\circ}C\right)$

APPENDIX D: RAW DATA TO FINAL RESULT

Raw data were collected during the test by data acquisition system in PEMS. The following calculations show how the raw data were converted into grams of CO, CO_2, and PM.

Carbon Monoxide

To get the CO in ppm, the data is multiplied by the calibration constant. The CO in grams is calculated by multiplying the raw data by calibration constant, mass flow rate (g/s) and change in time (s). Mass flow rate is calculated in Appendix C and the pressure differential is measured and recorded using the magnesense pressure transducer which is a part of PEMS. The change in time is always two seconds because the data is collected in every two seconds.

$$\overline{CO}_{cnst} = 0.02968\ ppm \quad \textbf{(D-1)}$$

$\overline{CO}_{cnst} = calibration\ \ constant\ for\ CO\ (ppm)$

$$\overline{CO} = Raw\ data \cdot \overline{CO}_{cnst}\ (ppm) \quad \textbf{(D-2)}$$

$$CO = \overline{CO} \cdot \dot{m} \cdot \Delta t\ \text{(g)} \quad \textbf{(D-3)}$$

$\dot{m} = mass\ flow\ rate\left(\frac{g}{s}\right)$

$\Delta t = change\ \text{in time}(s)$

The CO (g) is integrated with respect to the burn time to give the cumulative CO (g) at the end of the test.

Carbon Dioxide

The calculations involved in the conversion from raw data of CO_2 to grams are similar to carbon monoxide. But the calibration constant for CO_2 is different.

$$\overline{CO}_{2,cnst} = 1\, ppm \quad \textbf{(D-4)}$$

$\overline{CO}_{2,cnst} = calibration\, constant\, for\, CO_2\ (ppm)$

Particulate Matter

The two systems that measure the PM emission are gravimetric and scattering photometer sensor. Gravimetric system consisted of pump, particle separator, and filter paper. The particle separator allowed only particles equal or smaller to 2.5 micron meters in diameter to pass. The pump drew the flue gas through the particle separator and the PM was collected on the filter paper. Thus the total mass of the PM is taken by the difference of final and initial filter paper. The gravimetric is considered more accurate in comparison to the scattering photometer sensor (Jetter, et al., 2012). For all the tests, the gravimetric system was used to get the total mass of PM whereas the sensor was used to get the time resolved measurements. The total mass measurement obtained using the gravimetric system was used to express the estimate of the PM concentration obtained by the scattering sensor in mg/m^3.

Gravimetric:

$$m_{PM} = m_f - m_i\,(mg) \quad \textbf{(D-5)}$$

m_f = final filter paper mass (mg)

m_i=initial filter paper mass (mg)

$$\bar{c}\left(\frac{\mu g}{m^3}\right)=\frac{m_{PM}\cdot 1000(\mu g)}{\text{Gravimetric flow rate}\left(\frac{\mathrm{m}^3}{\mathrm{s}}\right)\times\text{Test duration time}(\mathrm{s})} \quad \textbf{(D-6)}$$

$\bar{c}=$ *average PM concentration from* gravimetry $\left(\frac{\mu g}{m^3}\right)$

The gravimetric flow rate = $2.78*10^{-4}$ m^3/s, is a constant value for the pump used in the experiments. To convert the $\bar{c}$ to PM, density of the flue gas is needed which is calculated using Equation (D-7). There is a thermocouple which measured the temperature of the flue gas. The temperature is found in the raw data. Equation (D-8) calculates the PM by multiplying average PM concentration from gravimetry by mass flow rate, change in time (s) and dividing by density. Mass flow rate is calculated in Appendix C.

$$Density\left(\frac{g}{m^3}\right)=\frac{Molecular\ weight\ of\ air\left(\frac{g}{mol}\right)\cdot Atmospheric\ pressure(Pa)}{Universal\ gas\ constant\left(\frac{J}{K\cdot mol}\right)\cdot Temperature(K)} \quad \textbf{(D-7)}$$

$$PM\,(\mu\mathrm{g})=\frac{c_i\left(\frac{\mu\mathrm{g}}{\mathrm{m}^3}\right)\cdot\dot{m}\left(\frac{\mathrm{g}}{\mathrm{s}}\right)\cdot\Delta t\,(\mathrm{s})}{\text{Density}\left(\frac{\mathrm{g}}{\mathrm{m}^3}\right)} \quad \textbf{(D-8)}$$

c_i = real time concentration with gravimetric scaling $\left(\frac{\mu\mathrm{g}}{\mathrm{m}^3}\right)$

$\dot{m}$ = mass flow rate $\left(\frac{\mathrm{g}}{\mathrm{s}}\right)$

Δt = change in time (s)

The PM (μg) is integrated with respect to the burn time to give the cumulative PM (μg) at the end of the test.

PM Sensor:

PM sensor is a red laser scattering photometer which records the time resolved measurement of PM emission. Time resolved measurement explains the behavior of emission in the process of combustion. PM sensor is a black case where a laser shines at a wavelength of about 635 nm (Aprovecho, 2012). Inside the case there is a photo sensor diode which acts as a receiver. When the case is clear, the laser shines through and returns very little signal to the receiver. But when there are solid particles the laser bounces of particles and gets deflected to the photo sensor.

Mass scattering cross section is the shadow area created by light scattering by a particle per mass and its value is assumed from the literature (Roden, Bond, Conway, & Pinel, 2006). The concentration measured by laser in real time is also provided by the manufacturer as shown in Equation (D-9) (Aprovecho, 2012). If the given concentration is used for a different type of stove or fuel then the PM calculation is not accurate. PM coefficient can be used to calculate the total PM, but it is considered less accurate (Jetter, et al., 2012). For the tests done for this thesis, it was found that the total PM from the sensor was about 50-75% lower than the gravimetry. The main reason behind this disparity is that the concentration measured by laser in real time which is given by the manufacturer was obtained from a different kind of stove or test. The stove, burning style, fuel being used in the tests for this thesis are very different from the test the manufacturer used to obtain the real time laser concentration value. To mitigate this inaccuracy, it is necessary

to calibrate and the calibration is done by scaling the gravimetric concentration which is specific for a test.

$$c_i^{'} = 4.2\ \frac{\mu g}{m^3} \tag{D-9}$$

$$c_i^{'} = concentration\, measured\, by\, laser,\, real\, time\left(\frac{\mu g}{m^3}\right)$$

$$\alpha_i^{'} = 3\ \frac{m^2}{g} \tag{D-10}$$

$$\alpha_i^{'} = mass\ scattering\ cross\ section\left(\frac{m^2}{g}\right)$$

σ_i is the real time scattering coefficient measured by the laser. Equation (D-11) gives the scattering coefficient $\left(\frac{1}{Mm}\right)$ for instantaneous time (Malm, Sisler, Huffman, Eldred, & Cahill, 1994). Scattering coefficient is a measure of attenuation of scattering light due to the PM acting as solid particles. It can also be defined as the cross-sectional area per unit volume of the particle.

$$\sigma_i\left(\frac{1}{Mm}\right) = c_i^{'} \cdot \alpha^{'} \tag{D-11}$$

$$\sigma_i = real\, time\, scattering\, coefficient\left(\frac{1}{Mm}\right)$$

In order to calibrate the real time concentration by gravimetric scaling, a new mass scattering cross section is derived from the gravimetric system. Average scattering coefficient $(\overline{\sigma_i})$ is the average of all the instantaneous scattering coefficient taken for the test period.

$$\bar{\alpha} = \frac{\bar{\sigma}}{\bar{c}} \quad \textbf{(D-12)}$$

$$\bar{\alpha} = mass\ scattering\ cross\ section\ derived\ \ from\ gravimetry\left(\frac{m^2}{g}\right)$$

$$\bar{c} = average\ concentration\ \ from\ gravimetric\left(\frac{\mu g}{m^3}\right)$$

$$\bar{\sigma} = average\ scattering\ coefficient\left(\frac{1}{Mm}\right)$$

The real time concentration with gravimetric scaling c_i, is the ratio of real time scattering coefficient measured by laser to mass scattering coefficient derived from gravimetry. Equation (D-13) is used to plot the PM emission with time.

$$c_i = \frac{\sigma_i}{\bar{\alpha}} \quad \textbf{(D-13)}$$

Change in Pressure (Delta P)

PEMS consists of magnesense pressure transducer that outputs a signal based on the pressure drop across the flow grid. The output signal is found in the raw data. There is also a magnehelic sensor, which provides the analogue pressure measurement (inches of water). PEMS records the data every two seconds and the change in pressure is always similar to the full flow reading from the analogue pressure measurement. However, to get better accuracy, the flow data from magnesense pressure transducer is combined with the full flow reading from the analogue pressure measurement.

The PEMS runs for at least 15 minutes as a background period before any test. There are two background periods. First background period is between when the PEMS is turned on and the blower fan is on. Second background period is between the blower fan on and two minutes before the test. Before the blower fan was turned on, the pressure gauge was made sure that it

pointed at zero making the $Flow_{GuageBkg1}$ always zero. When the blower fan is turned on, the full flow reading ($Flow_{GuageBkg2}$) of the Magnahelic pressure gauge is recorded on the test data sheet. Equation (D-13) combines the analogue pressure gauge and pressure transducer (raw data) to compute the change in pressure.

$$\Delta P\left(inches\, H_2O\right) = Flow\left(raw\, data\right) \cdot Flow\, Slope + Flow\, Intercept \quad \textbf{(D-14)}$$

$$Flow\, Slope = \frac{Flow_{GuageBkg\,2} - Flow_{GuageBkg1}}{Flow_{RawBkg\,2} - Flow_{RawBkg1}} \quad \textbf{(D-15)}$$

$$Flow_{GuageBkg\,2} = full\ flow\, reading\left(inches\, of\ water\right)$$

$$Flow_{GuageBkg1} = 0\left(inches\, of\ water\right)$$

$$Flow_{rawBkg1} = average\, of\ Flow\left(raw\, data\right)\ for\ first\, background\ period$$

$$Flow_{rawBkg\,2} = average\, of\ Flow\left(raw\, data\right)\ for\, second\, background\ period$$

$$Flow\, intercept = -Flow\, Slope * Flow_{rawBkg1} \quad \textbf{(D-16)}$$

Equation (D-15) has a negative sign because the first background period represents the data recorded before the blower fan was turned on.

APPENDIX E: RAW DATA

The raw data provided below is just a sample. All the raw data, conversions, and calculations can be found in the Co-firing DVD. There are eight different tests and each test is repeated three times. Therefore, there are 24 raw data in the Co-firing DVD. The conversions are explained in Appendix D. The PEMS runs for at least 15 minutes as a background period before any test. In the sample below, instead of the background period, the actual test is shown. Thus the time starts at 1001 seconds. The raw data consists of time, CO, temperature of the water, PM, flow, flue gas temperature, CO_2, and relative humidity. All the calibration constants were provided by the Aprovecho. The following sample is from test 1, biomass burned alone.

Date	3/13/2013													
Time	15:40:04													
Calibration	0.02968		0.1		4.2		1		0.00384		1		1	
	Raw		Raw		Raw		Raw		Raw		Raw		Raw	
Time (s)	CO	CO (ppm)	Temp Pot	Temp Pot (deg C)	PM	PM (ug/m3)	Flow	Δ P (in H2O)	FlueTemp	FlueTemp (deg C)	CO2	CO2 (ppm)	RH	RH (%)
1001	5087	151	280	28.0	2116	8887	41758	0.39	7924	30.4	1145	1145	20	20
1003	5862	174	273	27.3	2048	8602	41564	0.39	8031	30.8	1214	1214	21	21
1005	6031	179	277	27.7	1836	7711	41644	0.39	8143	31.3	1288	1288	21	21
1007	6233	185	288	28.8	1550	6510	41550	0.39	8238	31.6	1351	1351	21	21
1009	6401	190	304	30.4	1586	6661	41761	0.39	8337	32.0	1441	1441	21	21
1011	6435	191	295	29.5	1642	6896	41151	0.39	8444	32.4	1528	1528	21	21
1013	6772	201	309	30.9	1866	7837	40848	0.38	8543	32.8	1608	1608	22	22
1015	7176	213	285	28.5	2141	8992	41203	0.39	8650	33.2	1701	1701	22	22
1017	7311	217	295	29.5	2694	11315	41249	0.39	8748	33.6	1828	1828	22	22
1019	7682	228	292	29.2	2192	9206	41329	0.39	8855	34.0	1905	1905	22	22
1021	7884	234	300	30.0	2674	11231	41601	0.39	8970	34.4	2010	2010	23	23
1023	8288	246	305	30.5	2761	11596	41155	0.39	9099	34.9	2147	2147	23	23
1025	8692	258	305	30.5	3052	12818	40765	0.38	9223	35.4	2226	2226	23	23
1027	9350	278	309	30.9	2783	11689	40807	0.38	9354	35.9	2308	2308	24	24
1029	9792	291	318	31.8	3157	13259	40785	0.38	9491	36.4	2404	2404	24	24
1031	10230	304	304	30.4	3505	14721	41127	0.39	9640	37.0	2498	2498	25	25
1033	10653	316	318	31.8	3472	14582	41077	0.38	9778	37.5	2648	2648	25	25
1035	11098	329	324	32.4	3353	14083	40830	0.38	9931	38.1	2773	2773	25	25
1037	11559	343	320	32.0	3176	13339	41161	0.39	10081	38.7	2864	2864	26	26
1039	12007	356	330	33.0	3060	12852	41124	0.39	10217	39.2	2968	2968	26	26

Date	3/13/2013													
Time	15:40:04													
Calibration	0.02968		0.1		4.2		1		0.00384		1		1	
	Raw		Raw		Raw		Raw		Raw		Raw		Raw	
Time (s)	CO	CO (ppm)	Temp Pot	Temp Pot (deg C)	PM	PM (ug/m3)	Flow	Δ P (in H2O)	FlueTemp	FlueTemp (deg C)	CO2	CO2 (ppm)	RH	RH (%)
1041	12413	368	345	34.5	2913	12235	41073	0.38	10364	39.8	3063	3063	26	26
1043	12744	378	336	33.6	3328	13978	41158	0.39	10512	40.4	3170	3170	26	26
1045	13010	386	349	34.9	3266	13717	41194	0.39	10649	40.9	3281	3281	26	26
1047	13239	393	346	34.6	2390	10038	41347	0.39	10782	41.4	3403	3403	26	26
1049	13451	399	339	33.9	2834	11903	41487	0.39	10925	42.0	3506	3506	27	27
1051	13643	405	341	34.1	2262	9500	41529	0.39	11082	42.6	3634	3634	28	28
1053	13798	410	349	34.9	2190	9198	41280	0.39	11231	43.1	3723	3723	28	28
1055	13932	414	339	33.9	1899	7976	41465	0.39	11363	43.6	3825	3825	28	28
1057	14033	416	360	36.0	1583	6649	41300	0.39	11498	44.2	3953	3953	28	28
1059	14090	418	352	35.2	1773	7447	41301	0.39	11640	44.7	4071	4071	28	28
1061	14083	418	360	36.0	1625	6825	41285	0.39	11777	45.2	4172	4172	28	28
1063	14016	416	368	36.8	1435	6027	41252	0.39	11910	45.7	4268	4268	28	28
1065	13882	412	361	36.1	1592	6686	41327	0.39	12028	46.2	4397	4397	28	28
1067	13730	408	362	36.2	1505	6321	41260	0.39	12143	46.6	4501	4501	28	28
1069	13555	402	373	37.3	1564	6569	41107	0.39	12260	47.1	4611	4611	28	28
1071	13377	397	363	36.3	1298	5452	41066	0.38	12364	47.5	4709	4709	28	28
1073	13216	392	384	38.4	1286	5401	41413	0.39	12458	47.8	4816	4816	28	28
1075	13081	388	385	38.5	1585	6657	41350	0.39	12559	48.2	4917	4917	28	28
1077	12940	384	376	37.6	1490	6258	41387	0.39	12649	48.6	5012	5012	28	28
1079	12801	380	382	38.2	1647	6917	41294	0.39	12740	48.9	5081	5081	29	29
1081	12656	376	392	39.2	1356	5695	41206	0.39	12825	49.2	5199	5199	28	28
1083	12535	372	384	38.4	1607	6749	41354	0.39	12884	49.5	5227	5227	28	28
1085	12412	368	391	39.1	1926	8089	40990	0.38	12961	49.8	5284	5284	29	29
1087	12265	364	388	38.8	1933	8119	41077	0.38	13063	50.2	5347	5347	29	29
1089	12119	360	403	40.3	1617	6791	41118	0.39	13157	50.5	5396	5396	30	30
1091	12022	357	406	40.6	1293	5431	41157	0.39	13241	50.8	5460	5460	29	29
1093	11959	355	409	40.9	1200	5040	41027	0.38	13316	51.1	5503	5503	29	29
1095	11890	353	417	41.7	1345	5649	41263	0.39	13402	51.5	5575	5575	30	30
1097	11777	350	407	40.7	1288	5410	41302	0.39	13484	51.8	5640	5640	30	30
1099	11637	345	413	41.3	1162	4880	41149	0.39	13571	52.1	5662	5662	30	30
1101	11499	341	424	42.4	1233	5179	41382	0.39	13636	52.4	5765	5765	30	30
1103	11367	337	446	44.6	1122	4712	41235	0.39	13696	52.6	5802	5802	30	30
1105	11241	334	436	43.6	1091	4582	41351	0.39	13753	52.8	5883	5883	29	29
1107	11111	330	426	42.6	1158	4864	41627	0.39	13779	52.9	5936	5936	29	29
1109	10971	326	434	43.4	1173	4927	41444	0.39	13811	53.0	5981	5981	29	29
1111	10819	321	435	43.5	1142	4796	41159	0.39	13837	53.1	6019	6019	29	29
1113	10657	316	444	44.4	1229	5162	41182	0.39	13870	53.3	6012	6012	29	29
1115	10506	312	444	44.4	1159	4868	41293	0.39	13913	53.4	6064	6064	29	29
1117	10356	307	452	45.2	1156	4855	41210	0.39	13959	53.6	6087	6087	30	30
1119	10226	304	449	44.9	1199	5036	41575	0.39	14012	53.8	6087	6087	30	30
1121	10120	300	449	44.9	1450	6090	41297	0.39	14079	54.1	6147	6147	31	31
1123	10039	298	448	44.8	1353	5683	41208	0.39	14157	54.4	6155	6155	31	31
1125	9989	296	463	46.3	1318	5536	41285	0.39	14231	54.6	6170	6170	31	31
1127	9984	296	467	46.7	1134	4763	41303	0.39	14304	54.9	6193	6193	31	31
1129	10003	297	473	47.3	1253	5263	41038	0.38	14376	55.2	6170	6170	31	31
1131	10029	298	471	47.1	1371	5758	41200	0.39	14450	55.5	6186	6186	31	31
1133	10022	297	473	47.3	1415	5943	41122	0.39	14510	55.7	6224	6224	31	31
1135	10010	297	479	47.9	1443	6061	41118	0.39	14567	55.9	6247	6247	31	31
1137	9994	297	476	47.6	1315	5523	41118	0.39	14639	56.2	6247	6247	31	31
1139	10001	297	478	47.8	1623	6817	41039	0.38	14713	56.5	6247	6247	32	32
1141	10032	298	490	49.0	1537	6455	41263	0.39	14797	56.8	6301	6301	32	32
1143	10065	299	500	50.0	1963	8245	41448	0.39	14869	57.1	6362	6362	32	32
1145	10099	300	500	50.0	1700	7140	41048	0.38	14958	57.4	6308	6308	33	33
1147	10168	302	509	50.9	1882	7904	41108	0.39	15045	57.8	6301	6301	33	33
1149	10282	305	526	52.6	1767	7421	40964	0.38	15133	58.1	6339	6339	33	33
1151	10399	309	516	51.6	1649	6926	41031	0.38	15224	58.5	6362	6362	33	33
1153	10516	312	508	50.8	1565	6573	41155	0.39	15293	58.7	6440	6440	33	33
1155	10608	315	507	50.7	1705	7161	40985	0.38	15370	59.0	6433	6433	33	33

Date	3/13/2013													
Time	15:40:04													
Calibration	0.02968		0.1		4.2		1		0.00384		1		1	
	Raw		Raw		Raw		Raw		Raw		Raw		Raw	
Time (s)	CO	CO (ppm)	Temp Pot	Temp Pot (deg C)	PM	PM (ug/m3)	Flow	Δ P (in H2O)	FlueTemp	FlueTemp (deg C)	CO2	CO2 (ppm)	RH	RH (%)
1157	10668	317	528	52.8	1798	7552	40901	0.38	15455	59.3	6535	6535	33	33
1159	10720	318	527	52.7	2111	8866	40998	0.38	15543	59.7	6574	6574	34	34
1161	10752	319	532	53.2	2019	8480	40836	0.38	15633	60.0	6693	6693	34	34
1163	10811	321	536	53.6	1916	8047	41118	0.39	15712	60.3	6717	6717	34	34
1165	10913	324	540	54.0	2116	8887	40991	0.38	15773	60.6	6812	6812	33	33
1167	11048	328	545	54.5	2037	8555	40900	0.38	15842	60.8	6820	6820	33	33
1169	11182	332	543	54.3	2063	8665	41001	0.38	15902	61.1	6884	6884	33	33
1171	11303	335	547	54.7	1908	8014	40975	0.38	15963	61.3	6892	6892	33	33
1173	11420	339	556	55.6	1943	8161	41128	0.39	16023	61.5	6884	6884	33	33
1175	11512	342	552	55.2	1826	7669	41028	0.38	16085	61.8	6925	6925	33	33
1177	11584	344	554	55.4	2433	10219	40835	0.38	16163	62.1	6933	6933	34	34
1179	11652	346	559	55.9	2960	12432	40839	0.38	16230	62.3	6990	6990	34	34
1181	11705	347	583	58.3	3000	12600	41011	0.38	16282	62.5	7014	7014	34	34
1183	11812	351	573	57.3	2894	12155	41007	0.38	16337	62.7	7031	7031	34	34
1185	12003	356	572	57.2	2871	12058	41101	0.39	16386	62.9	7087	7087	34	34
1187	12223	363	578	57.8	2738	11500	41021	0.38	16452	63.2	7120	7120	34	34
1189	12437	369	593	59.3	3170	13314	40941	0.38	16522	63.4	7095	7095	34	34
1191	12658	376	590	59.0	3271	13738	40741	0.38	16597	63.7	7120	7120	35	35
1193	12847	381	601	60.1	3072	12902	40803	0.38	16668	64.0	7178	7178	35	35
1195	13044	387	595	59.5	3600	15120	40690	0.38	16734	64.3	7194	7194	35	35
1197	13250	393	594	59.4	3250	13650	40822	0.38	16794	64.5	7169	7169	35	35
1199	13467	400	611	61.1	3072	12902	40780	0.38	16852	64.7	7178	7178	35	35
1201	13711	407	618	61.8	2800	11760	40985	0.38	16899	64.9	7186	7186	35	35
1203	13947	414	614	61.4	2707	11369	40499	0.38	16943	65.1	7269	7269	35	35
1205	14131	419	625	62.5	2835	11907	40655	0.38	16982	65.2	7244	7244	35	35
1207	14259	423	623	62.3	3003	12613	40504	0.38	17035	65.4	7294	7294	35	35
1209	14328	425	625	62.5	3032	12734	40701	0.38	17095	65.6	7344	7344	36	36
1211	14417	428	637	63.7	2919	12260	40607	0.38	17145	65.8	7368	7368	36	36
1213	14551	432	642	64.2	2971	12478	40999	0.38	17202	66.1	7402	7402	36	36
1215	14706	436	642	64.2	2839	11924	41007	0.38	17248	66.2	7427	7427	36	36
1217	14850	441	647	64.7	2700	11340	40970	0.38	17300	66.4	7444	7444	36	36
1219	14951	444	648	64.8	3201	13444	40381	0.38	17350	66.6	7419	7419	36	36
1221	15008	445	658	65.8	2995	12579	40772	0.38	17394	66.8	7444	7444	36	36
1223	15067	447	656	65.6	2779	11672	40659	0.38	17435	67.0	7477	7477	36	36
1225	15141	449	665	66.5	3347	14057	40699	0.38	17478	67.1	7536	7536	36	36
1227	15242	452	665	66.5	3212	13490	40659	0.38	17535	67.3	7528	7528	36	36
1229	15354	456	679	67.9	3321	13948	40542	0.38	17593	67.6	7537	7537	37	37
1231	15485	460	670	67.0	3388	14230	40603	0.38	17644	67.8	7579	7579	37	37
1233	15626	464	671	67.1	3024	12701	40838	0.38	17688	67.9	7595	7595	37	37
1235	15760	468	684	68.4	2906	12205	40511	0.38	17733	68.1	7604	7604	36	36
1237	15887	472	688	68.8	2810	11802	40991	0.38	17772	68.2	7629	7629	36	36
1239	15954	474	697	69.7	2719	11420	40465	0.38	17818	68.4	7646	7646	36	36
1241	15949	473	699	69.9	2990	12558	40211	0.37	17848	68.5	7680	7680	36	36
1243	15897	472	705	70.5	3135	13167	40277	0.37	17885	68.7	7731	7731	36	36
1245	15822	470	701	70.1	3106	13045	40251	0.37	17921	68.8	7757	7757	36	36
1247	15758	468	705	70.5	3143	13201	40386	0.38	17957	69.0	7757	7757	36	36
1249	15707	466	705	70.5	3474	14591	40516	0.38	18007	69.1	7817	7817	37	37
1251	15630	464	714	71.4	3022	12692	40574	0.38	18063	69.4	7894	7894	37	37
1253	15567	462	719	71.9	3353	14083	40661	0.38	18108	69.5	7902	7902	37	37
1255	15551	462	736	73.6	3323	13957	40427	0.38	18146	69.7	7851	7851	37	37
1257	15532	461	750	75.0	3497	14687	40820	0.38	18176	69.8	7825	7825	37	37
1259	15512	460	754	75.4	3270	13734	40569	0.38	18206	69.9	7808	7808	37	37
1261	15522	461	751	75.1	3329	13982	40610	0.38	18253	70.1	7791	7791	37	37
1263	15539	461	744	74.4	3265	13713	40477	0.38	18293	70.2	7818	7818	37	37
1265	15553	462	747	74.7	3549	14906	40470	0.38	18337	70.4	7818	7818	37	37
1267	15554	462	751	75.1	3435	14427	40148	0.37	18386	70.6	7835	7835	38	38
1269	15544	461	755	75.5	3403	14293	40703	0.38	18432	70.8	7818	7818	38	38
1271	15527	461	771	77.1	3416	14347	40580	0.38	18482	71.0	7826	7826	38	38